Hungarian University of Agriculture and Life Sciences

Mixing efficiency of paddle and screw mixers

PhD dissertation

by

Seifeddine Garneoui

Gödöllő
2024

Doctoral school denomination: Doctoral School of Mechanical Engineering

Science: Mechanical Engineering

Leader: Prof. Dr. Gábor Kalácska, DSc
Doctoral School of Mechanical Engineering
Hungarian University of Agriculture and Life Sciences, Gödöllő, Hungary

Supervisor: Prof. Dr. István Keppler, PhD
Institute of Technology
Hungarian University of Agriculture and Life Sciences, Gödöllő, Hungary

Co-Supervisor: Dr. habil. Péter Korzenszky, PhD
Institute of Technology
Hungarian University of Agriculture and Life Sciences, Gödöllő , Hungary

....

Approval of the Head of Doctoral School Approval of the Supervisor(s)

CONTENTS

NOMENCLATURE AND ABBREVIATIONS

CoF	Coefficient of friction [-]
$CoRF$	Coefficient of rolling friction [-]
D	Strain [-]
D_R	Distance ratio [-]
e	Coefficient of restitution [-]
E	Young's modulus of the particle assembly [Pa]
E_1	Young's modulus of particle type 1 [Pa]
E_2	Young's modulus of particle type 2 [Pa]
E^*	Equivalent Young's modulus [Pa]
F	Force [N]
$F_{c,i}$	Contact force acting on particle i [N]
g	Gravity [m/s^2]
G	Shear modulus [Pa]
G^*	Equivalent shear modulus [Pa]
I	Nearest neighbor mixing index [-]
I_d	Uncertainty [-]
I_i	Moment of inertia [kgm^2]
k_n	Normal stiffness [N/m]
k_t	Tangential stiffness [N/m]
M	Mixing index [-]
m^*	Equivalent mass [kg]
m_i	Mass of particle i [kg]
M_i	Total torque [Nm]
N	Number of spheres in a clump [-]
N_{white}	Number of white particles [-]
N_{all}	Total number of particles [-]
P	Screw pitch length [mm]
$x_1(k)$	Number fraction of white particles in the cell k [-]
$x_2(k)$	Number fraction of black particles in the cell k [-]
R_1, R_2	Radius of particle 1 and Radius of particle 2 [-]
R^*	Equivalent radius [mm]
r_i	Position of particle i [-]
r_{ik}	Distance between i^{th} particle and a randomly selected particle [m]
$T_{Rayleigh}$	Rayleigh time-step [s]
Z_i	Height of particle i [mm]
σ	Variance [-]
ϑ	Poisson's ratio [-]
ρ	Density [kg/m^3]
ω_i	Angular velocity [rpm]
γ_n, γ_t	Viscoelastic damping constants [Ns/m]
v_{nij}	Normal component of relative velocity [m/s]
v_{tij}	Tangential component of relative velocity [m/s]
δ_{nij}	Normal overlap between particles i and j [m]
δ_{tij}	Tangential overlap between the two particles i and j [m]

DEM	**D**iscrete **E**lement **M**ethod
DoE	**D**esign **o**f **E**xperiments
HCP	**H**exagonal **C**lose **P**acking
BCC	**B**ody-**C**entered **C**ubic
CoF	**C**oefficient **o**f **F**riction
CoRF	**C**oefficient **o**f **R**otational **F**riction
AoR	**A**ngle **o**f **R**epose

1. INTRODUCTION AND OBJECTIVES

1.1. Background

Mixing granular material is a common process broadly used in production and processing companies. For instance, the active components of an agricultural product in some cases are evenly distributed to ensure efficiency. The mixing procedure is of vital importance in the dosage of solid granules. The historic range of granular types and applications has led to the development of numerous apparatuses, mixing concepts, and mixing descriptions. For this reason, methods developed to mix particles cannot be applied to all mixing processes.

In various areas of engineering practices, complications arising from specific mechanical behavior of granular materials can be encountered. Under specific circumstances, granular material behaves similarly to solids (particles preserve their strength and their shape), however under other conditions the same granular material modelled earlier as solids behaves similarly to liquids, this dissemblance makes the mechanical behavior difficult to describe, yet in some case none of those models can be practical (e.g., silo discharge). Consequently, technologies used in granular materials processing (agriculture, food, pharmaceutical industries, etc.) are usually determined by experiments for a specific process. The selected method could be inappropriate, which leads to numerous technological problems. For example, in the case of drying grains, it is crucial to use the proper technology due to the expensive operating costs and high quality requirements.

Diffusive mixing, convective mixing, and shear mixing mechanisms can be involved in mixing solid particles, which can lead to different mixture states namely: incomplete random, complete random and perfect mixture, and even to segregation where particles do not mix completely. sampling is required to evaluate the quality of a mixture where different techniques were used either invasively or non-invasively. For the invasive method, a sampling body is thrust into the material assembly to take samples by ceasing sequentially the mixing operation or without interrupting the mixing operation. A quantitative result is obtained by physical sampling; however, the operation could change the mixture state whenever the sampling devices make contact with the particles. The other non-invasive method is to analyze snaps by way of a high-speed camera. Even though many sampling techniques are available, not enough information about the mixing process such as particle velocity, particle coordinates could be identified.

Cundall and Strack established the discrete element method in 1979 (Cundall & Strack, 1979). This method allows us to investigate the flow of particles numerically. Over the decades, the discrete element method (DEM) was developed numerically and extended for various applications. Today, with the existence of numerical tools, the study of granules mixtures becomes more efficient, where many physical outcomes can be obtained such as particles positions in the 3D domain, particles velocity distribution, particles kinetic energy, etc. When dealing with a large bulk granular material, more computational resources are needed, however nowadays supercomputers do exist to help solve this large material in a convenient time. In addition, using coarser particles or decreasing particle stiffness would decrease the computing time, yet either the scale-up of particle geometries or the scale-down of particle stiffness should be verified.

Mixing indexes are used to quantify the uniformity of such a mixture. The mixing index always fluctuates between 0 and 1. 0 describes the total segregation state of the mixture, and 1 defines a perfect mixture. In my research, I used the Lacey mixing index and the Nearest neighbor mixing index to quantify the conducted mixtures. The Lacey mixing index requires the division of the

DEM system into cells, then it finds the mixing index based on a statistical calculation of the different types of particles. On the other hand, the Nearest neighbor mixing index quantifies the mixture based on the position of each particle in the 3D DEM domain. As an advantage, I can find the mixing index at any desired time throughout the mixture, also many other findings could be recognized such as de-mixing, unnecessary overmixing, and optimal mixer parameters.

In the literature, there is a lack of information about the improvement of mixing in paddled mixers and screw mixers (Asachi et al., 2018) (Soni et al., 2016) (Huang & Kuo, 2014). There is not enough information on what is the optimal number of paddles that must be used to mix a certain size of particles, similarly about the size of screw pitch length and screw diameter, etc. also there is no information on the use of a paddled drum mixer to improve the mixing homogeneity of bi-sized particles. Based on these deficiencies from the literature, I tackled the mixing of particles in screw mixers and paddled mixers to improve the mixing homogeneity by finding the optimal parameters that should be used and to support solving these open questions.

1.2. Research objectives

The goal of my research is to improve the homogeneity of particles by selecting the proper mixing apparatus, mixing parameters, and mixing time as over-mixing is costly and might result in segregation. The list of objectives set to achieve are the following:

- To find the optimal screw pitch dimension as a function of particle radius in a screw auger mixer.
- To improve the mixing effectiveness of a rotating drum mixer by adding paddles in the middle of the mixer. Identify the optimal number of rotations of the drum when mixing mono-sized and bi-sized particles, in which the mixing homogeneity is at its maximum.
- To build a single shaft paddles mixer and analyze its mixing efficiency.
- To find the optimal rotational speed of a paddled drum mixer in terms of mixing uniformity.
- To find the optimal number of paddles in a single shaft paddle mixer in terms of mixing uniformity.
- To find the optimal number of rotations of a single shaft paddle mixer in terms of mixing uniformity.

2. LITERATURE REVIEW

2.1. Mixing of particles: state of the art

In this section, I introduced the mixing of granular material and why mixing is needed, also I gave a description of the various mixing types namely: free flowing mixture, cohesive mixture and ordered mixture.

2.1.1. Definition of granular material mixing

Mixing granular materials involves the process of blending or combining various solid particles or granules to achieve a homogeneous mixture (Bhatt, 2009). This process is commonly used in various industries such as agriculture, food processing, pharmaceuticals, construction, and chemical manufacturing. Some common aims and objectives for mixing granular materials are the following: enhance the flow characteristics of granular materials, making them easier to handle and transport, reducing production time and cost savings by minimizing waste and ensuring consistent quality, ensuring even moisture distribution in granular materials can be essential in agricultural applications, such as fertilization and soil conditioning, mixing can be employed to apply a coating or layer of one material onto the surface of another. For example, coating pharmaceutical tablets or adding flavorings to food products, achieving a uniform distribution of different components within the mixture is a fundamental aim of mixing. This ensures that each portion of the mixture contains the same proportions of ingredients, resulting in consistent product quality.

Mixing is an indispensable operation in many manufacturing industries such as pharmaceutical, food, agricultural, and chemical. It is an inevitable process in many factories to acquire such a product (e.g., pharmaceutical powders, fertilizer, etc.), or even bring to light new products.

When dealing with mixing solid particles, two types of materials exist depending on the flow properties. First, cohesive materials which are characterized by the resistance to flow through openings (e.g., wet clay), second non-cohesive materials that are quite easy to flow (e.g., grain, dry sand).

Certainly, conducting a mixing operation aims to achieve one or more of the objectives listed below (Bhatt, 2009):

- Ensure the uniformity/homogeneity.
- Enhance the physical or chemical reactions (e.g., diffusion, dissolution, etc.).
- Avoid the waste of basic materials.
- Promote chemical reactions.
- Produce dispersion.
- Substance transfer between granules (e.g., heat).
- Coating of granules.
- Drying of granules.

2.1.2. Overview of mixing types

Particle mixing is a general term, which is broadly used in manufacturing of many industries, such as cement, ceramic materials, catalysts, pharmaceutical, and agricultural products. As defined below, three types of mixtures exist namely, free flowing mixtures, cohesive mixtures and ordered mixtures (Deveswaran et al., 2010).

a) Free flowing mixtures

This type of mixture could be subject to segregation during mixing and packing. It is characterized by the effective particle-wall contact and the minimal need for lubricant. The particle can move smoothly in a particular way due to the inter-particulate forces. This mixture requires care when packing products and applying vacuum before sealing.

b) Cohesive mixtures

These elements are not free to flow because particles might stick to each other and agglomerate due to some factors such as moisture, inter-particle solid bridges, electrostatic charges, and Van der Waals forces. The formed agglomerates lead to an augmentation in segregation intensity. To ensure a satisfactory mixing, in some cases agglomerates should be repeatedly broken down and redistributed during the process (e.g., preventing uneven product quality), however in other cases creating agglomerates is the intention from the mixing operation (e.g., agglomerates can have better mechanical properties, such as increased hardness and reduced friability, which is essential in tablet and pellet manufacturing).

c) Ordered mixtures

If one of the constituents of the granular material mix is added to a fine, micronized form then mixing the larger particles may adsorb some of these smaller particles to active sites on their surface where they are held tenaciously. Ordered mixtures are formed by mechanical, adhesion, or coating forces in the way that the ordered unit will be the smallest possible sample of nearly identical compositions to all other ordered units in the mix.

2.2. Mechanisms of granular mixing

Three types of mixing mechanisms exist namely: diffusive mixing, convective mixing, and shear mixing (Fan, 2001). Their definitions are described below:

Diffusive mixing: The motion of groups of particles within the mixture characterizes this type of homogenization. The components are subdivided into clusters. They are displaced relative to one another, and their size is reduced. This motion creates a contact area between different components and is carried out by mixing on a large scale. This mixing mechanism can be employed when the segregation effect is aimed. This mechanism requires minimal energy input compared to other mixing mechanisms. This can result in energy savings, making it suitable for processes where energy efficiency is a priority.

Convective mixing: The motion of individual particles within the mixture characterizes this type of homogenization. It carried out mixing on a fine scale. This mixing mechanism requires low energy input. This mixing mechanism helps achieve a uniform distribution of solid particles within a mixture. This mixing mechanism reduces the risk of particle agglomerations and processes the operation in a short time, also it can help mitigate segregation tendencies. Particles tend to separate

during handling or transport, but convective mixing redistributes them, preventing the formation of layers with varying compositions.

Shear mixing: The slipping of particles within the mixture characterizes this type of homogenization. Often, it is a combination of the two previous mixing mechanisms, however a specific operation should be considered. Shear mixing is highly effective at achieving homogeneity within a mixture. The applied shear forces disrupt particle agglomerates and ensure a thorough blending of solid components, resulting in a uniform mixture.

Depending on the extent of mixing, the distribution of particle mass after a mixing process can be one of the different mixing characteristics in Fig. 2.1.

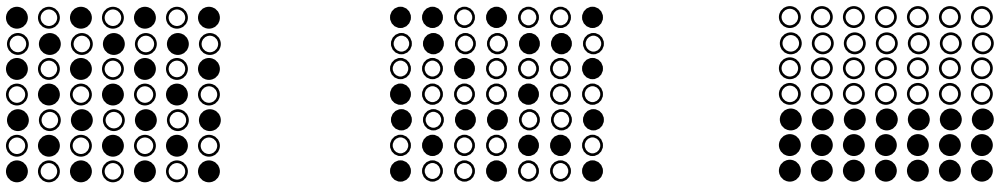

(a) (b) (c)

Fig. 2.1. Different types of mixing characteristics exhibited by granules: (a) perfectly mixed particles, (b) randomly mixed particles, and (c) unmixed particles (Lacey, 1954)

2.3. Factors impacting the mixing uniformity

Mixing particles is a complex process in which many factors interfere and influence the efficiency, thus the quality of the mixture. The impacting factors can be grouped namely: particle properties, mixer properties, and operating conditions.

2.3.1. Particle properties

2.3.1.1. Particle size

Venables and Wells revealed that particle relative size to the mixer apparatus as well as particle size distribution highly impact the mixture uniformity (Venables & Wells, 2001). For instance, tablets or capsules which are low-content dosage forms require an adequate number of particles to supply each dose.

It would be better to use fine particles to get better reproducibility and quality, particularly in small-dose preparation. Conversely, larger particles would lead to more influence of cohesive and adhesive particle interaction forces causing the so-called agglomeration in the mixture leading to unsatisfactory mixing results (Johnson M. , 1972). A cogent reason for this is Fig. 2.2 manifesting the evolution of drug dose when increasing the particle diameter.

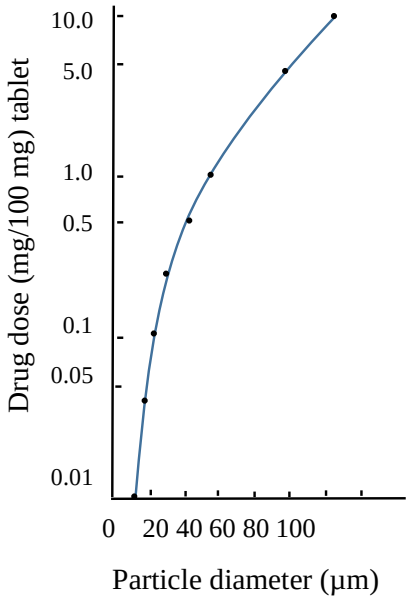

Fig.2.2. Limiting particle size as a function of the dose level for a coefficient of variance of 1 % in 100mg tablets (Johnson M. , 1972)

Furthermore, segregation can take form due to the large difference in size of the used non-interactive elements. The smaller particles may flow down through the voids between the larger particles when the kinetic energy is transferred to the system by shaking. Size segregation effects are crucial in powder metallurgy, pharmaceuticals, and the glass and paint industries. Size segregation refers to the separation of particles based on their size or mass, which can considerably influence the properties and performance of materials. For example, size segregation can change the distribution of particles in the end-product, changing its mechanical properties and structural integrity. In pharmaceuticals, it can impact the homogeneity and consistency of drug formulations, impacting their effectiveness and safety. Also, in the glass and paint industries, size segregation can influence the visual properties, texture, and coating quality of the end-products. Therefore, understanding and controlling size segregation effects are essential for optimizing processes and achieving the desired results in these industries. (Fig. 2.3) (Rosato et al., 1987).

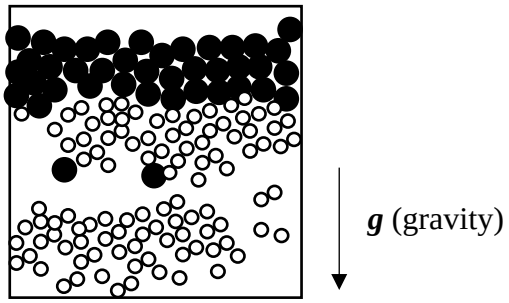

Fig. 2.3. Segregation of particles after shaking

Researchers found that the ratio between larger and smaller particles should be less than 1.2 to preclude segregation (Leuenberger H. , 2002).

2.3.1.2. Particle shape and surface

A sphere is the ideal shape because particles cannot interlock and stick, unlike the irregularly shaped particles that could highly impact the mixture state during a mixing process (Venables & Wells, 2001). Dubé et al., showed that an unexpected core segregation occurs when mixing particles having different shapes, also a smaller axial dispersion coefficient is obtained when mixing non-spherical particles compared to spherical ones (Dubé et al., 2013).

2.3.1.3. Density

Several problems can arise because of density variance in the mixture. First, due to gravitational force, the denser particles are dragged towards the bottom of the mixer leaving the less dense particles on the top layers which contributes to segregation (Hsiau & Chen, 2002; Venables & Wells, 2001). Second, mixing time is affected by the density, the denser particles need more time to mix (Fan et al., 1970). Practically, researchers stated that the size distribution is more significant to affect the mixing and segregation than the variance of particle densities (Venables & Wells, 2001).

2.3.1.4. Flowability

A precise definition of flowability is the capability of elements to stream in a desired way in a specific apparatus (Prescott & Barnum, 2000). Flow properties are of vital importance and must be considered whenever dealing with any granule's application such as tableting, encapsulation, brazing, mixing, etc. (Leuenberger & Lanz, 2005). A simple method to classify particle flow is by observing and describing the flow behavior inside the equipment (Prescott & Barnum, 2000). Variations in flowability are described in Fig 2.4. For non-interactive powders (free flowing) a first-in first-out flow sequence is usually observed, however, for interacting granules (cohesive) a first-in last-out sequence is seen. Those setups were distinguished during the discharge of solid particles from a hopper.

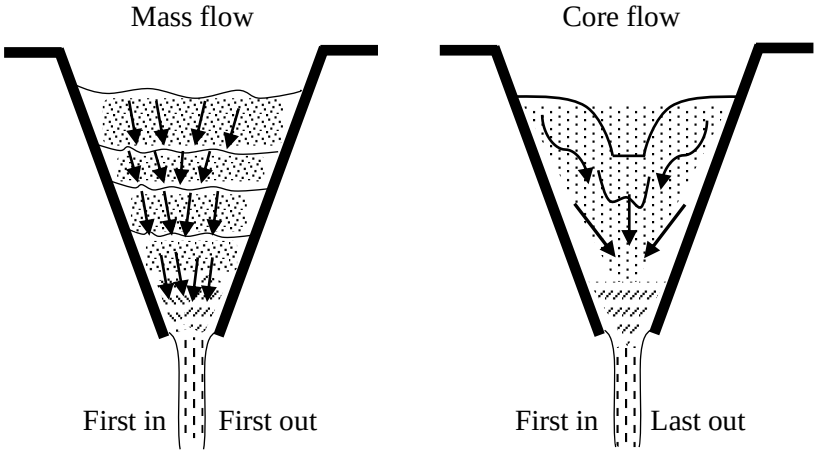

Fig.2.4. Classification of particle flow (Prescott & Barnum, 2000)

Particle mixtures can be categorized as non-interactive and interactive mixtures based on their flow pattern, but the flow properties of individual constituents cannot essentially determine the flow properties of a mixture. Conducting non-interactive mixing containing solely non-interacting particles would let particles move freely and fast because of the gravitational force which

expressed in mass flow. One drawback that may arise in this type of mixing is the so-called segregation, therefore this phenomenon should be considered during handling and storage of particles based on their density and size (Harnby, 2000). On the other hand, interactive mixtures comprise at least one cohesive ingredient, which underlies cohesive and adhesive forces, so particles are generally moving in clusters and particles stick to the equipment (core flow case) (Fan et al., 1990), thus agglomerations should be decomposed repeatedly to allow the relocation of individual particles.

2.3.1.5. Moisture content

The moisture in the environment has an impact on granules, in turn on granules mixtures which can display unstable moisture contents. The change in the moisture content may transform the surface forces where the growth of the relative humidity conditions comes across liquid bonds and dominates cohesive and adhesive forces (Duong et al., 2004). Therefore, a delay in the mixture arises due to agglomeration and adherence to the apparatus. So, it is of vital importance to keep materials under constant moisture conditions. Moisture content is a significant parameter in mixing granular materials as it could impact numerous characteristics such as size, shape, flowability, compressibility, stability, and storage properties. Controlling and optimizing moisture content is fundamental in mixing processes to guarantee product quality and consistency in different industries.

2.3.2. Mixer properties

Principally in any particle mixing process, the movement of particles followed by instability is imperative. Therefore, particle disarrangement should show the necessity of expansion in terms of capacity without any dead zones' formation inside the apparatus. In addition, particle dislocation in the mixer should be three-dimensional, fast, and random.

A universal design is not possible due to the fact of complexity of the aforementioned particle properties. Notwithstanding the above, mixers are designed based on the mixing mechanisms described in section 2.2.

Table 2.1. Advantages and disadvantages of mixers regarding their mixing mechanisms (Harnby, 2000)

Type of mixer	Advantages	Drawbacks
Diffusive mixer	- Both interactive and non-interactive mixtures can be handled.	- Segregation may occur due to differences in particle size and density. - Solely delicate agglomerations can be decomposed, however robust ones remain intact.
Convective mixer	- Can be used in a wide range of processes. - Decrease the segregation problem caused by the variance in particle size and density.	- Dead regions may be present inside the mixer.
Shear mixer	- Able to decompose all kinds of structured powders (agglomerates).	- Dead regions in the mixer can be located.

Mixer selection is quite a perplexing task whereas substantial factors namely, mixture quality, process requirement, costs, and operation mode are fundamental. Table 1 lists the advantages and disadvantages of several mixers based on their mixing mechanism (Harnby, 2000).

2.4. Operating conditions

Operating conditions of particle mixtures and equipment significantly impact the quality of the mixture. According to Fan et al., (Fan et al., 1990) several aspects affect the mixing result namely, the weight fraction of elements, the order and location of adding constituents, the pre-handling of particles like breaking down agglomerates, and discharging particles from the mixer. The volume level in the mixer is critical to allow the material to move freely around the mixer frame. The velocity of the mixer or agitator if existing should be accurately configured depending on the material mixed to remove agglomerations among particle structures. Additionally, mixing time should be optimized as over-mixing is unnecessary to reduce energy consumption, or in some cases to avoid segregation.

2.5. Choosing the right mixer

Before conducting any mixing process, many criteria should be considered for choosing the most suitable mixer. These criteria are the following (Harnby, 2000):

- The products, ingredients, and processes of the desired mixer.
- The necessary capacity for mixing.
- If any previous experience of the process is unavailable, then testing is a must.
- Safety when using the machine and products.
- The cleaning effectiveness.
- The mechanical design features (cooperation with the mixer supplier).

A variety of equipment available to conduct such a mixing process is listed in Fig. 2.5.

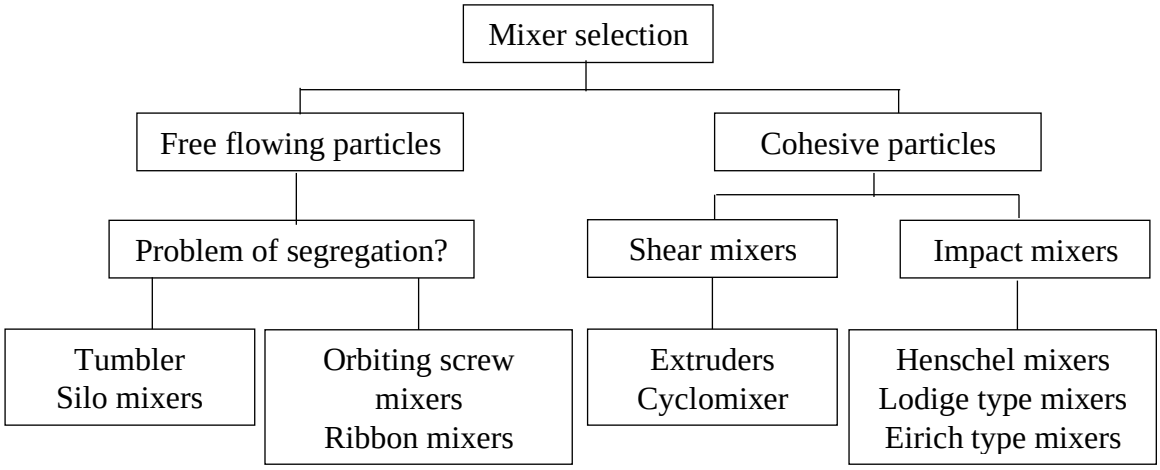

Fig.2.5. Selection of the appropriate mixer (Harnby, 2000)

There is a wide range of mixer geometries available. Mixers can be categorized into two groups. The first group is described by the rotation of the mixer itself while the material slops inside the mixer frame. The main mixing mechanisms for this type are shear and diffusion, examples are listed further below:

- *The cylindrical drum*: often, these mixers are horizontally placed in batch operation. These types are suitable for free-flowing materials; however, it is not efficient for materials that tend to agglomerate. Discharging is simplistic, but as with any mixers, internal segregation may occur at this stage. Cleaning is easy and it is very convenient for continuous operation.
- *The off-center drum*: one part of the drum mixer moves up and down while rotating with respect to the other part. This mechanism enhances the mixing in the axial direction by the slop of material backward and forward along the horizontal axis.
- *The double cone*: this mixer is an assembly of two parts. Each part is a conical section, and both are connected at the base of the cone. Shear and diffusion are the proceeding mechanisms. As the mixer rotates, a continuous rolling and interfolding of materials cause the mixing action. Agitating elements may be installed on the axis of rotation to break lumps and reduce the segregation effects.
- *The V mixer*: this batch mixer has two parts to form the V shape and has many similarities in features to the double cone. However, the material is subject to division inside the mixer sections, and interlocking ensues when the particles recombine.
- *Tote mixers*: these batch mixers have a vessel shape that is sealed, and then rotated around the mounted axis which can be horizontal or inclined at an arbitrary angle. The upper section of these mixers may be rectangular or circular. Utilizing asymmetry is the concept of breaking up flow for a better mixing result.

The second group where the shell is fixed, and the rotor/rotors is/are rotating inside of it engendering agitation. Bridgwater stated that convection is the dominant mechanism for centrifugal mixers and ribbon blenders (Bridgwater, 2012). Examples of this type are listed below:

- *The centrifugal mixer with a horizontal axis*: at low velocity, the particles are pushed circumferentially in the mixer, then displaced axially as far as the blade is removed from the material. At a high velocity, the material is centrifuged. This mixer is difficult to clean, but a broad type of materials could be processed.
- *The centrifugal mixer with a vertical axis*: at low velocities, the blades push the material around the mixer. At high velocities, a toroid of material forms next to the wall. It is effective in removing agglomerates. This mixer is relatively easy to clean.
- *Ribbon mixer*: this mixer is designed with one or two helical screws that can be used as blades. For the two-type screw, usually, one pushes in one direction close to the center and the other pushes in the opposite direction close to the wall, simultaneously. Materials are rolled, folded reversed in direction, and vertically and laterally displaced to achieve the maximum. Mixing dry powders granular materials or plowing pastes. Materials that tend to agglomerate can be mixed. Mixing in the axial direction is not as good as lateral. Segregation can occur on discharge. Easy to empty but can be difficult to clean.
- *Planetary mixer*: shear and convection are the governing mechanisms. A mixing blade rotates about an offset vertical axis to mix the bed. It is not effective to mix adhesive or very cohesive materials.
- *The draught tube and screw mixer* (Fig. 2.6(a)): the material is conveyed to the free surface by the rotation of a screw vertically in the tube/cylinder. Subsequently, the material is recycled to the base of the screw. The flow to the free surface adds diffusion.
- *Orbiting screw mixers* (Fig. 2.6(b)): this mixer has the shape of an inverted cone with a screw attached to the basis. It is limited to batch operation. The screw is rotated about its axis while processing the vertical axis of the cone at the same time. Governing mechanisms are

convection and diffusion. Segregation can be minimized by rotating the screw when discharging.

For both categories, the external shape of a mixer can be changed. Many empirical designs have been developed over the years to improve the mixing.

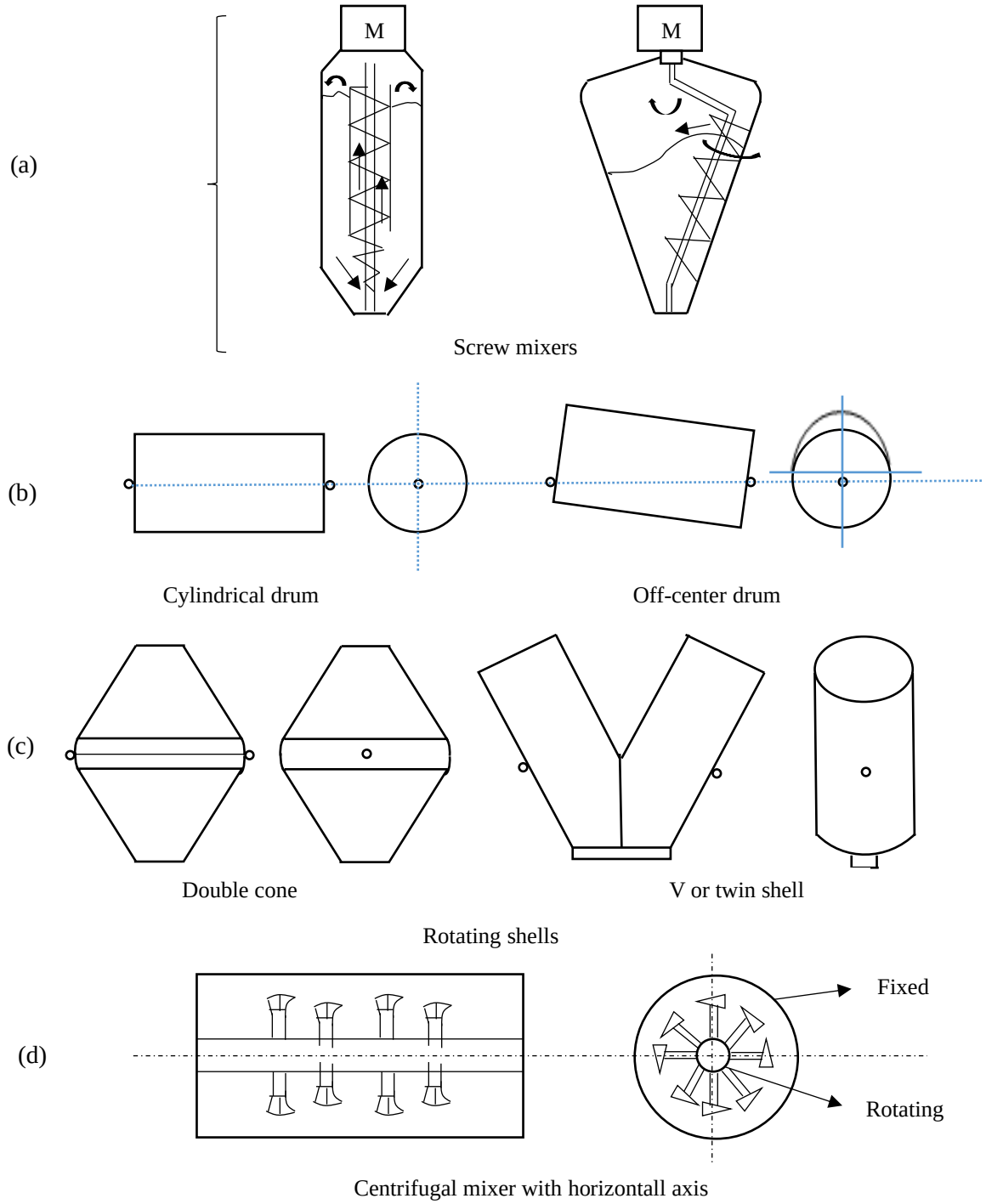

Fig. 2.6. Different types of mixers. (a) screw mixers (b) drum mixers (c) rotating shell mixers (d) centrifugal mixer (Bridgwater, 2012)

2.6. Mixing uniformity assessment

Researchers namely, Poole, Taylor, and Wall have established valuable methods to quantify the mixture of solid grains (Poole et al., 1964).

A homogeneous mixture is solely attained when the random state of mixing is achieved. To successfully reach this mixing state, some conditions should be considered: 1) enough space in the apparatus to allow the free movement of particles, 2) shear of particles by the input of lateral energy to gravity, 3) avoiding adhesion and cohesion between particles by pumping sufficient energy in the system which depends on the mixing speed and mixer type, 4) set the appropriate duration of energy (neither short nor long duration), and should not exceed the critical mass to avoid segregation phenomenon.

2.6.1. Various methods of mixing index calculation

Finding the index of mixing is very important to know to which extent the mixing is efficient. It is very challenging and time-consuming to find the mixing index experimentally. As an alternative, I can easily calculate the mixing indexes using the discrete element method. The mixer rate methods differ in terms of inputs such as number of particles, coordinates, type of particle, etc.

Based on the literature (Wen et al., 2015), the following methods are explained with detailed formulas hereinafter.

- Average height method
- Nearest neighbor method
- Neighbor distance method
- Lacey method
- Mixing entropy method
- Coordination number method
- Generalized mean mixing index

Average height method

Consider a bulk of mono-sized particles. Before mixing, the material is split into two sections, an upper section, and a lower section colored in black and white, respectively to distinguish the type of particles. At a given period of mixing, the average height of white particles is calculated by the subsequent equation (Hoomans et al., 2000):

$$Z_{white} = \frac{\frac{1}{N_{white}} \sum_{i \epsilon white} |Z_i|}{\frac{1}{N_{all}} \sum_{i \epsilon all} |Z_i|}. \quad (1)$$

Where N_{white}, N_{all} and Z_i are, the number of white particles, the total number of particles, and the height of particle i, respectively. Z_{white} equals 0.5 if the particles are completely unmixed and equals 1 if the material is perfectly mixed. Consequently, the mixing index is calculated as follows:

$$M = 2 \times (Z_{white} - 0.5). \quad (2)$$

The reference to calculate the height of each particle is the intersection or contact point between the lowest particle of type 1 and the highest particle of type 2 (in the middle). An example to better explain this method is given in Fig. 2.7.

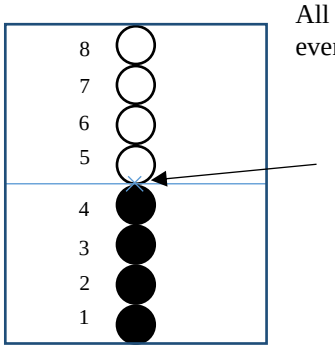

All particles have an even radius of 2mm

Reference of the system (0,0,0)

Height of particle 1 = -14mm
Height of particle 2 = -10mm
Height of particle 3 = -6mm
Height of particle 4 = -2mm
Height of particle 5 = 2mm
Height of particle 6 = 6mm
Height of particle 7 = 10mm
Height of particle 8 = 14mm

➔$\sum_{i\epsilon white}|Z_i| = 32$
➔$\sum_{i\epsilon all}|Z_i|$=64

Z_{white}

$Z_{white} = 0{,}5$ ➔ *M=0*

The mixing index is null (Total segregation)

Fig.2.7. An example to calculate the average highest index

Nearest neighbor method

This method is based on the position of particles in the 3D mixing domain. I have employed this calculation method of the mixing index in our study. It is explained in detail in the "Methods and Materials" chapter.

Neighbor distance method

This mixing index is based on the calculation of the distance between the two nearest particles. The distance between two specific particles is initially calculated, which is about one particle diameter if they are equal in size. The evolution of this inter-particle distance is not smooth because they tend to collapse and considerably change in position due to the continuous motion of the granular bed, however, the random selection of nearest particle pairs renders it smooth. This mixing index is calculated by the equation that follows (Wen et al., 2015):

$$M = \frac{\sum_{i=1}^{n}(r_{ij} - d)}{\sum_{i=1}^{n}(r_{ik} - d)}. \qquad (3)$$

Where, n is the number of closest pairs, d is the diameter which is the initial distance from center to center between two particles in contact, $r_{ij}$is the distance between i^{th} particle and its nearest particle in the vicinity and r_{ik} is the distance between i^{th} particle and a randomly selected particle. Both distances r_{ij} and r_{ik} can be calculated in all directions *x, y,* and *z*. So, the average mixing index is calculated as the mean value of the results obtained from all directions. A good feature of this method is that it is independent of the grid system.

Lacey method

This method is grid-dependent, it is calculated by the variance of particle concentration in the system (Lacey P. , 1954). I used this method to find the mixing index of particles in a screw mixer. A detailed description of this method is given in the next chapter.

Mixing entropy method

This method is based on the local entropy level in each cell of the DEM domain (Arntz, et al., 2008). The more entropy found; the better uniformity will be obtained. The local mixing entropy in a particular cell $e(k) = (k_x, k_y, k_z)$ is calculated using the Boltzmann's expression as follows:

$$e(k) = x_1(k) \ln x_1(k) + x_2(k) \ln x_2(k). \quad (4)$$

$x_1(k)$ and $x_2(k)$ are the number fraction of white particles and black particles in the cell k, respectively.

In case there are no particles or solely one type of particles is found in a cell, then the local entropy is null. Thus, the calculation of local entropies is calculated based on the number of different types of particles in a cell to provide the global entropy at a given time t. The last is calculated by:

$$E(t) = \frac{1}{N} \sum_k e(k,t) n(k,t). \quad (5)$$

$N = \sum k_n\,(k)$, is the preserved total number of particles. The perfectly segregated global entropy is zero and the perfectly mixed global entropy $E_{mix}(t)$ can be obtained. For simplicity, the global entropy can be normalized as $E_{norm}(t) = E(t)/E_{mix}(t)$, and $E_{norm}(t)$ varies from between 0 and 1, which refers to the mixing index (M).

Coordination number method

This method is calculated based on the number of contacts between particles (Carter, 1978). In the case of the distance between two particles' geometries in the mixture is less than 10 % of *d*, where *d* is the diameter of the smallest particle, then those particles are considered as in contact. The average number of particles in contact with one particle is known as the coordination number. The particles are divided by their type equally into particles of type A and particles of type B. Subsequently, the mixing index is calculated by the equation just below:

$$M = \frac{C_{AB}}{C_{AA} + C_{BB}}. \quad (6)$$

Where C_{AB}, C_{AA}, and C_{BB} are the contact number between particles different in type, contact number only between particles type A and contact number only between particles type B, correspondingly.

Generalized mean mixing index

In a 3D DEM system, the position of particles is registered by x, y, z of their centers.

$$GMMI_i = (GMMI_{xi} + GMMI_{yi} + GMMI_{zi})/3. \quad (7)$$

Where $GMMI_{xi}$, $GMMI_{yi}$ and $GMMI_{zi}$ are the Generalized Mean Mixing Indices in x, y, and z coordinates respectively.
$GMMI_{xi}$ is simply the mean of the x-coordinate of particle centers of type i divided by the mean of the x-coordinate of all particles. It is calculated as follows (Gorter et al., 2010):

$$GMMI_{xi} = \frac{\frac{\sum_{j=1}^{n}(x_j - x_{ref})}{n}}{\frac{\sum_{k=1}^{n}(x_k - x_{ref})}{N}}. \quad (8)$$

where n is the number of particles of type i, N is the total number of particles, z is the z coordinate of the position of the particle center and x_{ref} is the reference x-coordinate. Note that the x-mean is calculated relative to a reference x-coordinate such as the base of the hopper. Similarly, $GMMI_{yi}$ and $GMMI_{zi}$ are calculated.

2.7. Particle size scale-up method

Particle scale methodologies allow to replicate a bulk material response with a reduced number of particles by increasing their size. This is applicable for both cohesionless and cohesive particles.

The method of Pöschel et al., (Pöschel et al., 2001) is appropriate in a way that a physical problem is scaled down to a lab model in a try to mimic the original model. However this could still not effective if the number of particles is used in the lab model is yet abundant. An efficient solution to tackle this issue is by adjusting DEM parameters in a way that the large particles used in DEM simulation display similar results as small realistic particles in a real process after post-processing. This method is known as the coarse-graining approach.

Horváth et al, increased the diameter in the DEM model of hulled millet particles to reduce the computational capacity (Horváth et al., 2019). By sensitivity study, they revealed that increasing the size of particles by approximated spheres having diameters of 10 ± 2 mm to 18 ± 2 mm had no significant change on the model.

Compression, oedometric, and periodic triaxial tests are used for the calibration and validation of the particle scale-up method.

Compression test (Zhou et al., 2023)

A rectangular cuboid is filled with particles (Fig. 2.8), and then boundaries are applied along the *x* and *y* directions. First, a confined compression test is operated by setting periodic boundaries. The plate at the bottom is fixed, whilst the upper plate is moving along its vertical axis. Subsequently, an unconfined test is run by removing the cuboid mold. The last is conducted without any periodic boundaries until failure. For non-cohesive particles, the same experiments could be done by vibrating the system at a defined frequency and amplitude.

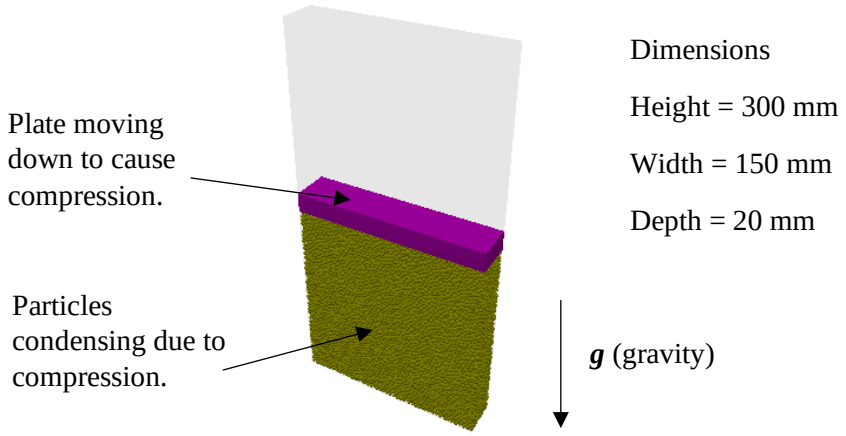

Fig. 2.8. Compression test simulation set-up (Thakur et al., 2016)

Oedometric test (Catalano et al., 2014)

This test procedure depends on the measurement of the vertical displacement of a granular material sample subject to a vertical load. An example of this procedure is a granular material sample having voids to allow water saturation, in turn, the water would slow down the strain of the sample. The rapid changes arise directly after the load application and then slow down continuously. The load is increased after descending and contrary during unloading. For every rise in the vertical loading, a curve of the variation in the height of the sample over time in a semi-logarithmic scale is plotted. The goal is to have insight into the variation in sample volume with a change in vertical load with the help of measured vertical displacements. The boundary conditions of the oedometer test are shown in Fig. 2.9.

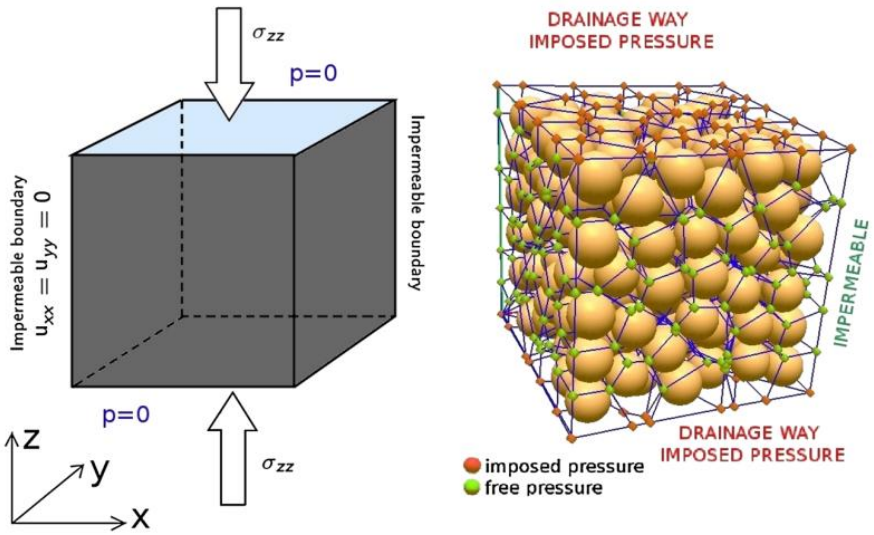

Fig. 2.9. DEM model of an oedometer test with boundary conditions (Catalano et al., 2014)

Periodic triaxial test

The periodic triaxial test consists of two stages: isotropic compaction and constant strain along the z-axis while maintaining constant stress laterally. Identical pressures are applied on all the walls towards the middle of the system in the isotropic compaction stage. Once the pressures reach the

magnitude of the projected pressure then they will be maintained constant, and the vertical compression will set at a constant strain rate until a prescribed axial test is attained.

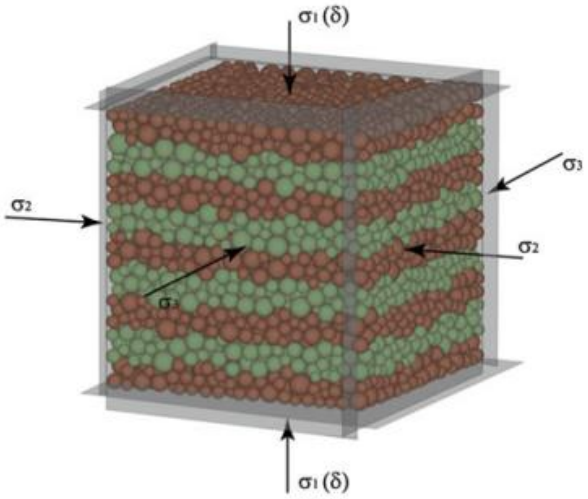

Fig. 2.10. Compression test simulation set-up. The main stress $\sigma_1(\delta)$ is acting parallel to the *z*-axis; σ_2 and σ_3 are equal in the case of homogeneous material and act parallel to axes *x* and *y*, respectively (Pawar et al., 2023)

All the three methods described above involve three steps; first run one of the above-described tests with a reference (original) particle size, second, increase the size of particles by scaling down the stiffness, then re-run the same experiment, and finally check to what extent the computationally reduced model correlates with the reference model through axial stress-strain plots. Stiffness scaling with particle radius is described analytically in the literature (Thakur et al., 2016).

To keep the mechanical and dynamic similarity, the contact model should be scaling invariant. The force-displacement connection in the linear spring contact model in a 3D model lies on the particle size and it is not scaling invariant. On the other hand, the stiffness in the Hertz-Mindlin contact model is scale-invariant for a 3D model. Therefore, the stiffness scale does not apply to the Hertz-Mindlin contact model.

Computationally reduced simulations (case of a drum mixer)

The needed computation time for a full-scale simulation may be in the order of a couple of days or weeks using a regular workstation. Building a hybrid model involving exact mixer zones within which the DEM code is applied could be useful to decrease the long simulation time (Trabelsi, 2013), that is to say:

1) For smaller mixer dimensions and a fixed number of particles.
2) For a reduced number of particles and a fixed mixer size (that of the laboratory apparatus).

First, the size of particles is given, and then the mixer dimensions are changed based on the number of particles to simulate, thus the mixer size changes in coordination with the particles number nevertheless, the evenness of radii to apparatus lengths ratios must be considered. It was observed that at a fixed rotational speed, a larger mixer decreases the period of particles' appearance on the surface, but it is complex to rely on the combined effect of these variables because speed and dimension together impact the forces applied to particles. Therefore, by only changing the size of

the mixer via the number of particles, and without changing the rotational speed. This allowed us to simulate the mixture with a reduced number of particles, and thus with low calculation time.

2.8. Evaluation of particle mixing

This section elaborates on the different sampling systems, and the two techniques used to assess a given mixing operation: invasive and non-invasive. In addition, the criteria to accept a sampling is explained with the related theories, and finally, I listed various engineering applications.

2.8.1. Generality

At the outset, it is necessary to estimate the information of granular material while mixing. Several techniques exist for the evaluation of particle uniformity which vary in accuracy, fundamental, basis, cost, and operating conditions. In this section, evolving techniques for powder content examination are enlightened and compared to assist in the choice of suitable and appropriate equipment for such a mixing process.

To choose the appropriate technique of sampling on bulk granular material, the following factors should be considered: *i*) population and sample size *ii*) sample collection and sample size reduction method *iii*) statistical analysis ratifying the stated level of acceptance of the sampling plan must be fully addressed (Gerlach & Nocerino, 2003). Fig. 2.11 illustrates the general schema for granular material sampling in mixing operation.

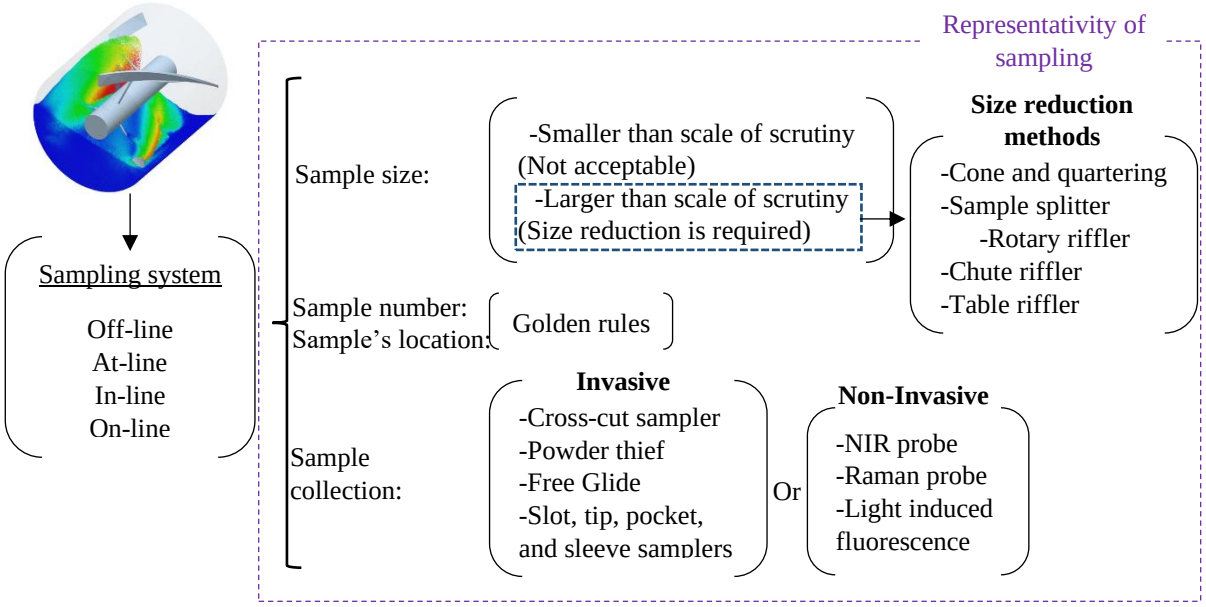

Fig.2.11. Framework for sampling powders all through mixing (Asachi et al., 2018)

The mixture homogeneity could mistakenly look unacceptable because the scale of scrutiny is minorly defined. On the other hand, if the scale of scrutiny is outsized, the uniformity of the mixture yields an overestimation (Fig. 2.12). Allen illuminated reliable sample reduction techniques whenever the scale of scrutiny is considerably less than the least sample amount that the sampler affords (Allen, 1997).

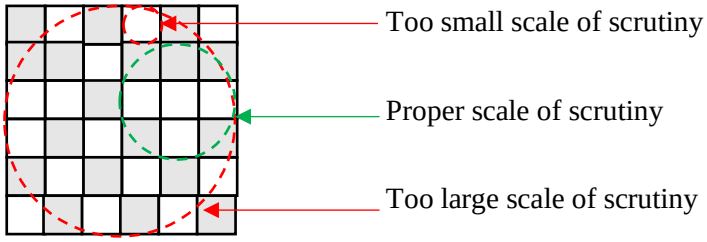

Fig.2.12. The outcome of the scale of scrutiny on mixing evaluation.

Golden rules must be entailed in granular material sampling when performing a dynamic mixing process; one, sampling must be carried out when in motion, two, instead of taking one part of the stream for the entire time, the entire stream of the mixture should be taken for various small increments.

The simple tools for granular material sampling are traditional samplers (e.g., thief and crosscut). Typically, using samplers is intrusive which would disrupt the mix, therefore distinct strategies and designs are needed to alleviate this drawback (Muzzio et al., 2003; Susana et al., 2011). However, non-invasive tools have been sophisticated without intrusion upon the mixing process. It is indispensable to monitor the concentration of the constituent inside the mixer, to govern the homogeneity of a mix and lessen its non-uniformity.

Not long ago, some non-invasive techniques were developed such as Near-Infrared spectroscopy (NIR) and Electrical Capacitance Tomography without any device intrusion in the mixture during the process (Benedetti et al., 2007). It helps to achieve the optimum mixing conditions by monitoring the concentration of particles inside the mixer. To achieve process monitoring, different analyzers are used namely: off-line, at-line, in-line, and on-line which are described in Table 2.2.

Table 2.2. Advantages and disadvantages of various analyzers (Asachi et al., 2018)

	Advantages	Drawbacks
Off-line	- Most accurate method. - Flexible in selecting the measurement method.	- Invasive and time-consuming. - Performed in a controlled location by a trained person.
At-line	- Quicker than off-line (it can be done with automatic facilities). - Robust devices used which rely on standardized procedures.	- Invasive.
In-line	- Extraction of samples is not required because sensors are placed directly into a process stream.	- Difficult to get a representative sample since the measurements could be influenced by immediate process fluctuations.
On-line	- Fully automated systems allow a large fraction of the product stream to be analyzed.	

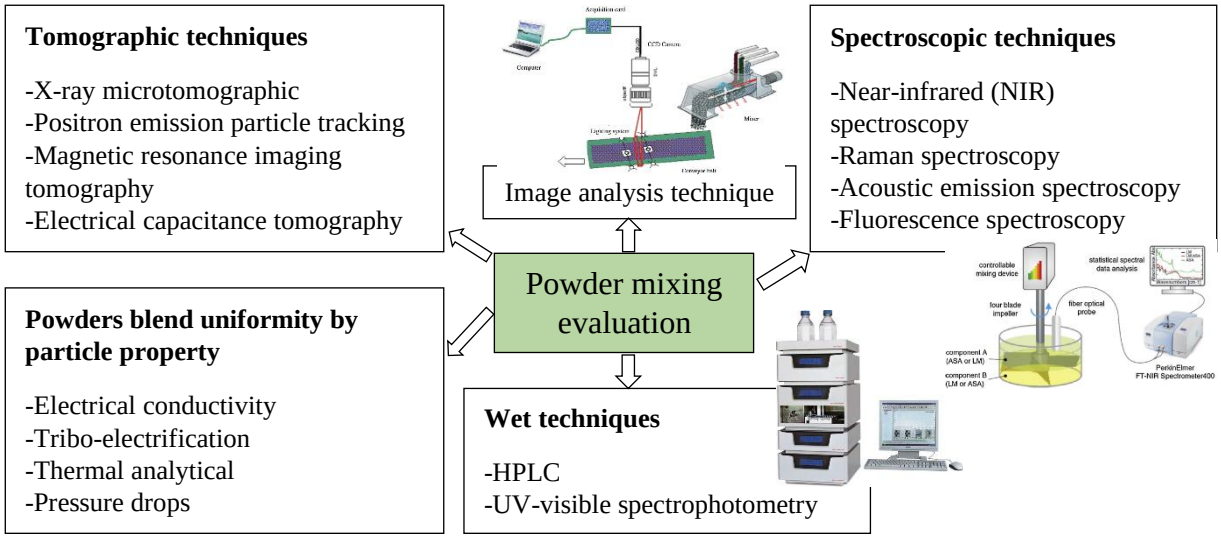

Fig. 2.13. Different evaluation techniques of powder mixing (Asachi et al., 2018)

2.8.2. Sampling

Sampling of a granular material bed is vital to analyze the mixture quality. Two major types of sampling could be distinguished: static sampling and dynamic sampling (Legoix, 2016). Static sampling could be effectuated only in a fixed granular bed and a sampling probe moves inside the material. Many types of probes are used for lateral sampling or sampling from the top. In all cases, the thrust of the probe disturbs the medium and could induce a measurement error. In contrast, dynamic sampling allows to directly collect samples directly in a flux of a flowing granular material. It could be taken at the end of the process during the emptying of the apparatus, or with the variation of particles stream throughout the process. This sampling is preferable because it induces fewer errors. The sampling collection is carried out in three steps: integration, cutting, and taking. Integration consists of choosing locations to collect samples in the form of points. Performed at random, each point of the granular bed has an equal probability of being sampled. A systematic sampling with random implantation corresponds to a first sample taken at random and the next ones will be carried out regularly. Regarding a randomly stratified integration, the mixture is defined in many equal sub-volumes, and a random sampling is performed in each of these volumes. Cutting is the realization of the shape and the volume of the sample around the points chosen previously, it determines the size of a sample and depends on the sampling tool used. Cutting generates an uncertainty I_d in function of particle number collected N_{part} (Legoix, 2016).

$$I_d = \frac{1}{\sqrt{N_{part}}}. \tag{9}$$

The taking corresponds to the isolation of these samples of the mixture of granular material. It can modify the mixture state because the granular material around the collected sample fills its place and alters the granular bed structure and the spatial disposition of components. The spatial dimension of a batch for sampling is an important parameter, dimensions may go from 0 to 3. A batch of three dimensions corresponds to a direct collection in the bed of granular material. A batch of two dimensions is possible when the mixture is spread with a uniform mixture if the spreading of the granular material has a negligible impact on the quality of the mixture. A batch of one dimension requires more manipulations and it is possible from spread mixtures with

uniform thickness and width. A batch of zero dimension can be realized on a final product already transformed, like for example tablets that form a single sample.

As soon as possible, a sampling of a granular material must be dynamic with random implantation and a simultaneous taking from all the samples where a batch of three dimensions. A full sampling of a granular material bed is ideal and can be performed mostly if the method of analysis allows us to evaluate the concentration of all samples.

For a given statistical law, with a determined sample size, the error committed on the observed variance to the true variance relates to the number of samples used. The greater the number of samples are, the less difference between variables is. In general, it is difficult to get an exhaustive number of samples that describe the whole mixture, for questions of time, money, or workforce needed to analyze all these samples. That is why by setting a reasonable margin of error, it is possible to reduce the number of samples considerably. The important thing is that this margin should be mentioned and considered upon interpretation of experiments.

2.8.3. Sampling techniques

There are various sampling techniques depending on devices and apparatuses used, some are simple, and some are complex to use. The characteristics and the mixture of a granular material permit the choice of an adequate technique for sampling (Fan et al., 1970). Most of the sampling methods are invasive through the thrust of a device into the bed of granular material after mixing. Examples of these tools are listed in Fig. 2.14.

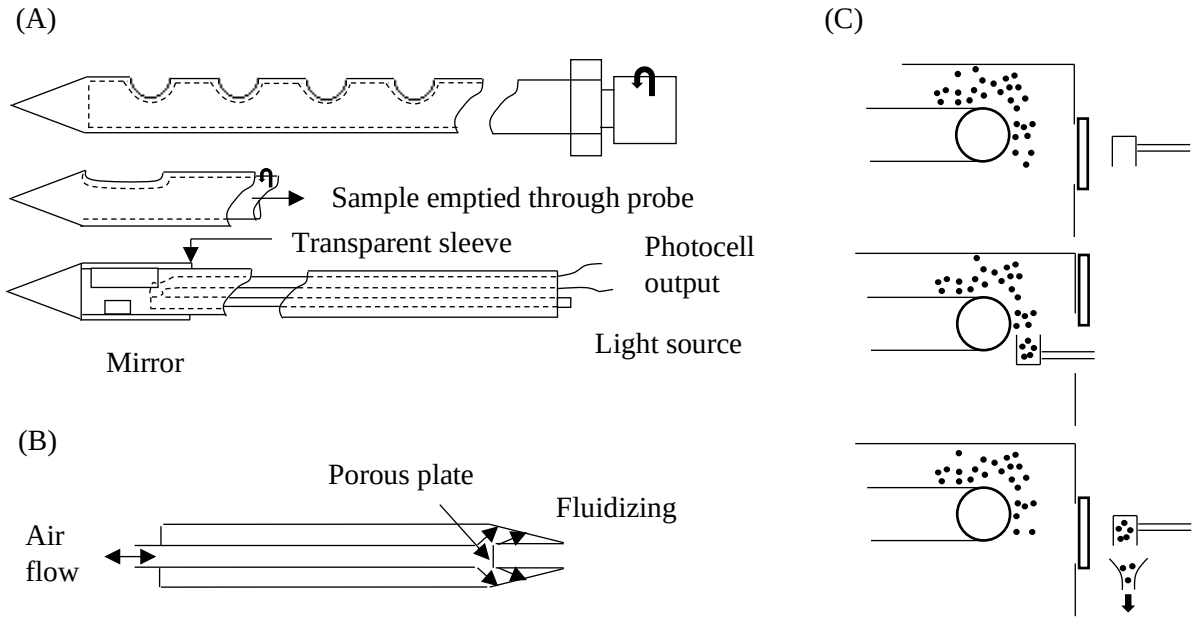

Fig. 2.14. (A) Sample thief (B) pneumatic lance (C) full-stream trough sample (Venables & Wells, 2001)

Using an invasive technique may disorder the mixture state, therefore caution is a must when using this method.

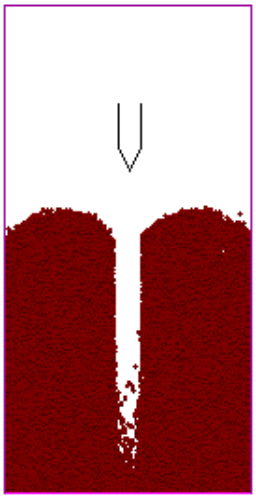

Fig. 2.15. Disordered mixture after the thrust of a thief sample

2.8.4. Criteria of sampling acceptance

Knowing the observation scale for which it is necessary to get a good mixture, a statistical method could be employed to quantitatively define the mixture quality (Schofield, 1976). It relies on the collection of a series of samples where the substance of each *i* sample must be analyzed (Fig. 2.16).

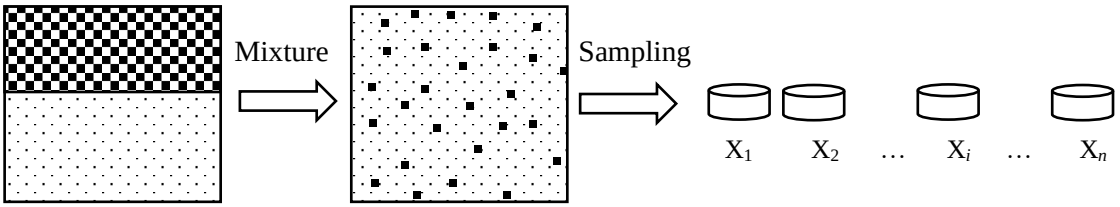

Fig. 2.16. Illustration of collection of *n* samples

Table 2.3 represents the basic mathematical expressions required for the study of a mixture quality (Poux et al., 1991).

Table 2.3. Concepts allowing to characterize a mixture

Name	Description	Expression
True average content	Key component fraction in the mixture.	μ
Content of a sample	Mass fraction by key component in sample n° *i*.	x_i
Sampled average content	Estimation of the composition with the *n* samples.	$x_m = \sum_{i=1}^{n} \frac{x_i}{n}$
True variance	The variance of the sample contents with a full mixture sampling of *z* samples.	$\sigma^2 = \frac{\sum_1^z (x_i - x_m)^2}{z}$
Observed variance	Estimated variance with a partial sampling of *n* samples.	$s^2 = \frac{\sum_1^n (x_i - x_m)^2}{n-1}$
Coefficient of variance	Variance relative to the average	$CV = \frac{S}{x_m}$

The variance for a completely segregated mixture σ_0^2 and the variance for a perfectly random mixture σ_R^2 could be calculated through the key component concentration in the granular material bed μ and the number of particles n_p in the mixture, according to equations 15 and 16 (Poux et al., 1991).

$$\sigma_0^2 = \mu(1-\mu). \tag{10}$$

$$\sigma_R^2 = \frac{\mu(1-\mu)}{n_p}. \tag{11}$$

From the measured variance in a mixture s^2 and these extreme theoretical variances σ_0^2 and σ_R^2, it is possible to define more descriptive mixture indices than a solely measured variance. These indices are numerous in literature and care must be taken before comparing different mixing experiments between them.

Engineering applications

In recent years, computing speed and power as well as programming have smoothed the path to create complex granular flow models using the Discrete Element Method (DEM), originally given in (Cundall & Strack, 1979). Several singular and interacting assembled discrete particles are used to model a particulate system. It has been used to investigate a variety of complex particulate systems, due to research advances, and the modeling of more complex models to capture the interactions at the particle level.

The DEM technique provides a profound study regarding the mechanisms governing particle flow. Moreover, numerical simulations post-processing can enhance fundamental understanding of the granular motion, thus helping the design and operation of systems involving particulate material (Cleary, 2000). DEM is capable of modeling complex geometry and their related kinematics. The developers of some commercial DEM packages such as DEM modeling software such as EDEM and LIGGGHTS emphasized the integration of DEM with CAD packages.

Until now, DEM is a valuable tool applicable in a wide range of industries such as chemicals, pharmaceuticals, ceramics, metal, food, and agriculture. Many DEM simulations have been conducted in the literature modeling a variety of granular processes as listed below:

- Comminution (Kruszelnicka et al., 2022).
- Granulation (Gantt & Gatzke, 2005).
- Flow in a hopper (Ketterhagen et al., 2009).
- Die filling for tableting (Wu, 2008).
- Fracture of agglomerates (Foldager et al., 2022).
- Packing of particles (Mathias et al., 2022).
- Bulk compression of particles (Jonsson et al., 2019).
- Flow in screw extrudes and conveyers (Wang et al., 2019).
- Vibratory screening, filling of dragline bucket, conveyor belt design, earth-mover bulldozer plate design.

2.9. Benchmark problems for mixing of solid particles

Mixing of particles in a horizontal drum mixer

A rotating drum mixer made of plexiglass (having Transparent walls) filled with spherical glass beads (Fig. 17) was used to study the uniformity of the two mixed particle types. As the velocity of the drum mixer increases, the dynamic angle of repose increases, and then the active profile of the granular motion becomes centrifuging rather than slipping (Mellmann, 2001). The dynamic AoR is the angle between the top surface of a rolling granular bed and the horizontal plane. Researchers revealed that the dynamic AoR increases with an increase in the drum mixer speed and decreases with an increase in particle dimensions (Yang et al., 2003). The mixing rate differs from radial to axial directions, the governing mechanisms are convective and diffusive, respectively. As a result, statistical assessment for sampling is challenging. A variety of experimental and numerical methods has been conducted to find the mixing state in different locations of the mixture, however the simple thief probe method has a drawback that generates disturbance in the surroundings of the insertion region.

Researchers developed a novel method to quantify the mixing rate that can predict the dead zone formation in a mixture.

Experimental set-up

Soni et al., (Soni et al., 2016) built a drum mixer made of plexiglass and has dimensions of 140 mm length and 280 mm diameter. Particles are glass beads of different sizes packed using dissimilar arrangements. The filling level is up to 75 %, and the velocity of the mixer varies between 2 rpm and 8 rpm.

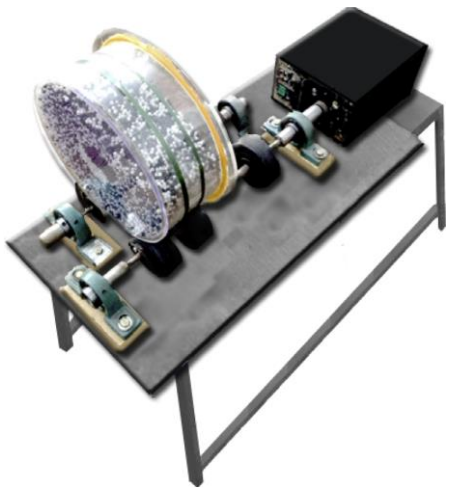

Fig.2.17. Apparatus design for real experiments (Soni et al., 2016)

Numerical simulations were carried out using LIGGGHTS DEM-based software. The list of simulations carried out is listed in Table 2.4, and the material properties are described in Table 2.5.

Table 2.4. List of simulations carried out by Soni et al., (Soni et al., 2016)

Case no.	Shape of mixer	Particle diameter (mm)	Packing arrangement	Mixer speed (rpm)	Filling level (%)
1	Cylindrical	5	Random	2	75
2	Cylindrical	5	Random	4	75
3	Cylindrical	5	Random	8	75
4	Cylindrical	5	BCC	4	75
5	Cylindrical	5	HCP	4	75
6	Cylindrical	7.5	Random	4	75
7	Cylindrical	7.5	Random	4	75
8	Cylindrical	10	Random	4	75
9	Hexagonal	5	HCP	4	75
10	Cylindrical mixer with baffles	5	Random	4	75

Table 2.5. Micro-mechanical properties used by Soni et al., in the mixing of glass beads in the rotational cylindrical mixer (Soni et al., 2016)

Properties	Particle (glass beads)	Wall (acrylic sheet)	Particle-wall
Density ρ (kg/m^3)	2700	1800	-
Young's modulus, E (GPa)	70	3	-
Coefficient of restitution, e	0.67	-	0.67
Poisson's ratio, υ	0.22	0.35	0.8
Coefficient of friction, μ	0.95	-	-

Important findings

When the filling level is low, a better mixture state is obtained. For filling levels greater than 50 %, dead zones have been detected. The dead zones are larger when mixing small particles due to low energy generation in the central region. In addition, for HCP and BCC and packing arrangements, the dead zone diameter is found to be larger.
The authors revealed that after 7 revolutions of the mixer, dead zones decreased from 22 % using 4 rpm to 17 % using 8 rpm mixer speed.

A simple design of a hexagonal mixer shape led to smaller dead zones formation; it improved the mixing state as well because the walls acted as lifters. However, the shape of the mixer did not change the shape of dead zones.

Mixing of particles in a cylindrical mixer by impeller

The impact of the impeller configuration described in Fig. 2.18 (blade diameter, blade number, and tilt angle) on the mixing of particles has been examined by Bao et al., (Bao et al., 2020), while maintaining a constant rotational speed and fill level of particles in the cylinder.

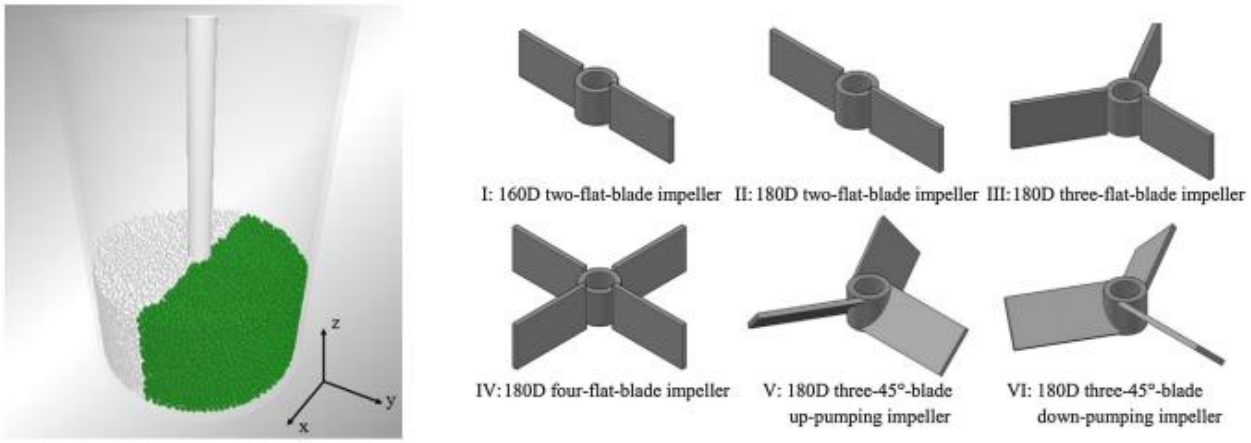

Fig. 2.18. Particles initial configuration and blade configurations (Bao et al., 2020)

Results shown in Fig. 2.19 reveal that the mixing efficiency improves by increasing the blade diameter; also, the mixing performance of the 3-flat-blade impeller is better than those of two and four blades, whilst tilting the blade angles either downwards or upwards had no significant effect on the mixing performance.

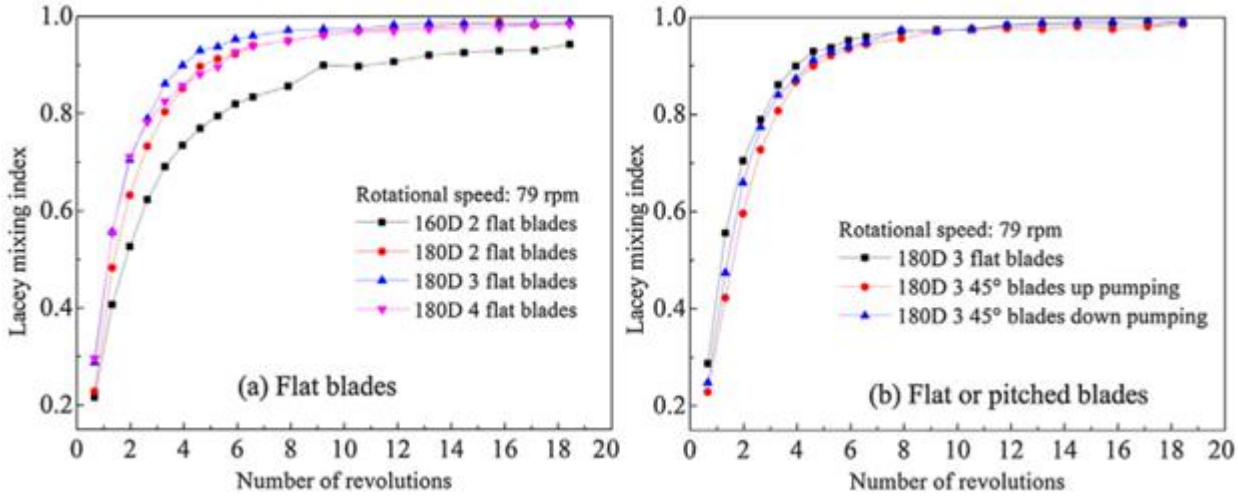

Fig.2.19. Evolution of the Lacey mixing rate using different blade configurations during the mixing operation (Bao et al., 2020)

Mixing of particles in a screw mixer

In some cases, only screw mixers are used like in silo dryers. It is very important to know the optimal time of mixing because over-mixing may deteriorate the quality of the mixture. So, this is a challenging task for engineers to find the optimal mixing intensity.

The old trial and error method is a costly experimental technique. In this section numerical simulations based on the DEM were conducted to imitate the real process and it showed good reasonable results that can be considered in a real process (Keppler et al., 2016).

Experiments

The screw mixer apparatus used is presented in Fig. 2.20. Its diameter is 450 mm, the wall has a thickness of 3 mm, and it is transparent. In the middle of the mixer' cylinder, there is a screw associated with an electric motor to control its velocity. The mixer is filled with wheat grains.

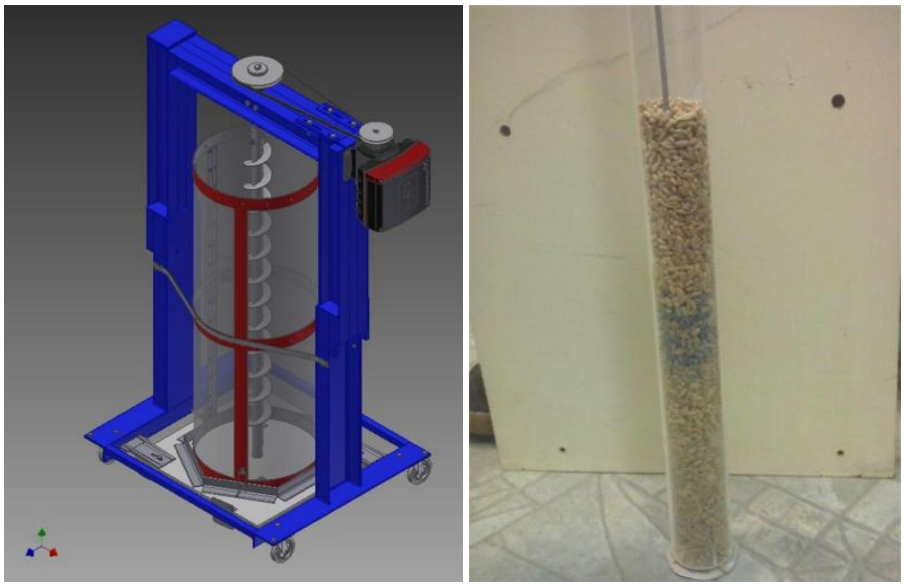

(a) (b)

Fig.2.20. (a) screw mixer apparatus (b) sampler used (Keppler et al., 2016)

Even though the mixer wall is transparent, it is still not possible to know the mixture homogeneity. Therefore, cylindrical tubes are thrust in different locations after stopping mixing to collect samples, consequently, assessing the homogeneity.

Important results

Simulations were able to detect the mixed and unmixed zones. In addition, the velocity of particles around the cavity could be determined as seen in Fig. 2.21. The velocity of particles nearby the screw is much higher than particles near the wall.

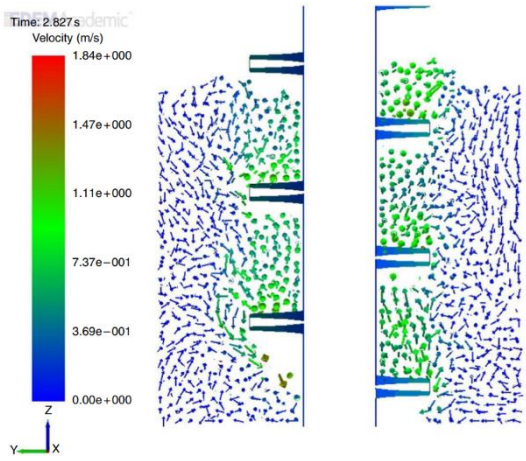

Fig. 2.21. Particle velocity distribution around an open mixing screw (Keppler et al., 2016)

The results of the simulations are illustrated in Fig. 2.22 and Fig. 2.23. The mixing efficiency improves with the increase of the rotational angular speed of the screw until 25 Rad/s after which the mixing efficiency drops. So, for practicing engineers there is an optimal rotation angular speed of the screw above which the mixing efficiency decreases significantly, where $e = r_e/r_m$ is the mixing efficiency. The mixing efficiency is calculated from the effective mixture radius and the radius of the mixer apparatus.

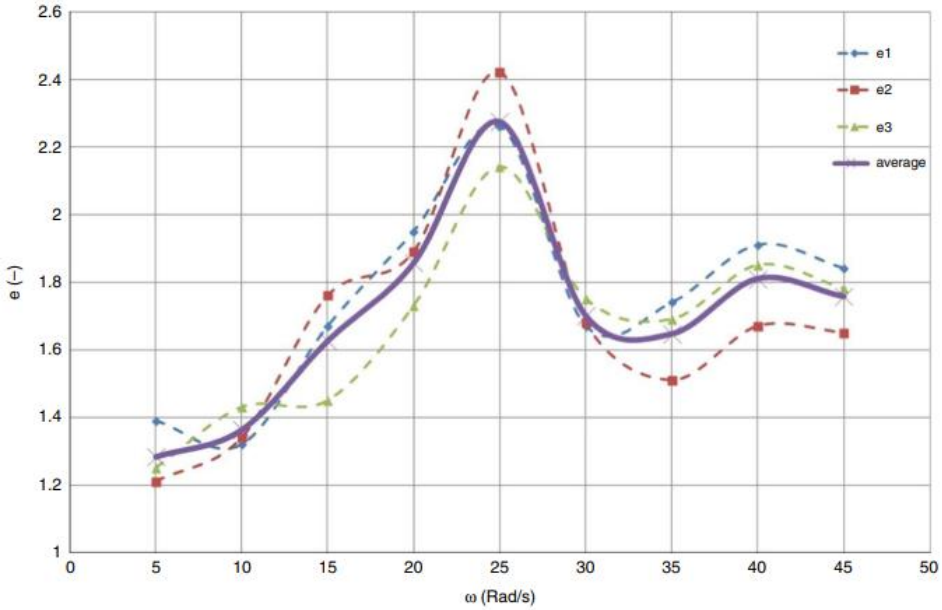

Fig.2.22. Mixing efficiency as the function of the screw rotation angular velocity (*e*: effective mixture radius, *ω*: screw angular velocity) (Keppler et al., 2016)

Fig. 2.23 shows, that the increase of the screw angular velocity causes the increase of the compressing forces acting on the individual particles. Although the value of the compressive forces is not larger than the breaking force magnitude related to an individual wheat particle. However, the increase of the screw angular velocity, contact forces, and number of collisions have a cumulative damaging effect, thus a negative impact on the quality of the mixed product.

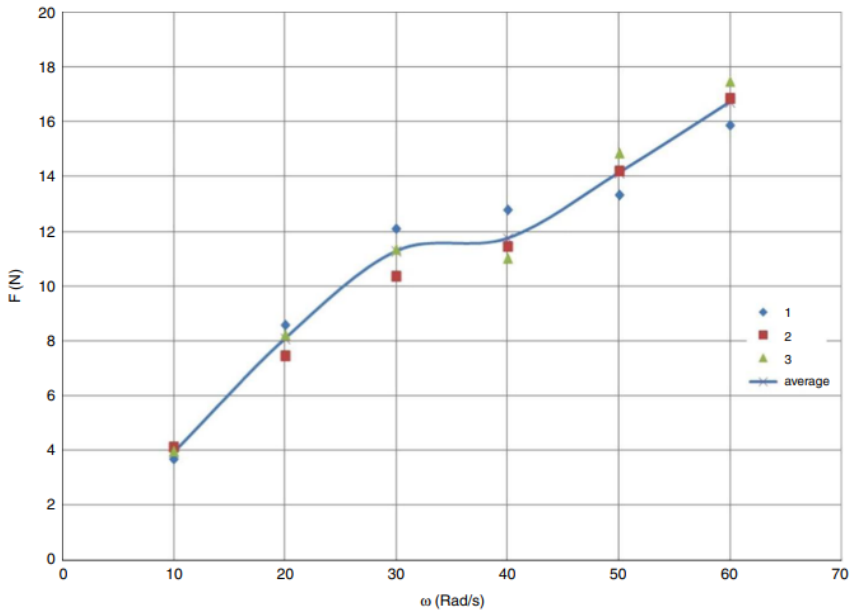

Fig.2.23. Evolution of the contact forces magnitude in function of the screw angular velocity (*F*: contact force, *ω*: screw angular velocity) (Keppler et al., 2016)

2.10. Conclusion

Many industries are using granular materials to produce their products, however, improving the quality of the end-products is challenging. In mixing particles, the trial-and-error experiments cost much time and money to achieve the desired mixture. The discrete element method is a numerical tool developed and improved by researchers until its accuracy and efficiency in modeling granular materials has been evidenced and has made it a robust tool that is used nowadays in laboratories and industries to simulate the behavior of particles.

Various studies about the mixing of particles using numerical simulations based on the discrete element method were conducted, however, this process is still not fully solved because the behavior of particles in the mixer is complicated and depends on numerous parameters, for example, the type of particles, shape of particles, mixer parameters (mixer type, rotational speed of a mixing rotor or mixer frame, etc.), and these parameters impact the micro-mechanical parameters (Young's modulus, friction coefficient, rolling friction coefficient, and coefficient of restitution), that identifies the accuracy of the DEM simulation. It could be computationally intensive to run a DEM simulation when dealing with a large number of particles, however advances in hardware resources have made it feasible, furthermore techniques to reduce the computational time of a DEM simulation could also be applied, for example by artificially increasing the particle size, the simulation time could be reduced, but the increase in size must be verified, or by using a lower magnitude of the Young's modulus.

In our study, I sought to improve the mixing effectiveness in terms of homogeneity. To quantify a mixture's homogeneity, a mixing index is used. There are many mixing indices in the literature, each method differs from the other. Some are grid-dependent means that the system must be divided into cells, and because of this, the mixing rate might alter based on the number of cells used, thus without choosing the appropriate cell number, the result will be inaccurate. Other indices are independent of the number of cells.

Ultimately, the numerical tools based on the discrete element method are powerful enough to build an accurate mixing model with an acceptable level of reliability that could be used by engineers in practice to solve a given mixing problem or improve a given mixing process. Visualizing results gives many important information that cannot be obtained experimentally, for example, the number of contacts between particles, torques and forces magnitudes, particle velocities, etc.

2.11. Study objectives

The majority of studies have analyzed the mixing of spherical artificial particles, but little work has been conducted to check the impact of mixer parameters on the mixture uniformity when mixing particles that are complex in shape. The practicing engineers don't have enough information regarding the mixing of solid particles in different types of mixers, precisely in screw mixers, paddle mixers, and drum mixers. For these reasons, the objectives of our work are the following:

- Build a lab-scale single-shaft paddle mixer to examine the mixing of corn particles.
- Create a DEM-based model that is capable of accurately mimicking the real experiments conducted to mix corn particles in a single-shaft paddle mixer and approximate its results by numerical simulation.

- Employ particle concentration variance to verify the accuracy of the single shaft paddled DEM model based on snaps that will be captured from the top of the mixer to display the distribution of particles and a grid will be assigned to each snap to get several cells to quantify the distribution of the particles which will be compared to the real experiments for the model validation. For quantification, the particle concentration variance method will be used which is the ratio of the number of one type of particle to the total number of particles and the average will be the sum of the particle concentration variances found in each cell divided by all the number of cells.
- Employ mixing indexes to quantify the mixture homogeneity during the mixing process.
- Improve the mixture of particles in a rotational drum mixer in terms of homogeneity by using paddles installed in the middle of the drum mixer frame and avoid segregation of particles by choosing an optimal rotational speed of the drum.
- Find the optimal screw pitch length to get the highest homogeneity level when mixing wheat particles in an open auger screw mixer.

3. MATERIALS AND METHODS

3.1. Introduction

Achieving the desired state of particle homogeneity in some mixing operations is still not fully solved based on the literature review. This study aims at optimizing the mixing quality in terms of homogeneity of different types of granular materials by numerical modeling using the discrete element method. I sight to predict average homogeneity when mixing solid granules using different mixing mechanisms. Using EDEM® and the open-source discrete element software LIGGGHTS-PUBLIC®, mixer apparatuses namely: drum mixer, single shaft paddle mixer, and screw mixer as well as granular material are described by the micro-mechanical properties after measurements and calibration, as it will be explained further in this chapter. The mixing quality is evaluated visually by looking at the structure of particles around and in the middle of the mixer. Also, the quantitative measurement is conducted which is rather significant since important phenomena could be detected throughout the mixing process such as segregation and over-mixing. The Lacey index based on the number of different elements and the nearest neighbor index which is a grid-independent index explained hereinafter were employed in our study.

3.2. The discrete element method

The behavior of a bulk granular material can be traced using the discrete element method. The interaction between granules is defined by a constitutive contact model. Motions of discrete elements are caused by external forces.

In a discrete element simulation, the flow of a granular material is solved iteratively by the law of motion and the force-displacement law for each element and contact, respectively. The equations are solved through an integration scheme where an adequate time step should be pre-defined to constantly update the velocities and accelerations through iterations.

Fig. 3.1 illustrates the calculation loop in every timestep. Initially, the boundary conditions are defined to know the positions of all elements, then the contacts and possible overlaps between elements are detected by the mean of a constitutive model, and the algorithm calculates the exerted forces by the force-displacement law. Finally, the calculated forces are introduced in the law of motion to calculate the velocity and acceleration of every element. This calculation loop is calculated at every timestep, and the obtained values are then updated to simulate a flow of granular material.

By importing the geometrical features and setting the boundary conditions, all elements and wall positions are known in the DEM model, and when launching the computation, the contact between elements is detected and the contact forces are determined promptly through the force-displacement law. In the following step, Newton’s second law of motion is applied to determine the element's velocities and accelerations to update the new position of each element in the discrete element domain. At each timestep, this cycle is repeated till the end of the set simulation time to obtain a granular material flow process.

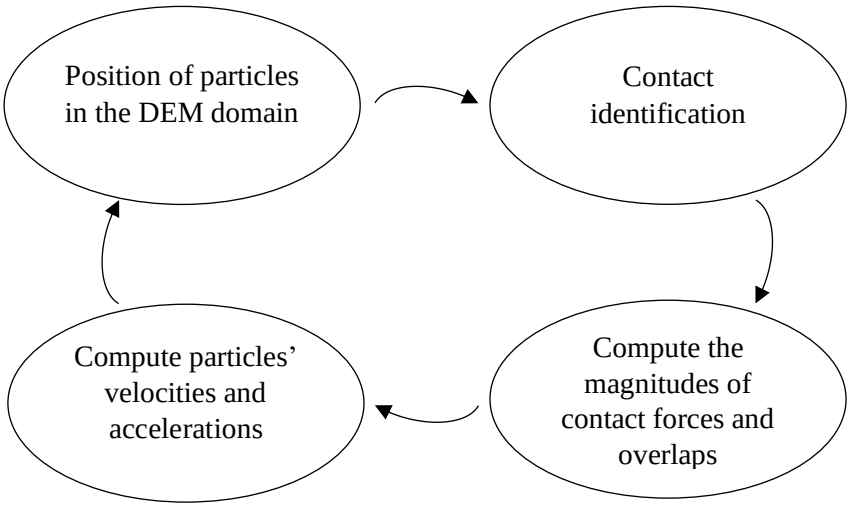

Fig. 3.1. Calculation loop in DEM

Particle shapes are defined as rigid bodies in DEM and overlapping may occur upon contact and its depth is related to the magnitude of the applied contact forces calculated via the contact model used in the discrete element model.

3.3. Set-up of the discrete element model

The translational and rotational motion of every element in a DEM domain is described by Newton's second law of motion. Those motions are calculated from the first time interval and updated in sequence at the following time intervals, and then full dynamics of granular material can be visualized. The equations are presented just below.

$$m_i \frac{d^2 r_i}{dt^2} = \sum_c F_{c,i} + m_i g. \tag{12}$$

$$I_i \frac{d\omega_i}{dt} = \sum M_i. \tag{13}$$

m_i, r_i, $F_{c,i}$, g, I_i, ω_i, M_i are the mass of particle i, the position of particle i, the contact force acting on it, gravity, the moment of inertia, the angular velocity, and the total torque, respectively.

3.3.1. Contact between particle-particle and particle-wall

The contact between every pair of particles and between every particle and wall is essential information in any discrete element model. Torques and forces are calculated at every contact point, hence the final state of particles is determined.

Finding the contact between all the particles costs time. The contact between a pair of particles is recognized if the shortest distance between two particles is either null or negative (particles overlapped). The number of necessary calculations is proportional to the square of the number of elements.

In the case of complex-shaped elements, then the shortest distance between two elements is determined by defining a bounding domain using a regular shape like a sphere to the complex shape in a way that it contains all the points of the complex shape, and similarly to the other

considered element. If the bonding domains do not touch or intersect, then the two elements are not in contact, and no further calculation is required.

3.3.2. Hertz-Mindlin contact model

This Hertz-Mindlin contact model (DCS, 2016) was used to describe both particle-particle and particle-wall interactions. The calculation force is the sum of the normal force and the tangential force. This is also called a soft-sphere method because it allows particles to overlap after a contact, therefore the frictional, elastic, and plastic components resulting from this overlap are calculated. The normal force is composed of a spring force and a damping force, and the tangential force is composed of a shear force and a damping force. The force equation and all the relative terms are calculated by the following expressions:

$$F = \left(k_n \delta_{nij} - \gamma_n v_{nij}\right) + \left(k_t \delta_{tij} - \gamma_t v_{tij}\right). \tag{14}$$

k_n and k_t are the stiffness constants, γ_n and γ_t are viscoelastic damping constants, vn_{ij} and vt_{ij} are the normal and tangential component of relative velocity, δ_{nij} is the normal displacement and δ_{tij} is the tangential displacement vector between the two particles i and j.

$$k_n = \frac{4}{3} E^* \sqrt{R^* \delta_{ij,n}}. \tag{15}$$

$$k_t = 8 G^* \sqrt{R^* \delta_{ij,t}}. \tag{16}$$

The equivalent Young's modulus E^*, the equivalent shear modulus G^*, and the equivalent radius R^* of the two contacting bodies are defined by:

$$\frac{1}{E^*} = \frac{1 - \vartheta_1^2}{E_1} + \frac{1 - \vartheta_2^2}{E_2}. \tag{17}$$

$$\frac{1}{R^*} = \frac{1}{R_1} + \frac{1}{R_2}. \tag{18}$$

Where E_1, ϑ_1, R_1 are respectively Young's modulus, Poisson's ratio, and radius of particle 1, and E_2, ϑ_2, R_2 are respectively Young's modulus, Poisson's ratio, and radius of particle 2.

$$\gamma_n = -2\sqrt{\frac{5}{6}} \beta \sqrt{k_n m^*} \geq 0. \tag{19}$$

$$\gamma_t = -2\sqrt{\frac{5}{6}} \beta \sqrt{k_t m^*} \geq 0. \tag{20}$$

Where $m^* = (\frac{1}{m_1} + \frac{1}{m_2})^{-1}$ is the equivalent mass of the two bodies in contact. β, normal stiffness k_n and tangential stiffness k_t are defined by:

$$S_n = 2E^* \sqrt{R^* \delta_{ij,n}}\,. \tag{21}$$

$$S_t = 8G^* \sqrt{R^* \delta_{ij,t}}\,. \tag{22}$$

$$\beta = \frac{\ln(e_r)}{\sqrt{\ln 2(e_r) + \pi^2}}. \tag{23}$$

Where, $G^*$is the equivalent shear modulus and e_r is the equivalent coefficient of restitution. G^* is calculated from the following expression.

$$\frac{1}{G^*} = \frac{2(2-\vartheta_1)(1+\vartheta_1)}{Y_1} + \frac{2(2-\vartheta_2)(1+\vartheta_2)}{Y_2}. \tag{24}$$

Forces and overlap between two particles upon collision are illustrated in Fig. 3.2.

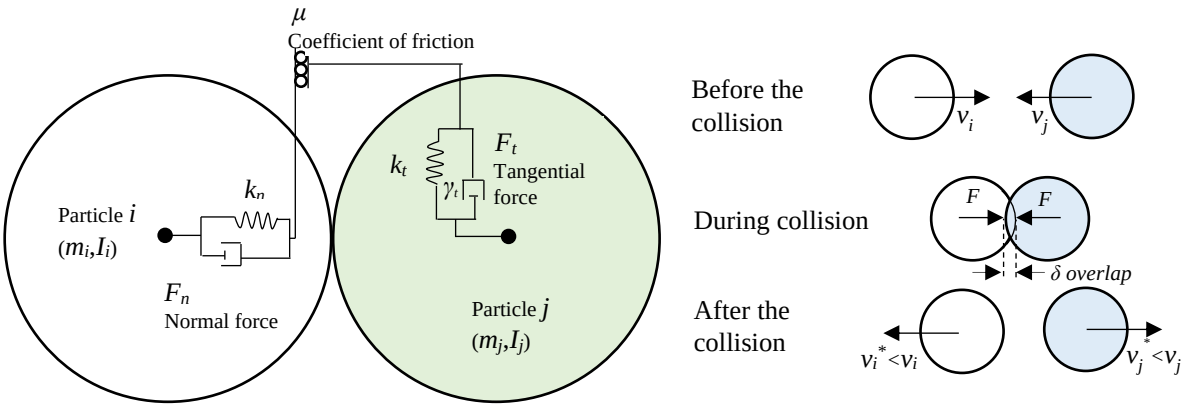

Fig.3.2. Illustration of the Hertz-Mindlin contact model between two particles (Capozzi et al., 2019)

The contact between particle and wall is calculated in the same method as the contact between two particles as described above in the condition that one of the two particles going to infinite radius and mass (flat wall), and the overlap between particle and wall is calculated via the shortest distance between the center of particle and the wall by the following expression:

$$\delta_{ij,n} = r_i - d_{iw}\,. \tag{25}$$

Where $\delta_{ij,n}$ is the overlap between particle i and the wall, r_i is particle radius, and d_{iw} is the shortest distance between the center of the sphere and wall.

The tangential overlap is calculated by the formula:

$$\delta_{ij,t} = d_{ab} + \theta \times r_i\,. \tag{26}$$

$\delta_{ij,t}$ is the tangential overlap, θ is the rotation and d_{ab} is the translation (Fig. 3.3).

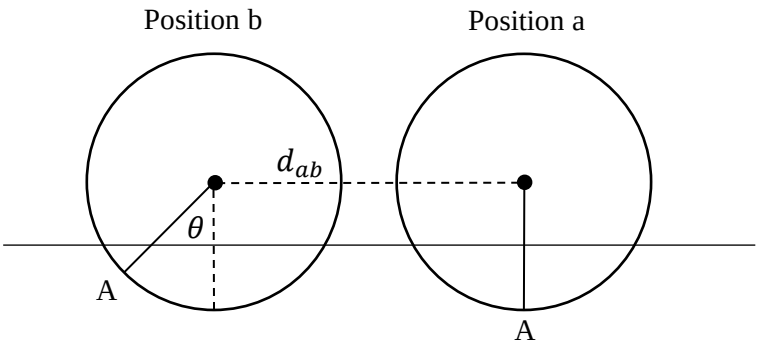

Fig.3.3. Definition of sphere displacement in the tangential direction

3.3.4. Timestep in DEM

The DEM typically uses an explicit numerical integration scheme to solve the equations of motion, however, errors could arise because an unsuitable timestep is used. The magnitude of the timestep should not exceed the magnitude of the Rayleigh critical time to stably run a simulation, otherwise, errors will show up causing the cease of a simulation (Jing & Stephansson, 2007). The principle of this methodology is that the energy cannot propagate from a particle past its adjacent particles in the vicinity in one-time step. The assumption is that all the energy transmitted by the system originates from these waves, which are Rayleigh waves, shear waves, and longitudinal waves. Shear waves and longitudinal waves together constitute about one-third of the radiated energy in the system (Johnson, 1985), which can then be neglected, and in the simulation, it is assumed that all energy is transferred by Rayleigh waves. Only contacts detected at the beginning of the time interval are considered and contacts detected afterward throughout the step are neglected, nevertheless, the torques are calculated to find the new contact for the next time interval.

The interaction between two spheres having radii R_1 and R_2, including the contact area and forces are shown in Fig. 3.4.

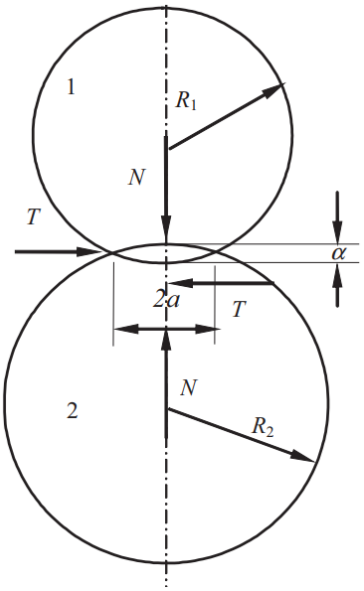

Fig.3.4. Illustration of the contact forces without adhesion between two particles in contact (Li et al., 2005)

Δt is the time-step in an incremental time scheme, while an incremental relative approach of the two spheres in contact is $\Delta\alpha$, then the incremental normal contact force is calculated by the following formula:

$$\Delta N = 2Y^* a \Delta\alpha. \tag{27}$$

Where $a = \sqrt{\alpha R^*}$ is the radius of the contact region.

When two surfaces in contact are subjected to an increasing tangential movement, δ, then relative slip is started at the boundary and progresses inward over an annular region of the contact surface. Because of the incremental tangential displacement $\Delta\delta$, the incremental tangential force ΔT depends on the loading history and the change of the normal force. Thus ΔT is obtained by the following formula (Thornton & Randall, 1988):

$$\Delta t = 8G^* a\theta_k \Delta\delta + (-1)^k \mu \Delta N(1-\theta_k). \tag{28}$$

Where θ_k depends on the loading status. If $|\Delta T| < \mu\Delta N$, then there is no slip and $\theta_k = 1$, if not the slip effect should be considered as following:

$$\theta_k = \begin{cases} \sqrt[3]{1 - \dfrac{T + \mu\Delta N}{\mu N}} & k = 0\ (loading) \\ 1 - \dfrac{(-1)^k (T - T_k) + 2\mu\Delta N}{2\mu} & k = 1,2\ (unloading\ and\ reloading) \end{cases}. \tag{29}$$

T_k is the historical tangential force from which loading or reloading started, and it needs to be updated as $T_k = T_k - (-1)^k \mu\Delta N$ to allow for the effect of change of the normal force.

For simplicity reasons the Rayleigh critical time is calculated based on the average particle size, or based on the smallest radius when using a clump of spheres, therefore the Rayleigh time-step is given by the following formula:

$$T_{Raileigh} = \frac{\pi R}{\beta}\sqrt{\frac{\rho}{G}}. \tag{30}$$

β can be obtained from

$$(2-\beta^2)^4 = 16(1-\beta^2)\left[1 - \beta^2 \binom{1-2\vartheta}{2(1-\vartheta)}\right]. \tag{31}$$

Witch can be approximated by (Thornton & Randall, 1988):

$$\beta = 0.8766 + 0.16316\vartheta. \tag{32}$$

Finally, the Rayleigh timestep is calculated as:

$$T_{Raileigh} = \frac{\pi R}{0.8766 + 0.16316\vartheta}\sqrt{\frac{\rho}{G}}. \quad (33)$$

Where R is the radius, ρ is the density, G is the shear modulus and ϑ is the Poisson's ratio of particles.

The time-step is excessively small when adopting a simulation using the explicit calculation scheme, however for practical purposes, the simulation time should be accelerated, and this could be obtained by only increasing the time step. A suitable approach to this is to decrease the value of the particle's shear modulus (Thakur et al., 2016) (Oldal et al., 2017). Also, the simulation time could be reduced by using a dynamic timestep (Horváth et al., 2022). A larger timestep can be applied at a given time interval with a small number of contacts, while the stability of the simulation is not declined. However, it is vital to choose an appropriate dynamic critical timestep coefficient. Also, it is important to set a maximum timestep which can be the critical static timestep. The choice of time step in DEM simulations is an important part of the setup of the simulation and often requires calibration and testing to ensure the stability of the simulation and the validity of the results.

3.4. DEM multi-sphere approach

In industrial and agricultural applications, most granular materials are complex in shape such as stones, pellets, corn grains, wheat grains, etc. Therefore, using a single sphere to model these shapes is unrealistic and yields untrustworthy simulations.

Non-spherical elements have distinct properties when it comes to rolling resistance. Modeling a complex-shaped element with a single sphere will roll on a flat/inclined surface in a different behavior, thus flawed motion of the particles will be obtained.

The multi-sphere method is used by clumping several spheres together as in one shape, knowing that the sum of the mass of spheres is the mass of the interlocking volumes because I used the keyword "use_density" density in LIGGGHTS(R)-PUBLIC which will use the specified mass and the specified density (LIGGGHTS(R)-PUBLIC Documentation, Version 3.X).

This approach is available in LIGGGHTS, for a better approximation of the real shape of non-spherical particles. This method is more expensive computationally, but it grants better results.

The number of steps required to find the contact is proportional to the number of spheres used to represent an element (Böhling et al., 2014), and it is calculated as follows:

$$N_{steps} = n_{spheres\ in\ the\ shape} \times n_{number\ of\ spheres\ in\ all\ particles} \times n^2 \quad (34)$$

For regular shaped elements like sphere, the center of mass is known, however, if a clump of spheres is used, then the centroid and the distance between the centroid and the centers of element spheres must be determined at the first cycle of a DEM simulation. In my study, I used axisymmetric irregular shapes, consequently, the centroid is straightforward to find based on the coordinates of centers of the spheres in an element shape. Far ahead, the coordinates of particles' centroids will be needed to calculate the mixing rates. For instance, representing an irregular shape by three spheres would let to get three different coordinates, however, to find the position of an irregularly shaped particle one coordinate should be used, and then the center to consider must be that of the centroid.

3.5. Generation of the discrete element model

In the work presented, the commercial software EDEM® and the open-source software LIGGGHTS were used to generate discrete element models. Surface models representing mixer parts and injectors are generated entirely with the pre-processor. Using EDEM®, the mesh is generated automatically, however, in LIGGGHTS meshing of parts must be performed independently before running any simulation especially that contains parts with curves to avoid significant errors. After a complete run of a simulation, a distinct program is needed to read the files generated by LIGGGHTS and post-process the results. The following chart shows all the steps required to get an effective mixing DEM model.

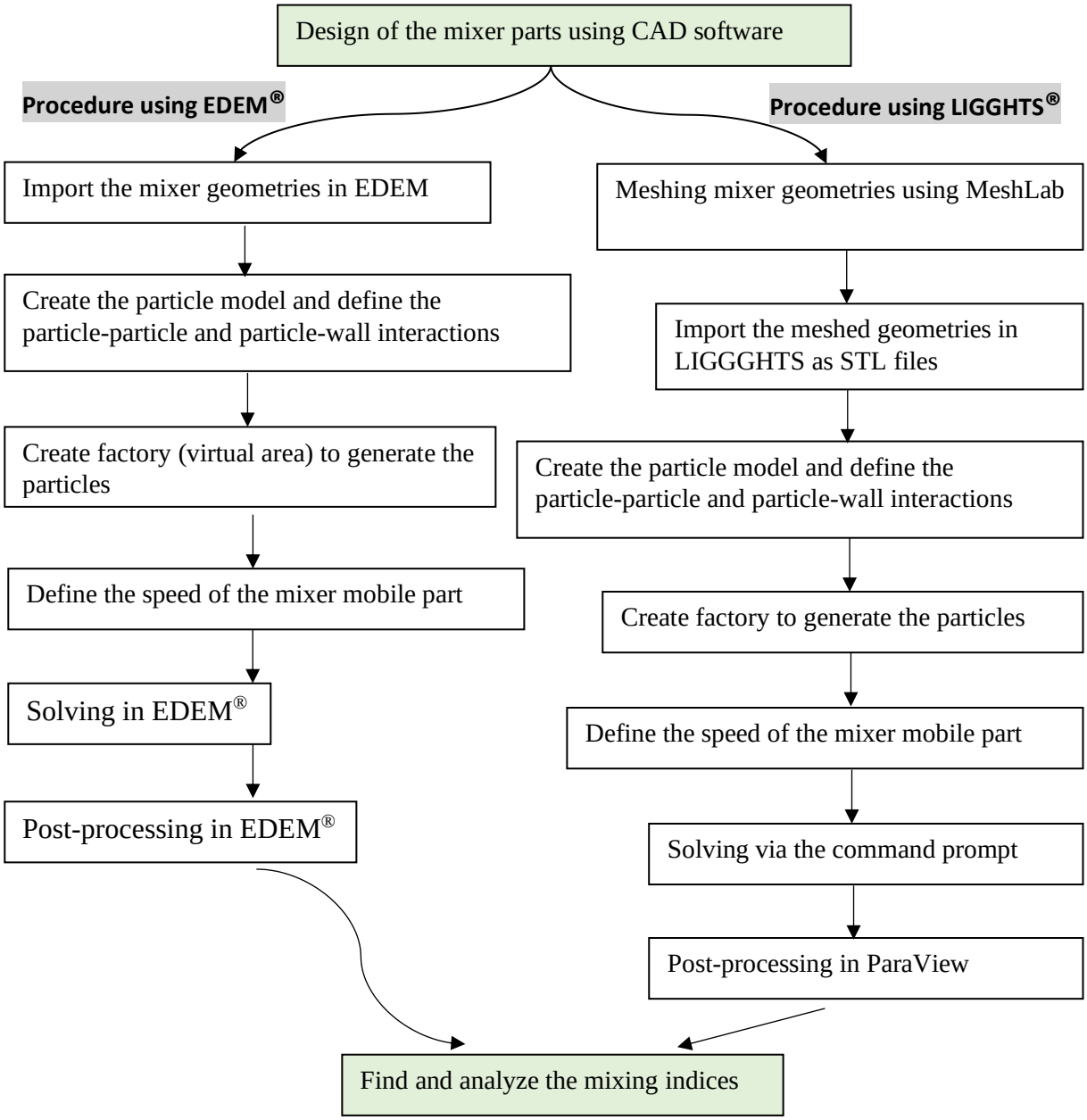

Fig. 3.5. Flow chart of the discrete element methodology either using EDEM® or LIGGGHTS®

Mixing particles of various types and shapes was tackled by employing the methodology illuminated in Fig. 3.5. Micro-mechanical properties, contact types, and particles loading were chosen and set to describe the particles and mixer wall.

3.6. Pre-processing with LIGGGHTS-PUBLIC®

LIGGGHTS is an abbreviation of the LAMMPS Improved for General Granular and Granular Heat Transfer Simulations, where LAMMPS is a standard simulator for molecular dynamics calculations. Thus, LIGGGHTS is a discrete element code to simulate the dynamics of particles, however, unlike commercial programs, this is an open-source software that requires an input deck before execution. The input deck typically entails four parts essential for the DEM modeling:

1. Initialization: define the DEM domain and units to be considered.
2. Setup: define particle type, size, and shape. Import geometries if needed, define the different micro-mechanical properties, and create a factory for particle generation.
3. Details: introduce the simulation time step, duration of the process, output information, etc.
4. Execution: give the run(s) command(s) and define the(ir) processing duration(s).

In the appendix, I presented one of our simulations' input decks to simulate a mixing process. The example will not give all the possible commands available in LIGGGHTS, however, it gives an insight for users to understand all the necessary parts of the simulations and allows them to develop their intended DEM models.

In pre-processing, I defined all the steps needed to run a simulation. In EDEM, it is straightforward to manipulate through the pre-processor, however, in LIGGGHTS I had to write all the steps in blocks of codes.

Particle creation and insertion

Calibrating a DEM model needs much time to select the appropriate particle geometries, number of particles, and their filling rate. The factors playing the role are the domain size, insertion region size, and computation power. The elapsed time intervals, the overall total kinetic energy of the system, the number of particles inserted, and warnings if there are any will be displayed in the command prompt terminal. In case the overall total kinetic energy of the system is exceedingly varying, then some parameters must be revised, which are the material properties and the filling rate. The particles could be inserted either by their mass or by their amount, also they could be generated through a volume or a geometry.

Best practices in the DEM input deck

The following recommendations were collected from previously conducted studies to achieve accurate results from the DEM numerical simulations (Shenouda & Hoff, 2020).

1. The timestep should be lower than the Rayleigh critical time. In practice, it would be better to keep the timestep equal or inferior to 20 % of the Rayleigh time, and to check the timestep magnitude in LIGGGHTS, I used the command line: *fix_check_timestep_gran* to verify our timestep magnitude by percentage according to Rayleigh time.
2. Deactivate the ignorance of particle loss during a run by the command line to avoid the shutdown of the simulation.

3. If the total kinetic energy of the system is not quite low and stable along a simulation, that means the timestep used is large and should be revised, otherwise it adversely impacts the flow of particles as they could intensely penetrate, resulting in a high total kinetic energy of the system in the course of a time interval.
4. If warning messages in the command prompt say, "particle insertion: fewer insertions than requested", means that the factory is trying to generate too many particles that are more than its capacity, therefore either a lower generation rate of particles should be used, or the factory surface should be extended regarding the container geometry to not allow particles to generate outside the container. Also, the initial velocity of particles could be increased to fill the container in a shorter period, but the speed rate should not be too high as the run might be unstable, and the reason behind this issue is that at a very high-speed particles collapse, and the domain might be extended, which it might force us to extend the simulation domain, and in turn slows down the simulation.
5. When the particles load without issue at the start, and then they suffer to load, and the desired number of particles cannot be reached, means that the initially loaded particles create a pile that intruded into the particles' factory (insertion zone).
6. It is generally a good idea to make sure a batch system is fully enclosed to avoid losing particles during the simulation. However, the presence of a lid can limit the ability to insert particles. If the lid is inserted as a separate object, it can be moved about before and after the particle insertion to facilitate the filling operation, or simply added to the system after all particles have been added.
7. Using different material types for different groups of particles, even if all the material properties are identical, can be a convenient way to identify particles and groups of particles during post-processing. This is especially true for mixing problems.
8. Of the three insertion methods (pack, rate/region, and stream), it is recommended to use the rate/region or stream methods. The pack method relies on being able to fill a volume with many particles at one time via random sequential addition, which will typically fill a volume to no more than 30 %. This can make it difficult to achieve the desired number of particles and will often leave a large empty space in the simulation domain that reduces the efficiency of parallelization. Using the rate/region or stream options allows you to use a much smaller insertion volume and insert material over time. Rate/region is preferred in general over stream solely because the user can define the insertion region from within the input deck and does not require the user to create and import some external CAD. That said, sometimes (e.g., filling an annular ring) is accomplished far more efficiently with the rate/stream option.
9. Reduce the geometry(ies) in a way to keeps only the parts that have contact with particles. Usually, parts with curves must be meshed before saving in the LIGGGHTS® directory, otherwise, the following error might show up: *particles have a high aspect ratio* causing the simulation to shut down. The meshing step is explained in detail in the next sub-section.
10. The value of the elasticity modulus could be decreased to significantly decrease the simulation time. Assigning a value of 10^7 Pa of the elasticity modulus is sufficiently high to capture the dynamics of particles without affecting the results of the simulation.

3.7. Meshing parts using MeshLab®

Before importing parts into LIGGGHTS® as Standard Triangle Language (STL) files, I checked their meshing to avoid substantial errors when running the code. To solve this issue, first I import every part to MeshLab software, and I refine its meshing through the remeshing command, then I export the part as an STL file to the designated folder. Fig. 3.6 shows the difference between some parts compositions before and after refinement.

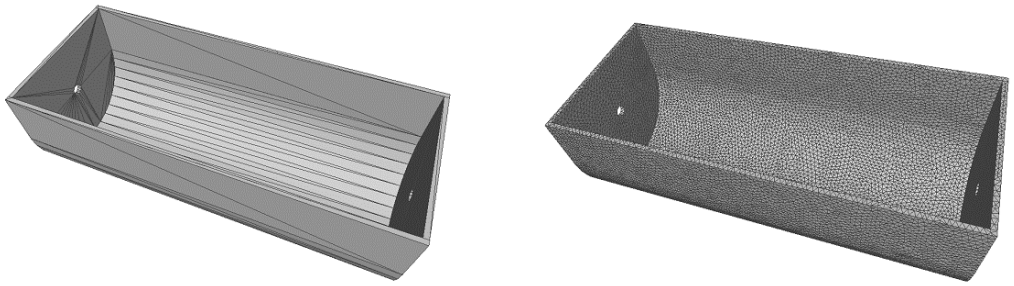

Before meshing After meshing using MeshLab

Fig.3.6. Meshing using MeshLab®

In a previous work, it was found that such dense meshing increases the computational running time, whilst it doesn't improve the simulation accuracy (Horváth et al., 2022).

I also found that refining the mesh of the mixer part has drastically increased the simulation computational time. Meshing the mixing paddles by 2242 and the mixer frame by 20979 vertices had 187 min computational time for a 29 s mixing time while meshing the mixing paddles by 7684 vertices and the mixer frame by 38855 vertices had a simulation time of 8920-minute for the same mixing time. As shown in Fig. 3.7, increasing the mesh density had no significant impact on the mixing index, therefore such dense mesh is unnecessary.

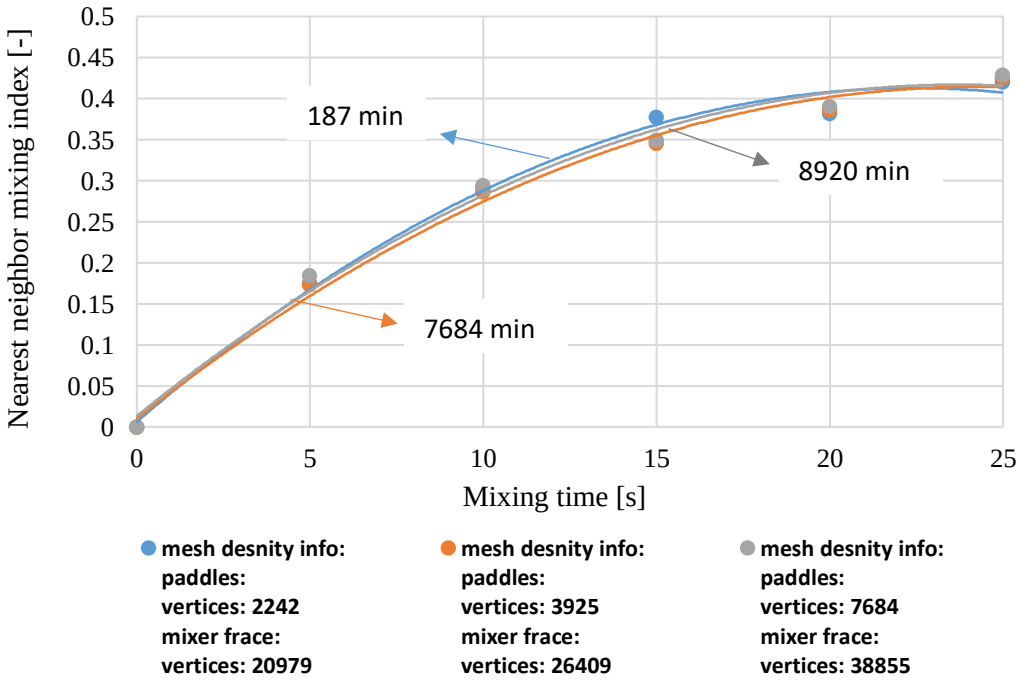

Fig.3.7. Impact of the mesh density on the mixing index and computational time

3.8. Determination of the micro-mechanical properties

In this section, I explain how the micro-mechanical properties of the corn particles are determined namely: particle density, Young's modulus, coefficient of restitution, coefficient of friction and coefficient of rolling friction.

3.8.1. Density and Young's modulus

The density of a grain is a fraction of its mass by its volume, and it could be determined either theoretically or experimentally. The theorical approach requires a precision scale to weigh the mass of a grain and approximate its volume by regular shapes which the most fits the real volume of the particle. On the other hand, the density could be determined by the pycnometer method. A mass of particles is loaded in a vessel pre-filled with a definite volume of water or alcohol if particles are buoyant until the loaded particles displace the water/alcohol volume. 5 samples of 20-40 grains were used and the average density obtained is from a previous study is 1163.3 kg/m^3 (González-Montellano et al., 2012).

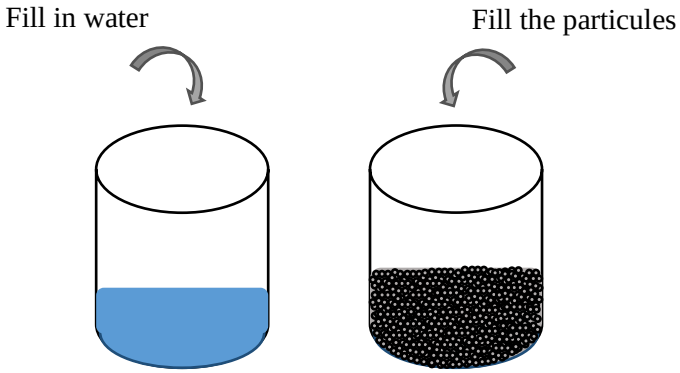

Fig.3.8. Illustration of the measurement of particle density

As shown in the above illustration, particles are filled in the vessel, which is pre-filled with a liquid until particles reach the top surface of the liquid and don't exceed it. The volume of the liquid will increase after the filling of the particles, and the volume of that number of filled particles is measured via the change of the liquid in the vessel, subsequently the average volume of each particle could be calculated, and its mass could be measured using a microscale.

The XT2 Texture Analyzer which is a piece of laboratory equipment used for measuring the mechanical properties of various materials was used to measure the Young's modulus of a corn grain as described in Fig. 3.9 and the Poisson's ratio was determined by the ratio of the transversal to longitudinal strain (González-Montellano et al., 2012). This analyzer consists of a motorized probe or arm that applies controlled force to a sample while sensors measure the response. The grain was placed on a flat fixed part and a 4.8 mm spherical mobile part presses gradually from the top of the grain until cracking occurs.

In this case of contact between a spherical indenter and a spherical surface (grain surface), according to the ASAE standard 386.4 (S368.4, 2000), the particle's Young's modulus is calculated by equation 35.

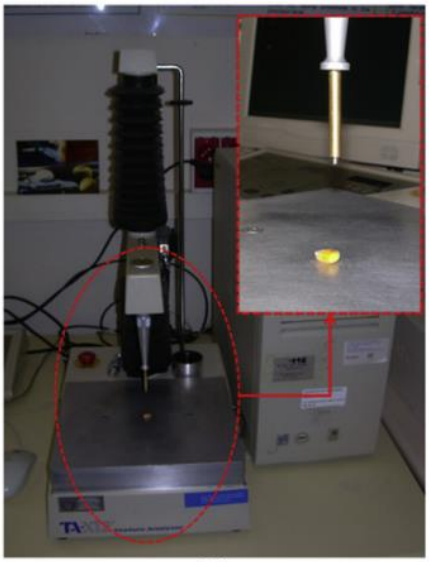

Fig. 3.9. XT4 texture analyzer being used

$$E = \frac{0.338F(1-\vartheta^2)}{D^{1.5}} K_U^{\frac{3}{2}} \left(\frac{1}{R_U} + \frac{1}{R'_U} + \frac{4}{d}\right)^{1/2} \quad (35)$$

F is the loading force of the compression tool, ϑ is the Poisson's ratio, D is the strain due to the applied force, R_U and R'_U are the minimum and maximum curvatures between the compression tool and the corn grain, respectively, K_U is a known constant in the aforementioned standard document, and d is the diameter of curvature of the spherical indenter. 20 samples were performed, and the average value of the particle's Young's modulus calculated is 2.98×10^8 Pa.

3.8.2. Coefficient of restitution

The coefficient of restitution characterizes the bouncing capacity of a particle as it collides with another particle or a wall. This value is always between 0 and 1, 0 means that the collision of the particle is totally plastic, and 1 means that the collision of the particle is totally elastic.

Grain-wall coefficient of restitution

The grain-wall coefficient of restitution determines the rebound distance when a particle hits the mixer wall. For this purpose, I carried out drop experiments by releasing one particle without an initial velocity towards a plate having the same mixer material (Fig. 3.10). A high-speed camera is used to capture the position of a particle before and after bouncing. The coefficient is calculated as follows:

$$e = -\frac{v_1}{u_1} = \sqrt{\frac{H_2}{H_1}}. \quad (36)$$

In this experimentation, the particle-wall coefficient of restitutions found is 0.505. This result is the average value of 50 replications by releasing two distinct corns from 200 mm and 300 mm heights (H_1 in Fig. 3.10).

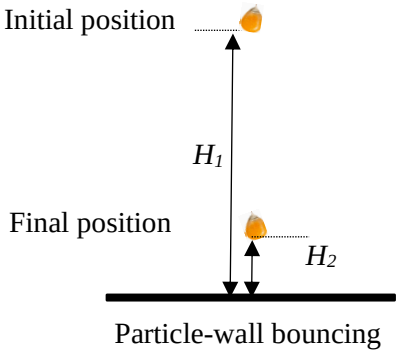

Fig.3.10. Measurement illustration of the particle-wall coefficient of restitution

Grain-grain coefficient of restitution

The measurement of the grain-grain coefficient of restitution was taken from the literature because repeating the same experiments is unavailing. Researchers (González-Montellano et al., 2012) used an apparatus composed of two equal pendulums connected to a vertical fixed beam. On each free extreme of the pendulums, one corn is tied up. A pendulum is pulled up towards one side while the other remains fixed, then it is released from height H_1 towards the other pendulum so that particles will collide forming new heights H_2 and H_3 as described in Fig. 3.11.

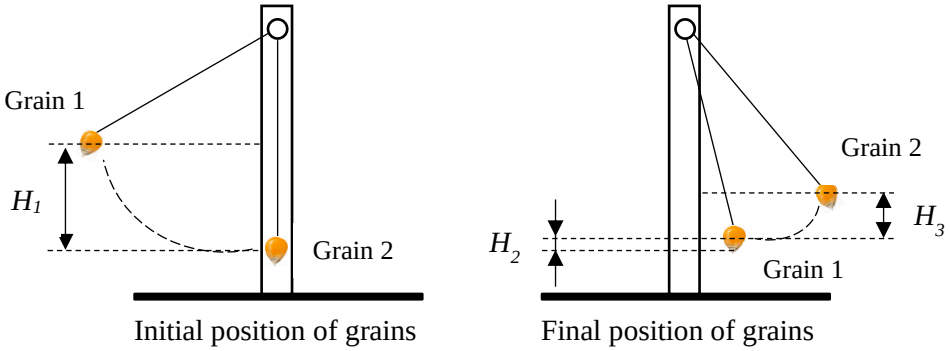

Fig. 3.11. Appliance used to calculate the grain-grain coefficient of restitution (a) initial position before collision (b) position of grains after collision

The formula applied to calculate this coefficient is the following:

$$e = -\frac{v_1 - v_2}{u_1} = \frac{\sqrt{H_3} - \sqrt{H_2}}{\sqrt{H_1}}. \tag{37}$$

After a set of repetitions were carried out by using different grains and varying the initial angle between the two pendulums, the average coefficient calculated is 0.25.

3.8.3. Coefficient of static and rolling frictions

The corn grain has a complex shape, modeling this grain with a simple sphere is unrealistic and results will diverge, therefore I employed the multi-sphere approach in LIGGGHTS® to thoroughly mimic the real shape of a corn particle. I used a clump of 5 spheres as described in Fig. 3.12. This DEM shape is used after some trials using other number of spheres for validation, which are 4

spheres in a clump (same shape and size in Fig. 3.12 excluding the smallest sphere in the clump) and a single sphere (radius = 4 mm). I found that this shape is the best to represent the corn grain by comparing the magnitudes of the slope angles found from DEM and real experiments shown in Fig. 35.

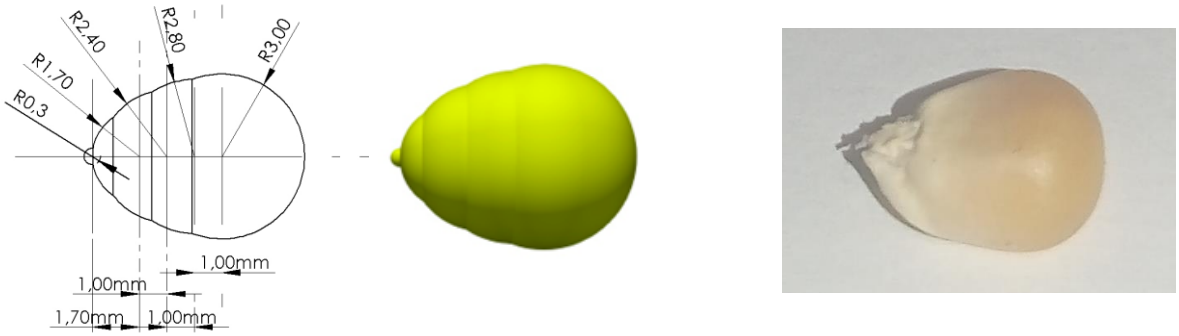

particle size and shape in DEM real corn particle

Fig. 3.12. DEM particle shape and size of a corn grain

To measure the coefficients of static and rolling frictions, I conducted the storehouse unloading experiment. A roofless box having the dimensions of 75 mm ×75 mm ×75 mm is fixed on a flat base. The box was loaded with 1000 grains, then one side of the box was pulled out, as a result the loaded material will freely slide out the box in a way that it will form a slope. Calibration experiments using DEM experiments were performed to find the optimal values. Various static and rolling frictions were tested (Table 8.1 in appendix). Fig. 3.13 shows the results that I found from the real experiments and DEM simulations.

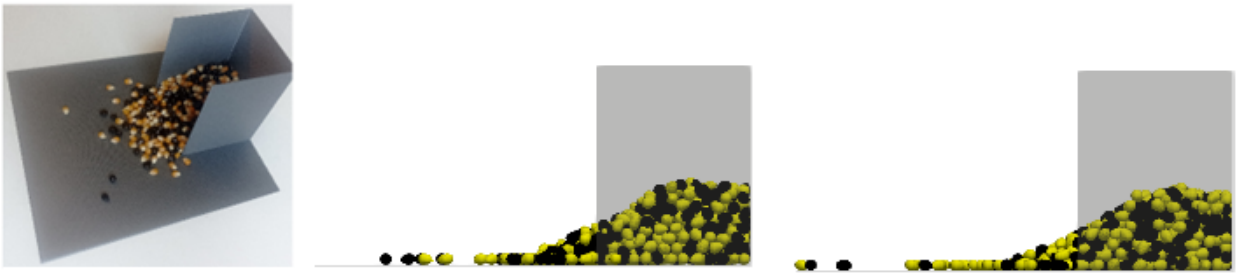

(a) Slope angle = 22.6° (b) Slope angle = 22.7° (c) Slope angle = 23.7°

Fig. 3.13. Slope angles calculated: (a) real test (b) numerical test using real value of E and 20 % Rayleigh timestep (c) numerical essay using $E = 5 \cdot 10^6$ Pa and 20 % Rayleigh timestep

As the material is opaque, I used a protractor to find the slope angle and compare it to numerical results. The slope angles obtained by the real experiment and the numerical simulation with smaller values of Young's moduli were 22.6° and 23.7°, respectively, which closely matched.

Post-processing using PARAVIEW

PARAVIEW is an open-source application. It is used to visualize and analyze the data generated by LIGGGHTS qualitatively and quantitatively. By default, after loading the files in PARAVIEW particles will be displayed as points representing the centers of every sphere, however, these points

could be scaled according to their radii (Fig. 3.12). The flow of elements could be displayed at the desired time interval considering the data saving interval used in LIGGGHTS inputs. For instance, saving results could be set to 1s time, then LIGGGHTS will generate files every second during the run, as an advantage, this option allows to generate less volume in the disk.

3.9. Qualitative analysis

In the post-processor, the particles could be distinguished by their type using different colors, and the mixer parts could not be visualized on the interface, consequently, a clear interpretation of the mixture state could be read. In addition, the granular volume could be divided into slices, and the internal structures could be forecasted visually using the clipping feature in the post-processor.

Initially, particles will be displayed as points in the interface of PARAVIEW®. These points represent the centers of particles; however, they could be represented by volume according to their radii by switching the representation option to 3D Glyphs (to show particles' real shape), and in properties change the scale mode to magnitude, setting the scale factor = 1.0, glyph type to sphere and radius = 1.0, then the particles will be displaced as in Fig. 3.14.

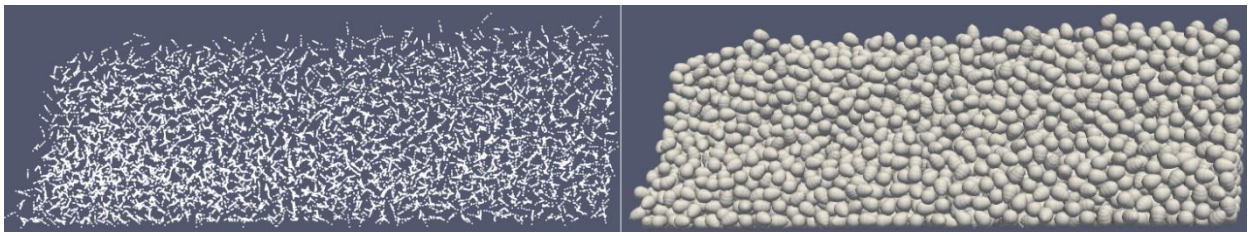

Particle initially displayed as points Rendering points as spheres

Fig. 3.14. display of particles in PARAVIEW®

LIGGGHTS® generates files sequentially every time interval until the end of a run in a post folder. To view particles and other geometries, the saved files in the post folder should be imported into PARAVIEW®.

In the case of using the multi-sphere approach to represent one particle, then the coordinates are extracted in order. For example, if 3 spheres are used as a clump, then the coordinates will be extracted as follows: (x_1, y_1, z_1) (x_2, y_2, z_2) and (x_3, y_3, z_3) for particle 1, 2, and 3, respectively, and so on in the DEM system for other clumps.

3.10. Image analysis of the mixing dynamics using the variance method

To check the reliability of the DEM models, I have used a high-speed camera to take snaps along the mixture from the top of the single shaft paddled mixer (Fig. 3.15). This would give an insight into the structure of the mixture from the top layer and then I divided each structure into several cells and then applied the particles variance method to quantify these mixing states of particles.
The variance method is a useful technique to quantify the distribution of particles from a 2D image (Liu et al., 2015). I used a high-speed camera to capture the arrangement of the particles from the top layer of the single shaft paddled paddle mixer along the mixing time without interrupting the mixing as described in Fig. 3.15. Images captured must be divided into a certain number of cells, and the quality of the mixture is quantified by the concentration variance of the system as explained by equations 38, 39, and 40.

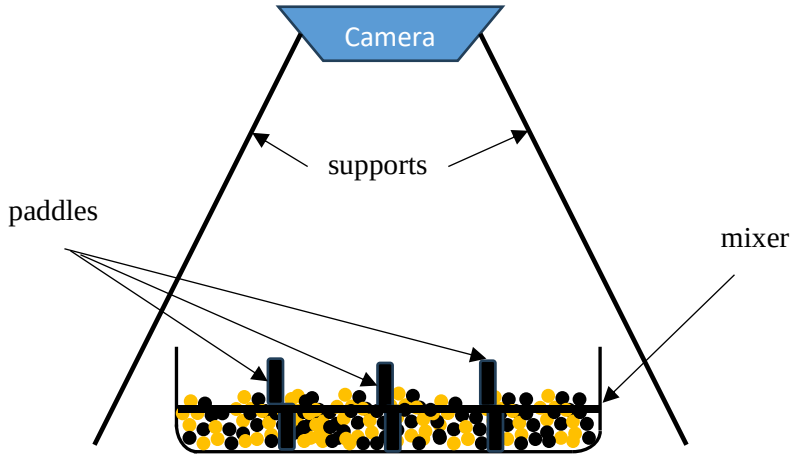

Fig. 3.15. Description of the setup used to capture particle distribution by images

$$\sigma^2 = \frac{1}{n-1}\sum_{i=1}^{n}(C_i - C)^2. \tag{38}$$

Assume mixing a bi-component material distinguished by color white and black, then the concentration of a particular component in cell *i* is calculated by:

$$C_i = \frac{number\ of\ black\ particles}{number\ of\ black\ particles + number\ of\ white\ particles}. \tag{39}$$

And C is the average value calculates as follows:

$$C = \frac{1}{n}\sum_{i=1}^{n} C_i. \tag{40}$$

σ^2 equals 0.5 if the particles are segregated, and σ^2 approaches 0 if decent homogeneity of particles is attained.

I used this quantification method to plot the different mixing curves and find the difference between results found from the real experiments and the DEM simulations in the rotational drum mixer and the single shaft paddle mixer.

3.11. Mixing indexes calculations

The mixing indexes used in our study are the Lacey mixing index and the nearest neighbor index. The lacey mixing index is grid-dependent, a partition of the DEM domain into cells is necessary to calculate the mixing rate, because it relies on the number of elements by their type, while the nearest neighbor index is a grid-independent method. The latest is based on the position of particles described by their coordinates (*x*, *y*, *z*) in the 3D DEM domain.

3.11.1. Lacey mixing index

This method is grid-dependent, which means that the system of granular material must be divided into cells (Gorter et al., 2010). The mathematical model to find this mixing index is presented by the following equations:

$$M_{Lacey} = \frac{x_0^2 - x^2}{x_0^2 - x_r^2}. \quad (41)$$

$$x_0^2 = x_m(1 - x_m). \quad (42)$$

$$x_r^2 = \frac{x_0^2}{n}. \quad (43)$$

$$x^2 = \sum_{i=1}^{N} \frac{(x_i - x_m)^2}{N - 1}. \quad (44)$$

In which N represents the number of cells, n is the average number of particles in each cell, while x_m, x_i respectively represent the average number fraction of white particles and the number fraction of white particles in each cell. Lacey index depends on the number of cells. The Lacey mixing index would be higher when divided into more cells.

x^2 is the variance of the number fraction of white particles in each cell, x_0^2 and x_r^2 is the variance of fully demixed system and fully mixed system.

In this work, I used an excel sheet to import the number of particles in each cell filtered by their type. Then I implemented the above equations sequentially to expedite the calculation.

3.11.2. Nearest neighbor mixing index

This mixing rate is calculated using the coordinates of all types of particles in the DEM domain (Gorter et al., 2010). The 12 nearest particles to each particle are identified by iteration, then the equation (47) is applied to find the mixing rate of the concerned element, and similarly for all other particles, finally a mean value is calculated of the mixing rates found of each particle to describe the homogeneity level of the whole mixed material bed.

$$M = \frac{1}{N} \sum_{i=1}^{N} \frac{2 \times n_{diff}}{n_{nb}}. \quad (45)$$

N, n_{diff}, n_{nb} are the total number of particles, the number of particles different in type, and the number of neighboring particles, respectively.

A slight modification could be introduced in case of using unequal quantities of particle types are used. For instance, a material bed composed of 1000 particles of type *A* and 2000 particles of type *B.* In this case, the perfect mixture of particle *i* is attained only if 4 type *A* particles and 8 type *B* particles are found as the nearest particles.

For this method, I created a java script that finds the rate by reading the coordinates from a CSV file because it is smooth and practical. In the appendix, I presented a script of this method.

3.12. Open auger screw mixer set-up

A hopper base screw mixer was studied in this work. I used paddles mounted to screw to obtain a more homogeneous mixture. I investigated on the one hand the number of mounted paddles and

their orientation. On the other hand, I studied the impact of the initial filling configuration of particles and the screw pitch length.

3.12.1. Paddles mated to the screw

A simple screw or screw-mated-paddles was placed in the middle of the mixer cavity. The different structures of the screw-mated paddles are presented in Fig. 3.17. This model could be used as a mixer to mix granular materials such as agricultural and chemical powders. The screw was rotating in the clockwise direction at a given linear rotational speed. It could have several functions, one is to decrease the moisture content between particles, two, to mix different types of particles and keep the stock homogeneous, and by mixing the under-dried particles with the over-dried ones, it helps to homogenize the mixture and initiate moisture exchange between the particles. The screw has the following dimensions: shaft diameter = 15 mm, screw diameter = 40 mm, screw length = 300 mm, and screw pitch = 20 mm.

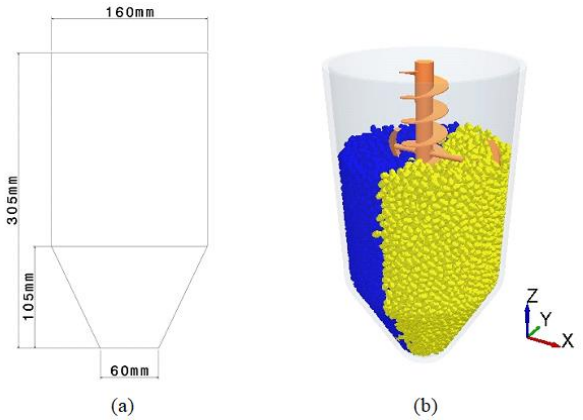

Fig. 3.16. (a) mixer geometry (b) filling configuration

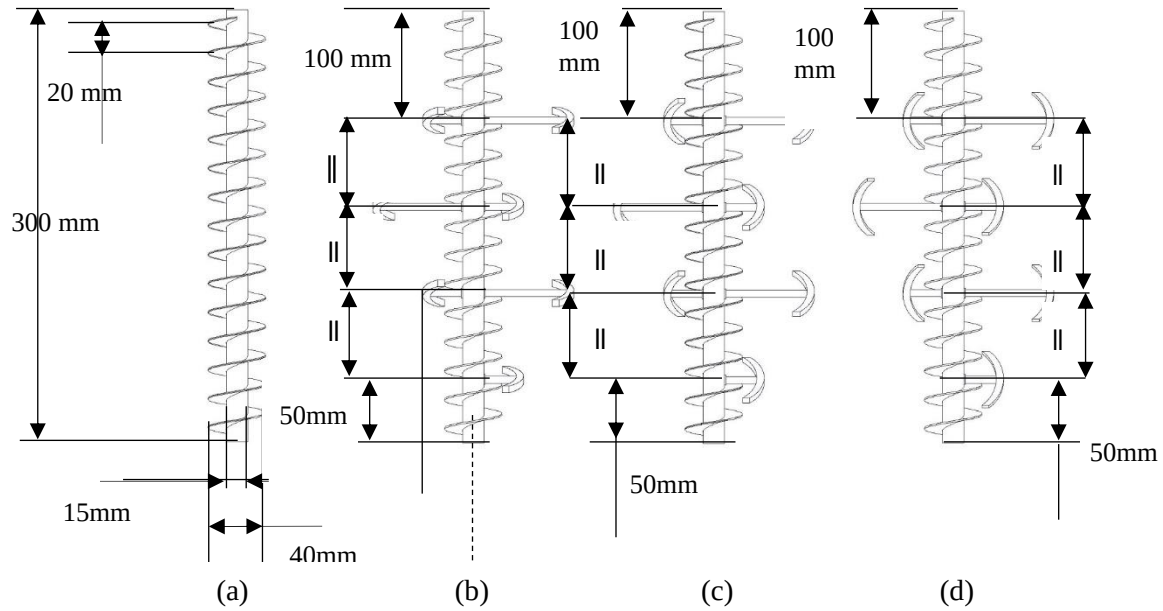

Fig. 3.17. The geometry of the screw with different tilted paddles used in the simulations. View from the front, with the screws, rotated in the clockwise direction: a) simple screw, b) screw-mated -paddles asymmetrically oriented by 20° (c) screw-mated-paddles asymmetrically oriented by 45° and (d) screw mated paddles asymmetrically oriented by 70°.

The simulation system consists of 11200 particles, corresponding to a 70 % fill fraction by volume. The 70 % value, unlike to low filling volume, gives an intense flow of particles that makes the mixing more challenging. The simulation started by placing particles separated into the mixer (side-by-side loading) to know the performance of the mixer from a totally segregated particles state. Particles were loaded under the influence of gravity for 2 seconds, while the screw/screw-mated paddles were static. After particles loading, the screw/screw-mated paddles are set in the clockwise rotational motion around its vertical axis with 60 rpm rotational speed, corresponding to 1 rotation per second. Eight simulations were carried out, the first run using a simple screw, the second to the fourth run using 1, 2, and 4 paddles mated horizontally to the screw axle tilted asymmetrically by 70°, fifth to eighth simulations using 4 mated paddles to the screw having different tilt angles (Fig. 3.17). The thickness of these paddles is 2.5 mm, and they have crescent shapes on both sides and the length from each far side of the paddle to the screw axle is unequal, also they are reversely mated along the screw axle (Fig. 3.18). The gap between the lengthier chunk and shorter chunk of the mated horizontal paddle and mixer wall are 5 mm and 20 mm, respectively. Each simulation lasted for 32 seconds, 2 seconds for particles filling, and 30 seconds for particles mixing until the material bed becomes almost steady. The particle' model shape used of wheat particles is shown in Fig. 3.18 and the micromechanical properties and the mixer apparatus were found in the literature and used in our simulations (Table 3.1).

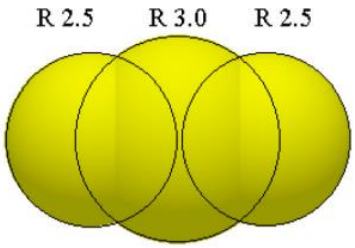

Fig. 3.18. Geometry of the mixer and screw geometrical parameters studied.

Table 3.1. Micro-mechanical parameters used in the drum mixer simulations (Keppler et al., 2016)

Parameters	Particle (wheat)	Mixer wall (steel)
Poison ratio υ	0.4	0.3
Shear modulus G (Pa)	$3.58 \cdot 10^9$	$8 \cdot 10^8$
Density ρ (kg/m^3)	1460	7500
Coefficient of restitution e	0.5	0.6
Coefficient of friction CoF	0.3	0.25
Coefficient of rolling friction $CoRF$	0.01	0.01

3.12.2. Screw dimension and initial filling configuration

In this part, I investigated the impact of the screw diameter and screw pitch length described in Fig. 3.19 and I used the same mechanical properties listed in Table 3.1.

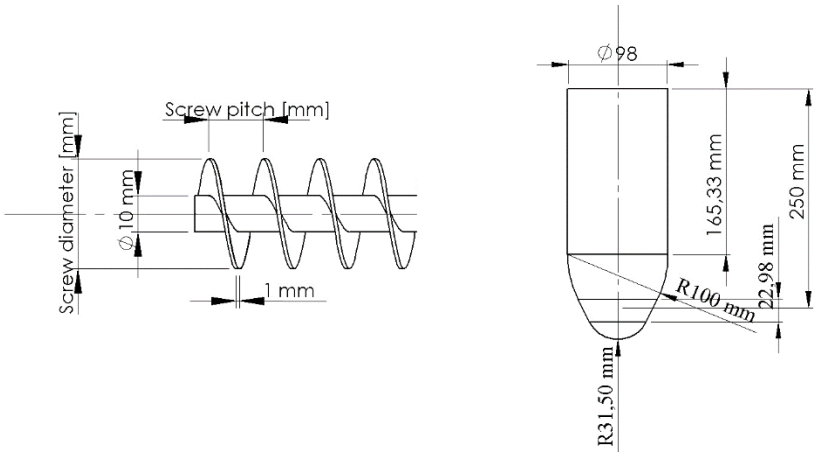

Fig. 3.19. Geometry of the mixer and screw geometrical parameters studied.

I changed the screw dimensions and removed the paddles, and I checked the effect of the screw rotational direction and filling pattern of particles on the mixing index. The simulation scenarios with the related parameters conducted are listed in Table 3.2.

Table 3.2. List of the conducted numerical simulations for the screw mixer

Runs	Initial configuration of particles	Screw direction of rotation	Screw pitch length (mm)	Screw diameter (mm)	Screw rpm
Run 1	Top-bottom	clockwise	10	10	60
Run 2	Side-by-side	anticlockwise	10	10	60
Run 3	Side-by-side	clockwise	10	10	60
Run 4	Side-by-side	clockwise	20	10	60
Run 5	Side-by-side	clockwise	30	10	60
Run 6	Side-by-side	clockwise	40	10	60
Run 7	Side-by-side	clockwise	50	10	60
Run 8	Side-by-side	clockwise	30	20	60
Run 9	Side-by-side	clockwise	30	20	40
Run 10	Side-by-side	clockwise	30	20	50
Run 11	Side-by-side	clockwise	30	20	70
Run 12	Side-by-side	clockwise	30	20	80

3.13. Paddled drum mixer set-up

I used a literature reference to create a DEM model of a cylindrical drum mixer assigned with acrylic material having a diameter of 280 mm and a width of 140 mm, to find the reliability by comparing my results to that of Li et al., (Li et al., 2009). The mixer was filled and maintained at 75 % filling fraction by volume for all simulations with spherical glass beads, segregation state was set before mixing by generating two groups of particles from separate inlets on the top of the mixer separated by a cross-sectional splitter placed in the middle of the mixer to study the homogeneity of particles mixture from a totally inhomogeneous mixture state, knowing that particles filling time is 1 s. For the mono-disperse mixing, the diameters of the two types of particles selected are 10 mm, and for the bi-disperse mixing, the diameters of the two types of particles selected are 10 mm and 5 mm. A 1:1 filling volume ratio was maintained for all simulation cases inside the drum. After complete filling of particles, the splitter was removed and the material bed settled down until it reached a stationary state in the mixer under the influence of gravity for 1 s time, followed by the rotation of the mixer vessel for 75 s time to ensure the mixing to reach its highest rate. In this work, the micro-mechanical properties provided by Yanjie et al., (Li et al., 2009) displayed in Table 3.3 were used to define the mixer wall and particle materials and describe particle-particle and particle-wall interactions, and the DEM timestep that I used for all the simulation is 40 % of the Rayleigh timestep. I designed a new drum by installing uneven paddles in the middle of the mixer frame, and I examined the impact of paddles number on the mixture. The drawings of the paddled mixer configuration are shown in Fig. 3.20. The radius of the blade of each paddle has the shape of a semi-cylinder and its radius is 50 mm.

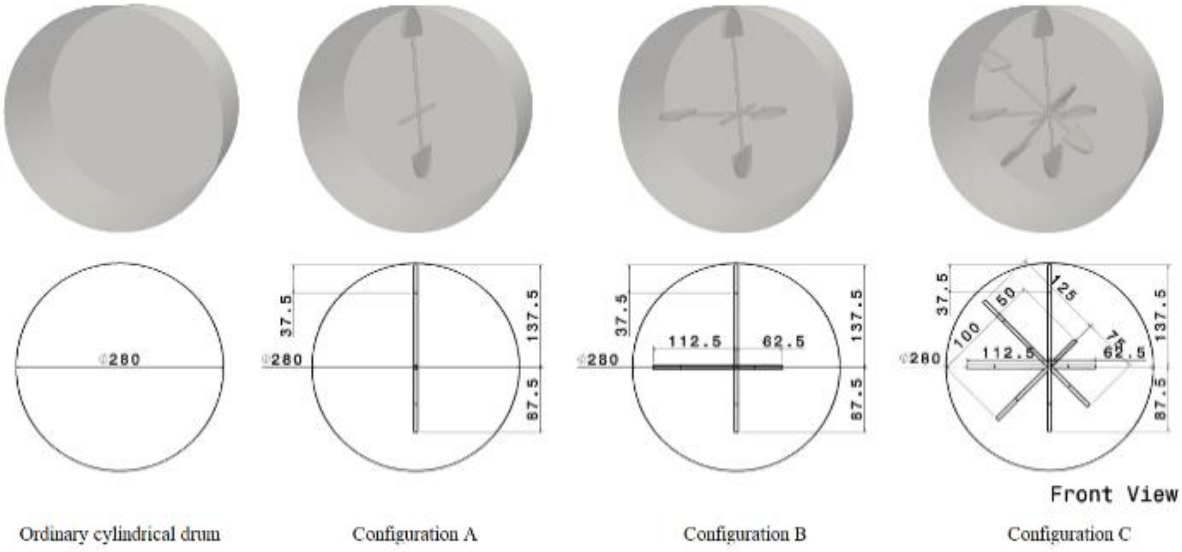

Fig. 3.20. Set-ups of the cylindrical drum used in simulations

Table 3.3. Micro-mechanical parameters used in the drum mixer simulations (Li et al., 2009)

Properties	Particles (glass spheres)	Mixer wall (acrylic sheet)	Particle-wall
Density, ρ (kg/m^3)	2700	1800	-
Young's modulus, E (Pa)	10^7	10^7	-
Coefficient of restitution, e	0.67	-	0.67
Poisson's ratio, υ	0.22	0.35	-
Coefficient of friction, *CoR*	0.95	-	0.8
Coefficient of rotational friction, *CoRF*	0.05	0.05	-

The simulation scenarios are described in Table 3.4. Initially, simulation cases 1 to 4 and 5 to 8 were conducted at an 8 rpm fixed drum speed to check the efficacy of the different mixer designs in terms of mixture uniformity for mono-disperse and bi-disperse materials, respectively. Eventually, the mixer speed was varied only for the finest mixer set-up in terms of mixing efficacy for the bi-disperse material because it is more challenging. Simulation cases 9 to 15 tackled the impact of mixer rotational velocity (configuration C) on the bi-disperse mixture quality.

Table 3.4**.** Design of numerical experiments of the rotational drum mixer

Simulation cases	Mixer set-up	Material bed	Mixer rotational speed
Cases 1 to 4	Ordinary drum	Mono-disperse	8 rpm
	Configuration A		
	Configuration B		
	Configuration C		
Cases 5 to 8	Ordinary drum	Bi-disperse	60 rpm
	Configuration A		
	Configuration B		
	Configuration C		
Cases 9 to 15	Configuration C	Bi-disperse	16 rpm
			24 rpm
			32 rpm
			40 rpm
			48 rpm
			60 rpm
			70 rpm

3.14. Single-shaft paddle mixer

For the real mixing experiments, I built a single shaft paddle mixer as described in Fig. 3.21. The apparatus has a frame, two supports to hold the frame, a mixing rotor, and an electric controllable-speed motor. The different parts of the mixer were 3D printed using PLA material. The mixing rotor is changeable to change the number of paddles. The mixer was filled with corn grains, and these grains were partitioned equally into two types distinguished by color and an initial

segregation state was set. A high-resolution camera was placed above the mixer to capture high-quality snaps during the mixing process. These snaps would give an insight into the mixture quality and compare the particle distribution on the surface to that of the developed DEM models for correlation check. After particles filling, the motor was turned on, the paddles were rotated in the clockwise direction and grains were moved in the mixer for 40 s mixing time until a steady state was reached.

Table 3.5. Micro-mechanical parameters used in the single shaft mixer simulations

Properties	Particles (corn)	wall	Particle-wall
Density, ρ (kg/m^3)	1163.3	1250	-
Young's modulus, E (MPa)	$5{\cdot}10^6$	$5{\cdot}10^6$	-
Coefficient of restitution, e	0.25	-	0.505
Poisson's ratio, υ	0.4		0.235
Coefficient of friction, *CoF*	0.6	-	0.7
Coefficient of rolling friction, *CoRF*	0.05	-	0.05

I used the box discharging method described in section 3.8.3 to calibrate the micro-mechanical properties. The obtained values are listed in Table 3.5. The timestep used is 20 % of the Rayleigh timestep in all the simulations

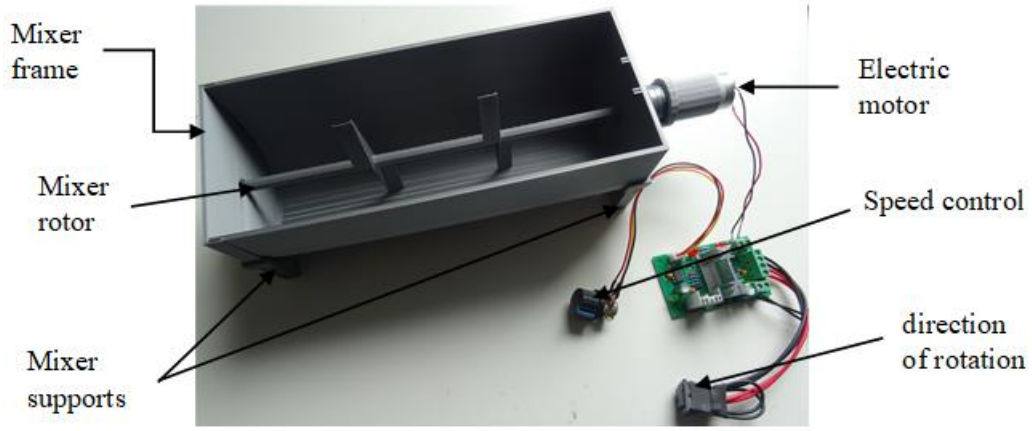

Fig. 3.21. Set-up of the single shaft paddle mixer (dimensions are in Fig. 8.1 and Fig. 8.2 in the appendices)

The technical drawing of the mixer is in Appendix 3. I used two types of paddles in the mixer. The paddles are illustrated in Fig. 3.22, and they are equally distant on the axle between.

The list of conducted simulations with the configurations set is listed in Table 3.6.

Table 3.6. Listed of simulations conducted for the single shaft paddle mixer

Run	Paddles' shape	Number of paddles	Initial filling type	Particles shape
1	B	2	Side-wise	Mono-shaped
2	A	2	Side-wise	Mono-shaped
3	A	3	Side-wise	Mono-shaped
4	A	4	Side-wise	Mono-shaped
5	A	5	Side-wise	Mono-shaped
6	A	6	Side-wise	Mono-shaped
7	A	7	Side-wise	Mono-shaped
8	A	5	Top-bottom	Mono-shaped
9	A	6	Top-bottom	Mono-shaped
10	A	7	Top-bottom	Mono-shaped
11	A	5	Top-bottom	Bi-shaped
12	A	5	Top-bottom	Bi-shaped

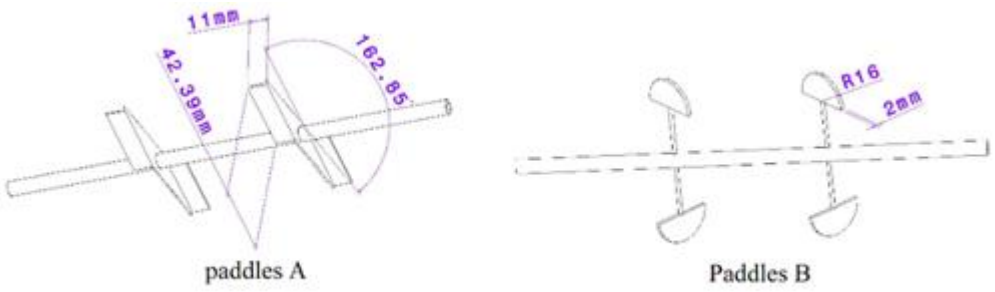

Fig. 3.22. Particles' initial configuration. (a) side-by-side (b) top-bottom

4. RESULTS AND DISCUSSIONS

4.1. Introduction

All the results obtained from the DEM simulations are evaluated qualitatively by visually analyzing the mixture arrangements from the mixer apparatus' periphery as well as the internal structures with the help of the DEM post-processor clipping function, and quantitatively using the mathematical models described in the methods chapter to calculate the mixing rates, thus find the influential factors on the quality of mixed particles.

Various types of mixers were utilized: open auger screw mixer, drum mixer, single shaft mixer, and a static mixer utilized to mix a bi-component solid particle. In this chapter, important findings are discussed and parameters for optimal mixing are given for each type of mixer used.

4.2. DEM models

For each DEM model, contact information, material properties, and boundary conditions are specified, then the DEM model is executed. The simulations are carried out using EDEM® or LIGGGHTS® programs. In the case of using the latter, generated data are opened with PARAVIEW® to visualize results.

4.2.1. Open auger screw mixer

4.2.1.1. Impact of screw dimensions on the mixture of wheat granules

I assessed the impact of particle filling type, screw rotational direction, screw pitch length, screw diameter and screw rotational speed on the mixture quality by qualitative and quantitative analyses. EDEM® post-processor allows us to see the mixture state not only through the mixer periphery but also in the middle of the material using the clipping function. In this way, snapshots were captured along the mixing process to qualitatively evaluate the mixture quality from the simulations. On the other hand, I used the nearest neighbor's method to quantitatively evaluate the different mixtures.

4.2.1.2. Effect of particles' initial configuration and screw rotational direction

The first 3 simulations from Table 3.4 were conducted to investigate the impact of the initial filling pattern and screw rotational direction on the mixture uniformity. Two different configurations of the particles were arranged before mixing: sidewise and top-bottom filling patterns. The sidewise filling pattern is the filling of each type of particles from one half of the mixer while the top-bottom filling is the filling of one type of particles in the whole mixer then the filling of the other type of particles from the top of it. The calculated mixing indexes based on the nearest neighbor's method showed that the homogeneity of particles is higher when considering the sidewise filling pattern of particles, and the rotational direction of the screw has no significant impact (Fig. 4.1).

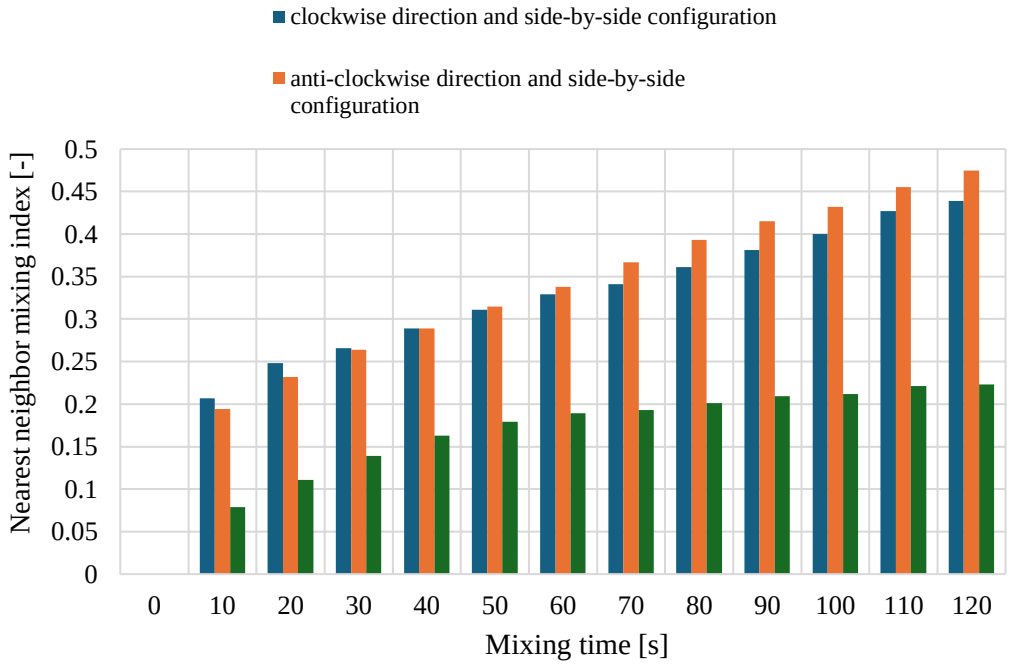

Fig. 4.1. Mixing index curves in terms of screw direction of rotation

4.2.1.3. Effect of the screw pitch

Simulations 4 to 8 listed in Table 7 were carried out using a screw having the following pitch lengths: 10mm, 20mm, 30mm, 40mm, and 50mm, while the screw diameter and screw speed maintained constant. The arrangement of particles from the mixer wall doesn't give adequate information about the mixing quality, therefore I clipped the system longitudinally along the *z* direction to have an insight into the particles state in the middle of the mixer. Snapshots were taken each 30-second mixing time for all the simulations (Fig 4.3).

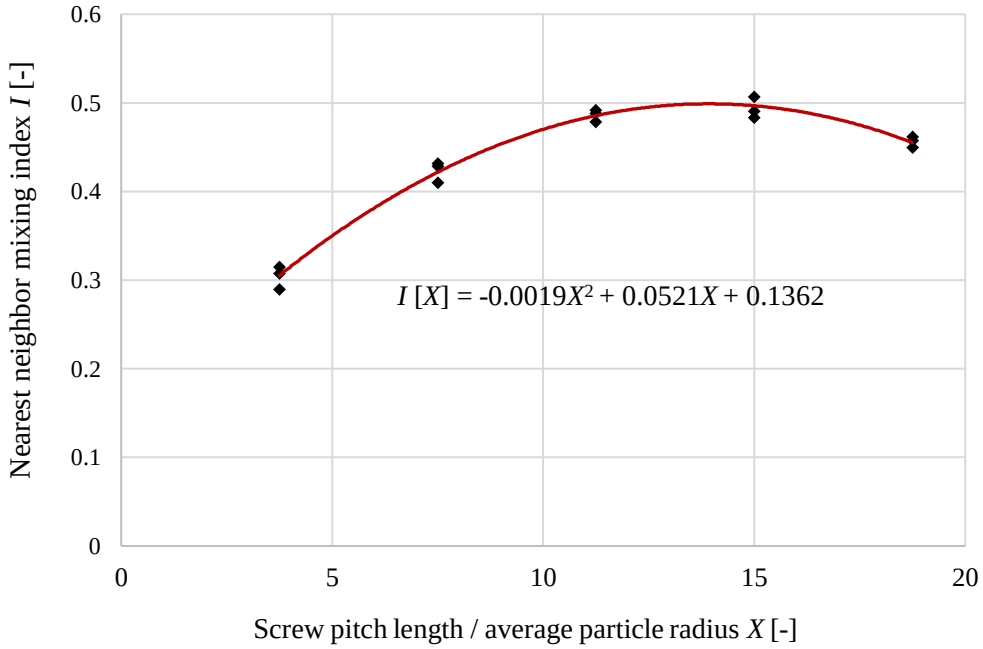

Fig. 4.2. Optimal mixing index in function of screw pitch length to average particle radius ratio

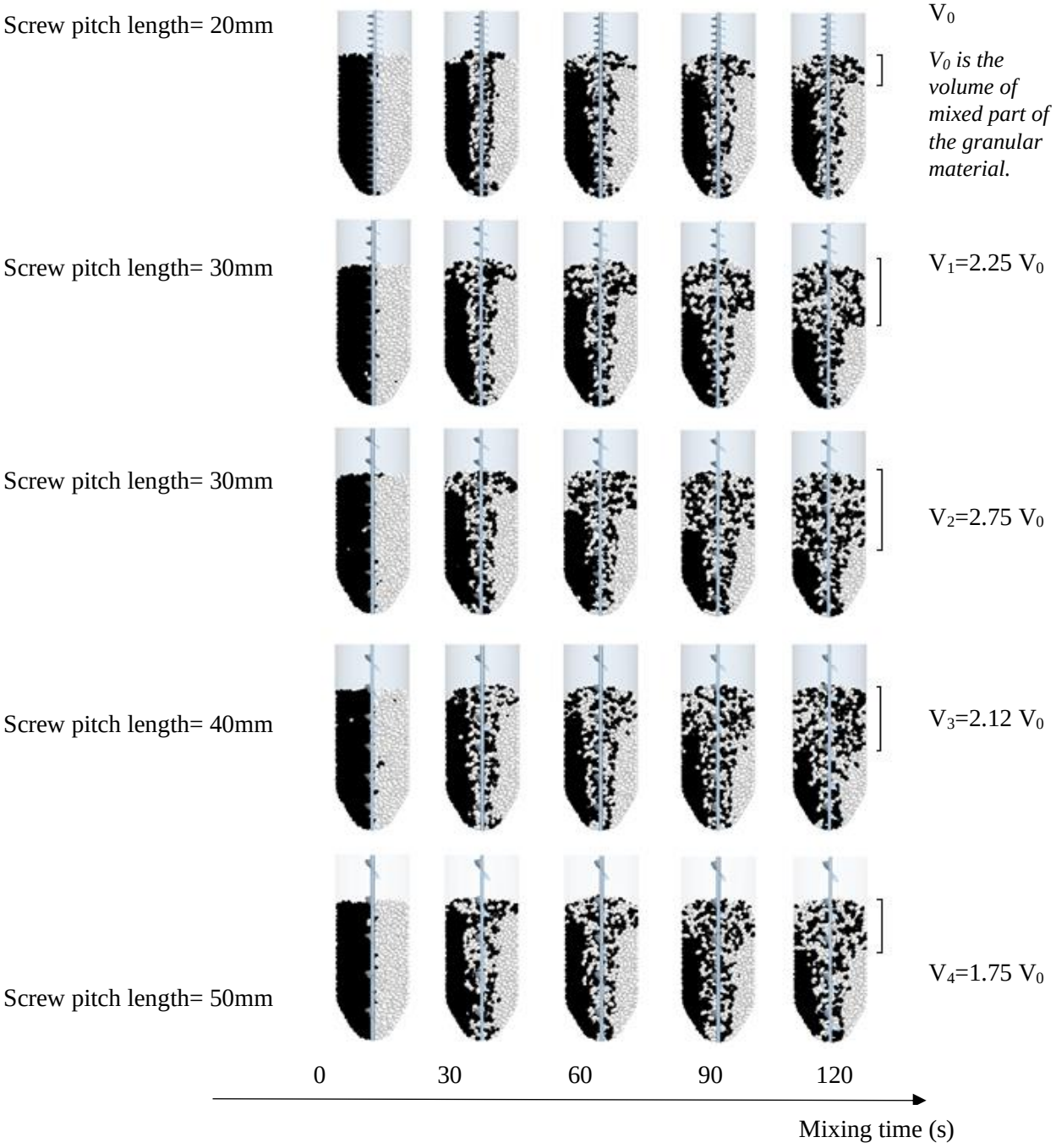

Fig. 4.3. Series of internal structures of the mixture along mixing time when using different screw pitch dimensions

Snapshots of the midplane of particles reveal that the homogeneity is at its maximum when using a screw pitch length of 30 mm and the homogeneity is at its minimum when using a screw having a 10 mm screw pitch length. Also, increasing the length of the screw pitch above 30 mm adversely impacts the mixing quality as revealed when using 40 mm and 50 mm screw pitches.

Furthermore, I calculated the average mixing index in function of the screw pitch length to average particle radius ratio for an elapsed simulation time t=20s (Fig. 4.2), where results revealed that the mixing uniformity reached a peak at X=15 while increasing this value doesn't improve the mixing

I found that the best mixing effectiveness in terms of mixing uniformity in the screw mixer is based on the screw pitch length and particle average radius rapport which can be approximated using the following polynomial equation.

$$I(X) = -0.0019X^2 + 0.0521\,X + 0.1362 \tag{46}$$

Where: $I(X)$: Nearest neighbor mixing index [-], X: Screw pitch length to average particle radius ratio [-]. The equation is valid on the condition that X ranges from 3.75 to 18.75, and the coefficient of determination is 0.985.

4.2.1.4. Effect of screw diameter

Considering the results obtained from the previous section, I evinced the optimal length of the screw pitch. I furthered a simulation with this optimal value and having a bigger screw diameter to check the differences.

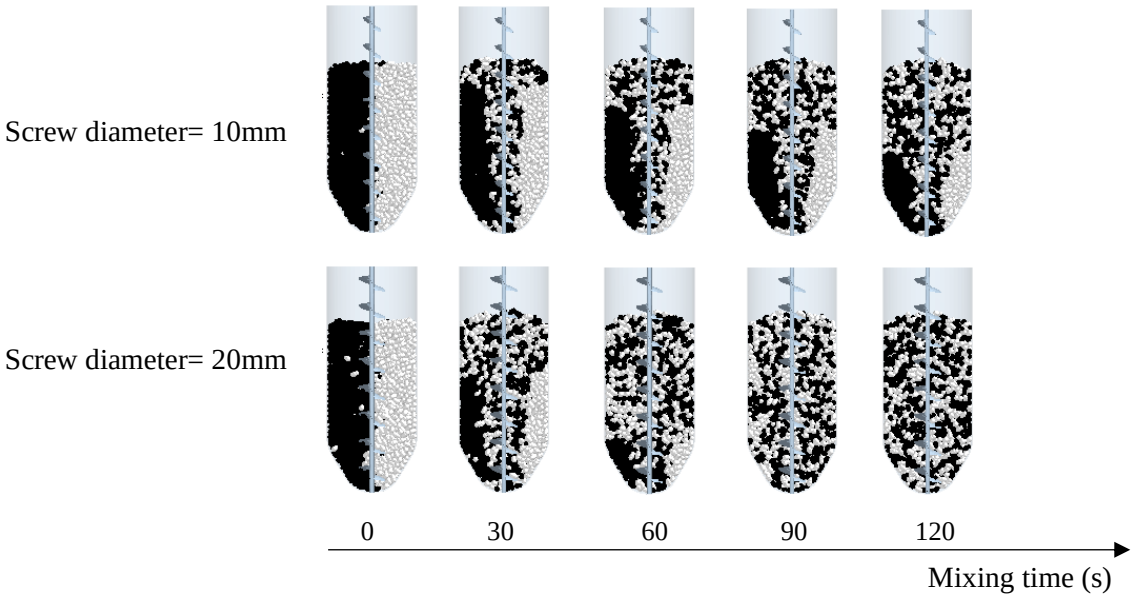

Fig. 4.4. Series of internal structures of the mixtures along mixing time when using different screw diameter dimensions

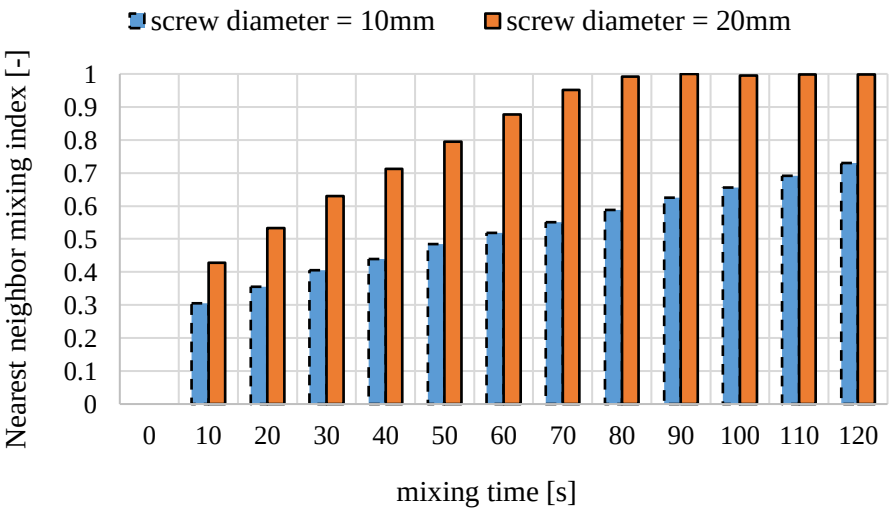

Fig. 4.5. Mixing index curves in terms of mixing diameter

As done before, I screened the internal structures and the evolution of the mixing indices curves. Distinctly, results showed that using a 20 mm screw diameter gives a better mixing quality to the same mixing time.

4.2.1.5. Effect of screw rotational speed

The velocity of the screw has an important impact on the mixture. Intuitively, a low rotational speed of the screw would lead to less uniformity among the mixed particles. In addition, high screw rpm could damage the quality of grains due to excessive shear, thus an 80 rpm screw velocity was set as an upper limit. The afore-cited intuitive approach has been confirmed by calculating the mixing indices for various screw rotational velocities (Fig. 4.6). Furthermore, the curves depict the optimal mixing time that should be pre-set, for instance, mixing of the material above 70 s at 60 rpm is unnecessary as over-mixing is time-consuming and costly.

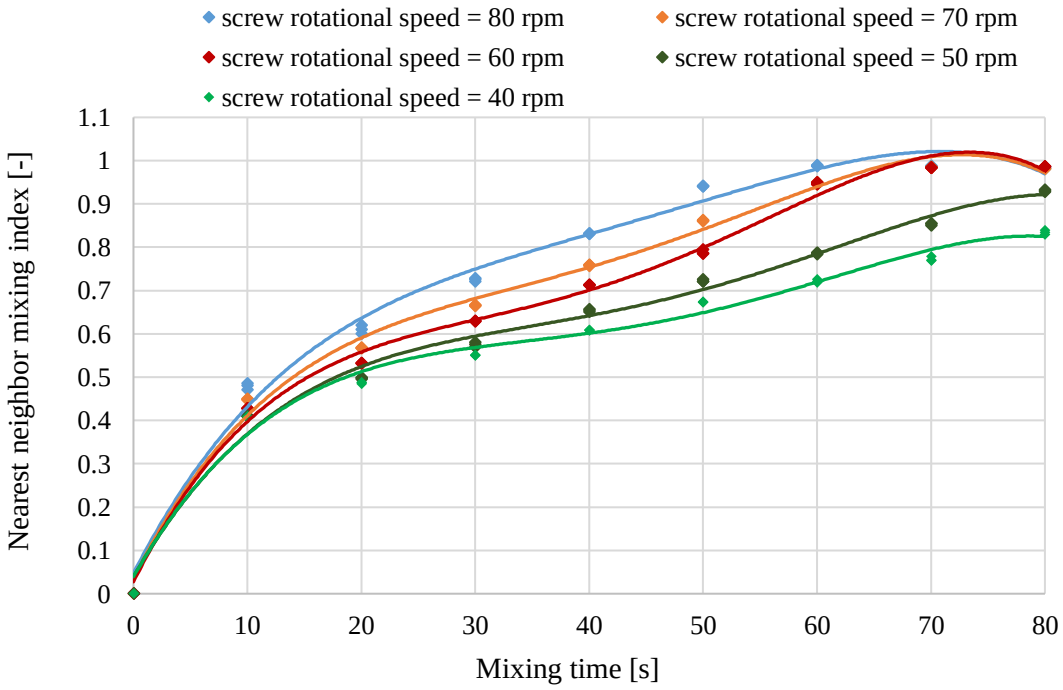

Fig. 4.6. Mixing index curves in terms of screw rotational speed

4.2.2. Paddled screw mixer

4.2.2.1. Qualitative analyses

The clipping function in EDEM® would let us see the arrangement of the particles from the interior of the material bed. Screenshots were taken each 10 seconds of the mixing time (Fig. 4.7). There were no significant differences between the different screw-mated-paddles tilt angle configurations, however, the most marked observation to emerge from visual observation was the state between mixed particles with a normal screw and the number of mated paddles to the screw axle.

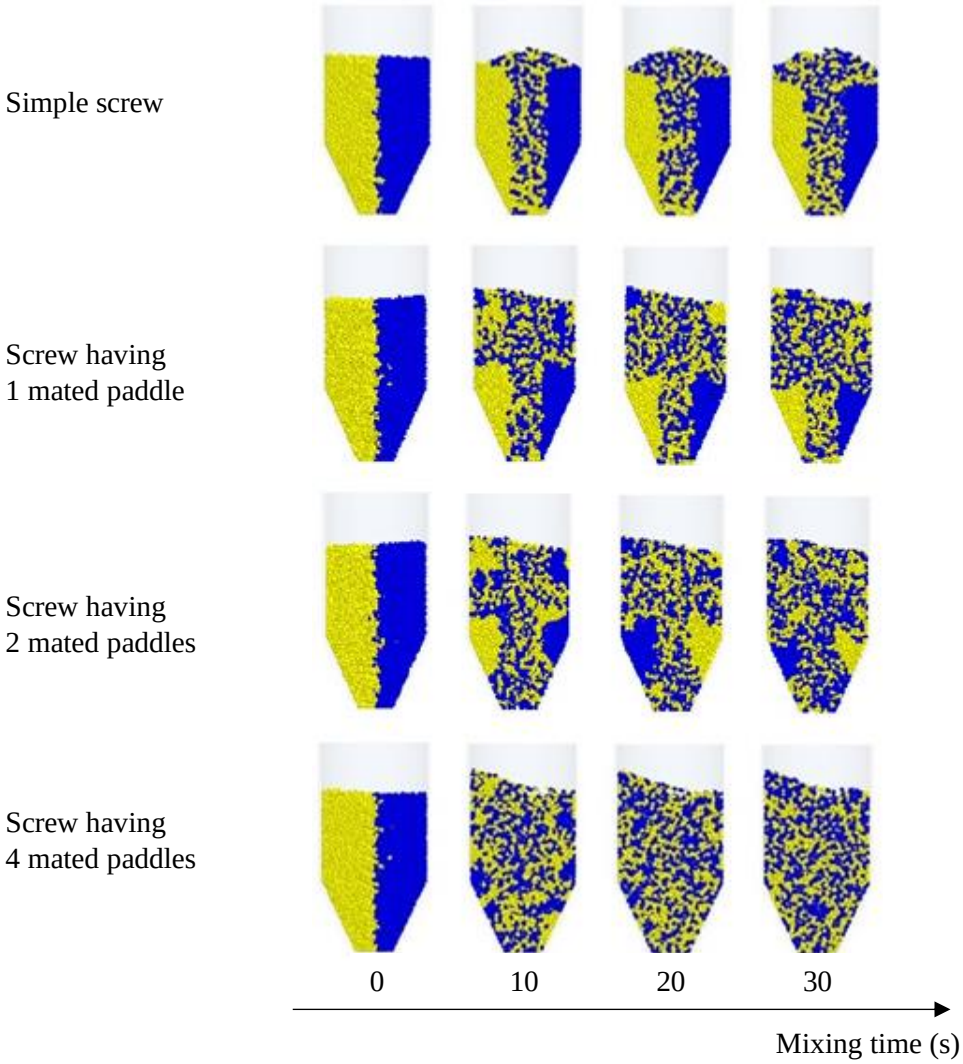

Fig. 4.7. Series of screenshots comparing particles displayed in the middle of the mixer when using a simple screw and screw having 1, 2, and 4 horizontal paddles, all tilted by 70° along with simulations.

Some dead regions exist in the mixer wall vicinity when using a normal screw because only particles in the vicinity of the screw were moving upright toward the material bed surface. The mated paddles have drastically improved the mixture by letting particles move in all the mixer regions. Further analysis of particle velocity has been assessed (Fig. 4.8). It is obvious that 4 mated paddles to the screw axle have improved the mixture homogeneity.

The fringes of particle velocity at the end of the process showed that the average velocity of particles is much higher when using paddles. This result has further strengthened our trust in the mated horizontal paddles to transform the dead zones into active zones, hence improving the whole mixture.

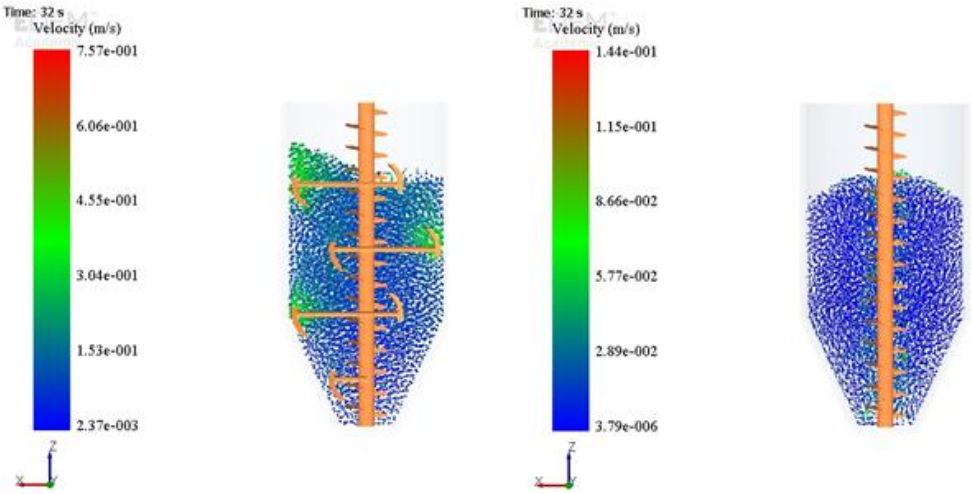

Fig. 4.8. Velocity distribution of particles in case of mixing with screw-mated-paddles (4 paddles) and a normal screw

4.2.2.2. Quantitative analysis

To quantitatively describe the mixing degree of the binary mixture, the described lacey mixing index in the previous chapter was utilized. Fig. 4.9 shows the variation of the Lacey index over time for a simple screw and screw having a different number of mated paddles to the screw axle and Fig. 4.10 shows the evolution of the lacey mixing index when using 4 mated paddles to the screw having 20°, 45°, and 70° tilt angles. The value of the lacey mixing index was calculated for every rotation in all simulations. The steady state was reached at 20 s mixing time after which the index varies slightly. The curves reveal that mixing in the hopper bottom mixer with screw-mated-paddles is much better than that without mated paddles, yet the mixer using 4 paddles mated to the screw axle showed relatively high efficiency to mix the particles, however, the paddles tilt angles had no important impact on the mixture.

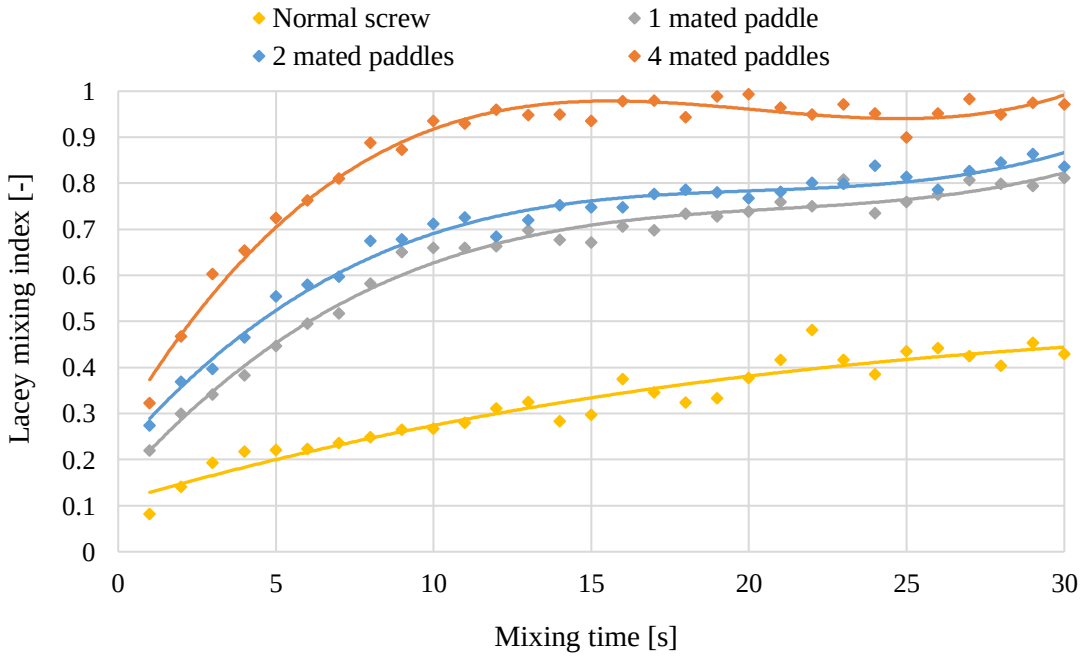

Fig. 4.9. Evolution of the Lacey mixing index from an initially unmixed state for different numbers of paddles mated to the screw axle

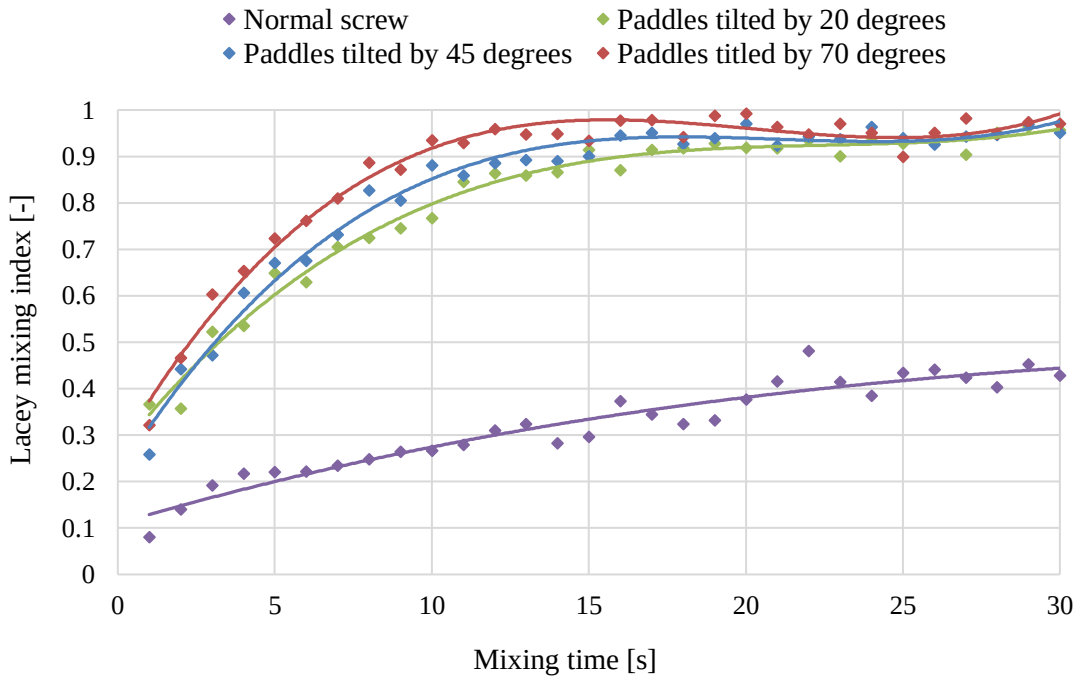

Fig. 4.10. Evolution of the Lacey mixing index from an initially unmixed state for different tilt angles of the mated paddles

4.2.3. Drum mixer

To check the reliability of the drum mixer DEM model, I conducted three simulations with the same parameters set used by Soni et al., (Soni et al., 2016) and I compared the distribution of particles by taking snapshots from the side of the mixer wall to the real experiments (Fig. 4.11). I applied the system concentration variance method described in section 3.10 in the previous chapter to quantitatively examine the difference between results. I used the same grid for all results with 8 cells to find the difference in the number of particles. The average difference in the system concentration variance between the experiments and the DEM simulations is the following:

- 9 % using 10 mm particles' diameter at a 4 rpm drum rotational speed (Fig. 4.12)
- 2.5 % using 5 mm particles' diameter at a 4 rpm drum rotational speed (Fig. 4.13)
- 4.5 % using 5 mm particles' diameter at an 8 rpm drum rotational speed (Fig. 4.14)

As a result, the concentration variance found proves that the DEM model has an acceptable level of accuracy and could be used to study the mixing of particles.

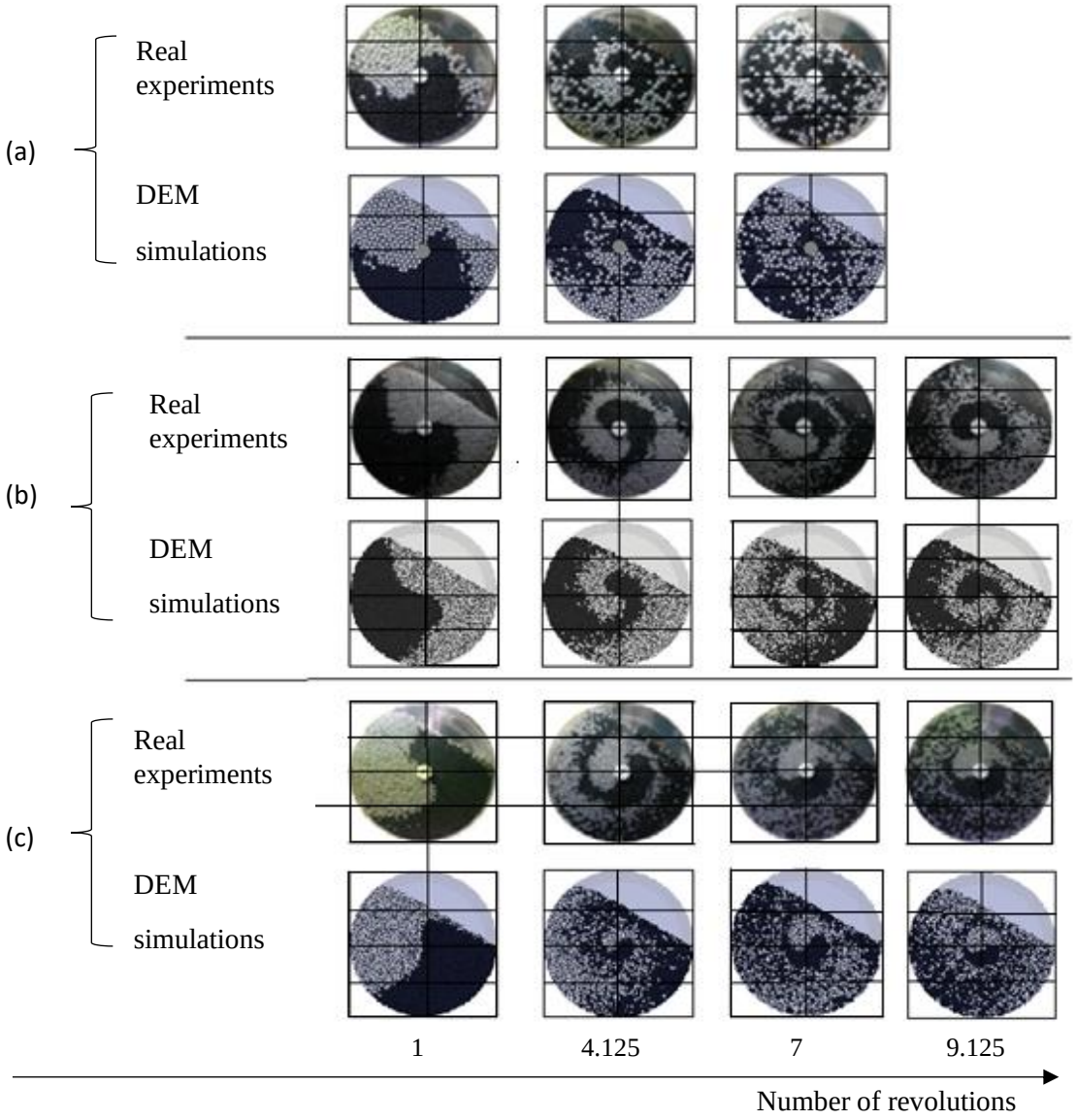

Fig. 4.11. Mixing states of real experiments obtained from literature and numerical simulations at 4 rpm drum rotational speed (a) drum rotational speed 4 rpm and particle diameter 10 mm (b) drum rotational speed 4 rpm and particle diameter 5 mm (c) drum rotational speed 8 rpm and particle diameter 5 mm

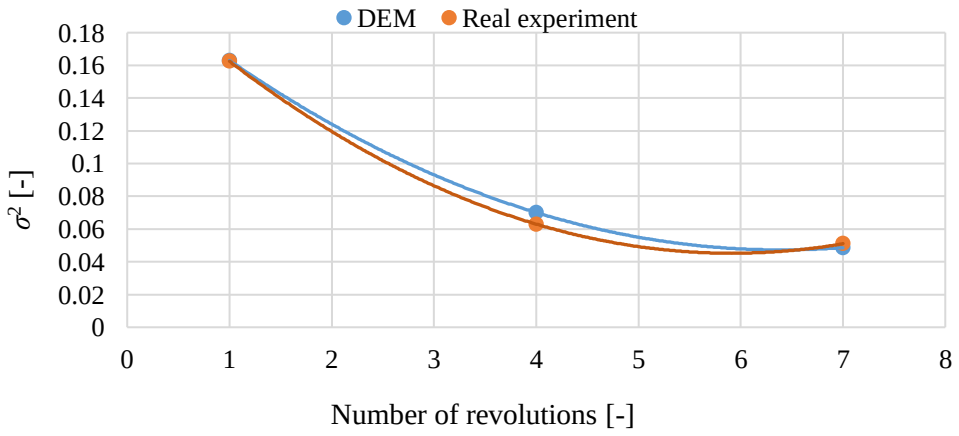

Fig. 4.12. Concentration variance of particles using 10 mm particles' diameter at 4 rpm drum rotational speed

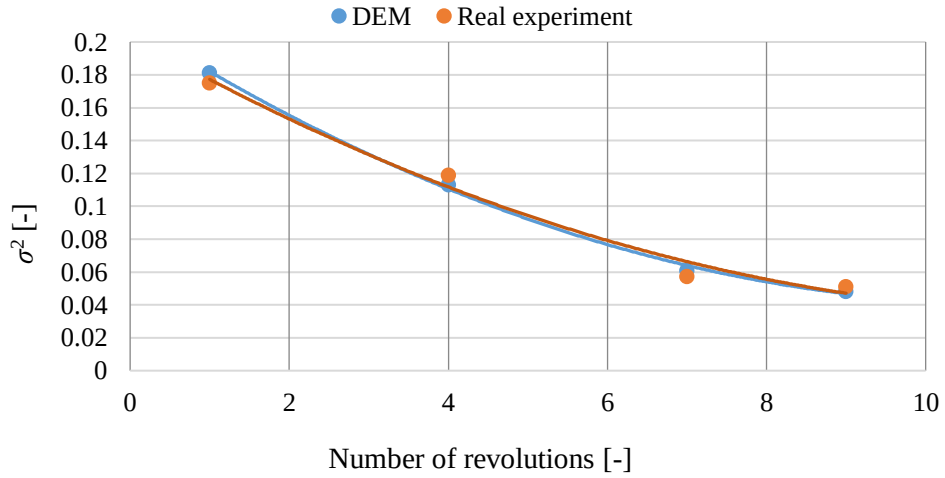

Fig. 4.13. Concentration variance of particles using 5 mm particles' diameter at 4rpm drum rotational speed

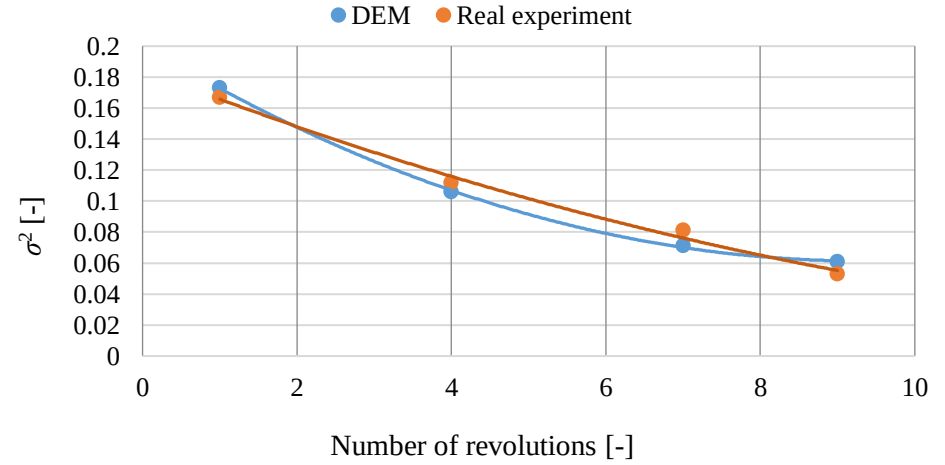

Fig. 4.14. Concentration variance of particles using 5 mm particles' diameter at 8 rpm drum rotational speed

4 groups of simulations were carried out (listed in Table 9), the first group involved 4 simulations to investigate the impact of the paddle structures shown in Fig. 3.20 on the mixture quality of mono-sized particles. An identical number of simulations were also carried out to investigate the impact of the aforementioned structures when mixing particles having different sizes. Then, 7 more simulations were conducted by varying the rotational speed of the best drum structure obtained to improve the mixing quality of bi-disperse particles and find an optimal mixing model and speed for the drum. Finally, I furthered a sensitivity analysis of the mixture homogeneity on the coefficient of rolling friction by conducting numerical experiments at various values of the rolling friction coefficient. Results were post-processed by reading files generated from LIGGGHTS® in PARAVIEW® which is an open-source, multi-platform data analysis and visualization application. The state of particles at a specific time could be visualized either near the mixer wall or in the middle of the mixer by clipping the 3D model. Also, I could track particles' velocity and their exact locations.

4.2.3.1. Mixing of mono-disperse particles

Fig. 4.15 shows the variation of the mixing rates through mixing time for the different drum set-ups. Mixing uniformity improves as it approaches 1, hence reading the graphs reveals that "Configuration C" (all configurations are described in Fig. 3.20) of the drum enhanced the mixture quality. This could be explained by the approach that both particles near the mixer wall and paddles received maximum energies induced by them to improve the granular assembly, resulting in a diffusive mixing. Thus, paddles avoided dead zone formation in the middle of the mixer because without them in the mixer, little energy would be received among particles far away from the mixer wall.

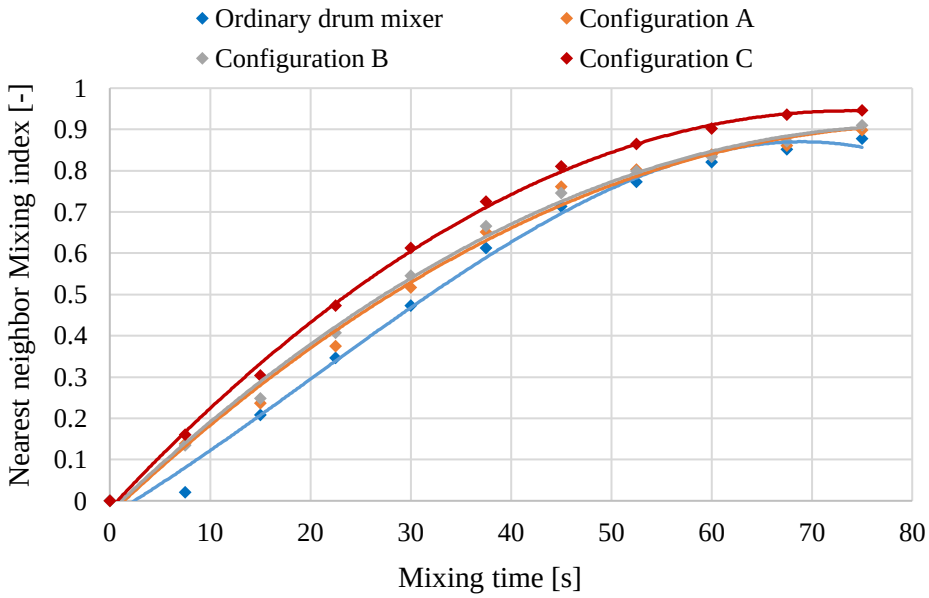

Fig. 4.15. Variation in the overall mixing index of mono-disperse material bed during 75 s of mixing

4.2.3.2. Mixing of bi-disperse particles

In this part, I tackled the mixing of unequally sized particles. In this case, three mechanisms should be deemed: convection, diffusion, and segregation. The first two mechanisms sustain mixing. Convective mixing is also known as macro mixing which helps the granular material bed to turn around the mixer frame from one side to another and diffusive mixing involves the random displacement of a particle within a material bed, letting particles change their position relative to one another. However, segregation (the opposite term of mixing) disfavors mixing due to the so-called stratification phenomenon, as smaller particles tend to slip down the material bed through the voids between larger particles. This has been elucidated due to the uneven displacement of larger particles against smaller particles during mixing (Yong-Zhi et al., 2008). Because of segregation mechanism could arise, then an appropriate mixing time should be selected to avoid insignificant over-mixing.

Simulation cases 5 to 8 described in Table 9 were conducted. In the interest of improving the mixing state, various numbers of paddles, as described in section 4.2.3, were installed in the middle of the mixer along the axis to intensify particle mixing. Fig. 4.16 shows how the homogeneity index of the binary system evolves during mixing time for the different drum set-ups.

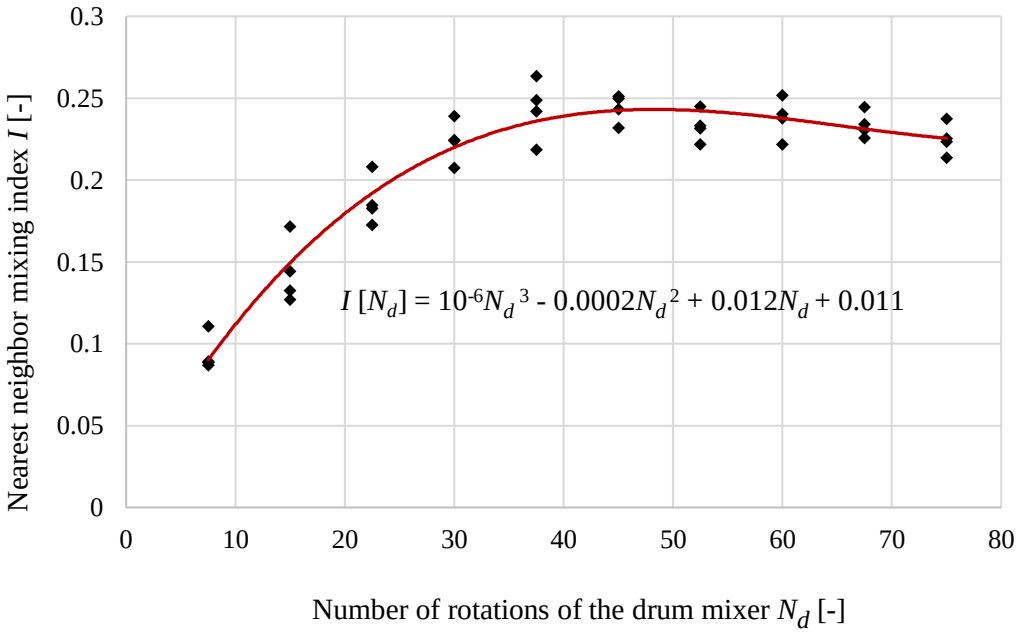

Fig. 4.16. Variation in the overall mixing index of bi-disperse (diameters are 10 mm and 5 mm) particles for different rotations of the paddled drum mixer

While mixing a bi-disperse material bed at 60 rpm fixed rotational speed, a mixing to de-mixing transition can be perceived from the curves of the mixing indices for all types of paddled drum mixers. Mixing beyond the optimal number of rotations causes de-mixing for all configurations, independently of the shape and spatial configuration of the paddles.

Using regression analysis, I obtained the following polynomial equation:

$$I(N_d) = 10^{-6}{N_d}^3 - 0{,}0002{N_d}^2 + 0.012N_d + 0.011. \quad (47)$$

Where: $I(N_d)$: Nearest neighbor mixing index [-], N_d: Number of rotations of the drum mixer [-]. This result is valid for ordinary drum mixer and all paddled mixer configurations from 7 to 75 rotations of the mixer. The coefficient of determination is 0.936.

Among the advantages of the discrete element method, I can visualize particle distributions in the middle of the mixer. Observations of occupancy snapshots in the middle of the drum were described in Fig. 4.17. It can be seen from these snapshots that smaller particles tend to compact in the middle of the whole material bed, elucidating the low mixing degrees obtained even though paddles were being used in the drum.

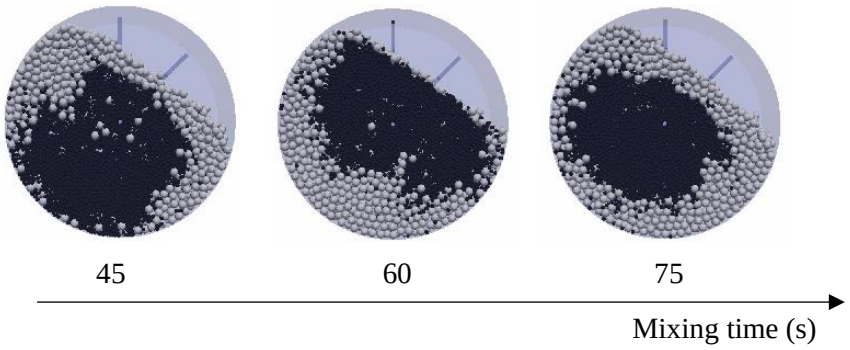

Fig. 4.17. Variation in the overall mixing index of bi-disperse material bed during 75s of mixing

4.2.3.3. Optimal rotational mixer velocity

According to results obtained in the previous sub-sections, it is obvious that the mixing of bi-disperse particles is rather complex and requires enhancement. For this purpose, I furthered simulations by gradually increasing the drum speed from 8 rpm to 16 rpm, 24 rpm, 32 rpm, 40 rpm, 48 rpm, 60 rpm, and 80 rpm. Related homogeneity indices along the mixing process were calculated as average for an elapsed mixing time of 80 s and illustrated in Fig. 4.18.

By increasing the drum speed, the mixture quality improves, whereas increasing the drum speed above 60 rpm is inefficacious as confirmed at 70 rpm and 80 rpm.

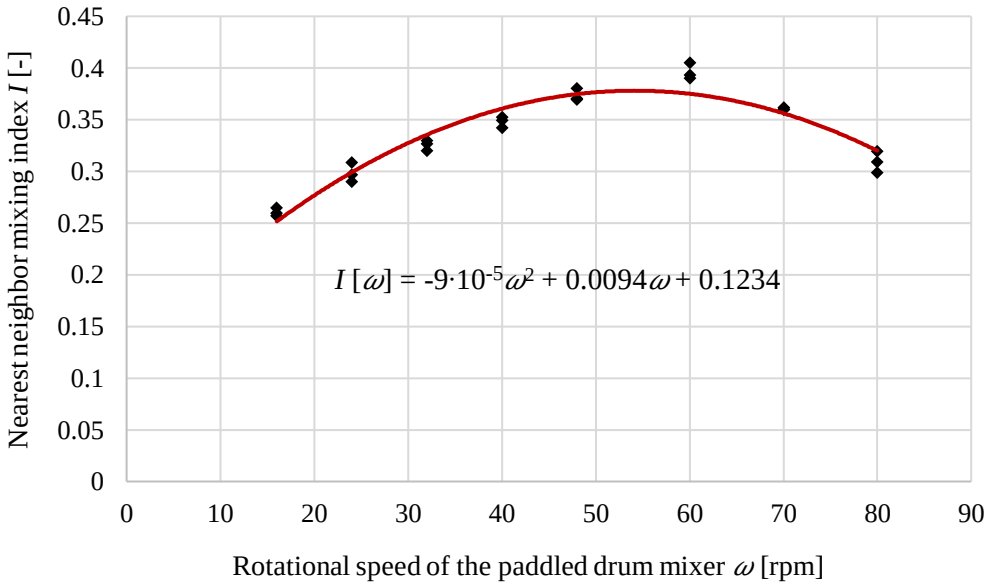

Fig. 4.18. Optimal number of rotations of the drum mixer for 80s fixed mixing time

I found that in a paddled drum mixer the mixing uniformity increases until it reaches the peak based on an optimal number of rotations of the drum mixer, while further increasing the number of rotations of the drum will result in a deficiency of the mixing efficiency.
Using regression analysis, I obtained the following polynomial equation:

$$I(\omega) = -9 \cdot 10^{-5}\omega^2 + 0.0094\omega + 0.1234. \quad (48)$$

Where: $I(\omega)$: Nearest neighbor mixing index [-], ω: rotational speed of the drum mixer [rpm]. The equation is valid on the condition that n ranges from 15 to 80 rpm. The coefficient of determination is 0.916.

4.2.3.4. Sensitivity study of the mixing index on the rolling friction

I furthered numerical experiments to investigate the impact of the rolling friction on the mixture homogeneity in the drum mixer. According to previous studies about the mixing of glass spheres in drums, the coefficient of rolling friction didn't exceed 0.01 between particles (Huang et al., 2021; Marigo et al., 2012).

I studied the impact of the rotational friction on the mixing by systematically changing the rolling friction value ranged between 0.001 to 0.1. Fig. 4.19 shows the results of the mixing indices for the different above-mentioned values of the coefficient of rotational friction. The mixing time was

set at 25 seconds because previous results of the bi-disperse mixture with the 'configuration C' mixer design showed that 60 rpm is the optimal speed of the drum and particle uniformity at this speed did not give rise to an increase after 25 s as it reached a steady state. Each value of the mixing index plotted in the graph is the average value of the indices calculated every 5 seconds of mixing time for every simulation. Results revealed that the coefficient of rotational friction has little to no effect on the mixture uniformity of particles in the cylindrical drum when mixing glass beads.

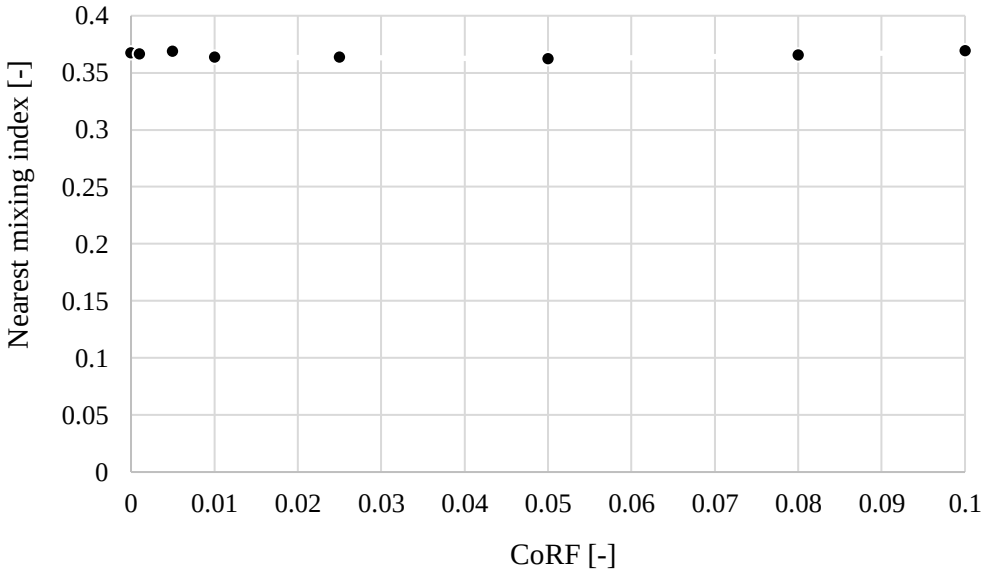

Fig. 4.19. Variation of the average mixing index in relation to the coefficient of rolling friction (mixing of bi-disperse material case in "configuration C" set up of the mixer at 60 rpm drum speed)

4.2.4. Single shaft paddle mixer

In this part, I investigated the effects of filling configuration and the number of paddles on the mixing rate in a single shaft paddle mixer. I used bi-colored corn grains as solid particles, and I employed discrete element simulations using LIGGGHTS-PUBLIC®. To calculate the static friction, rolling friction, and the coefficient of restitution, I performed box discharging technique. The coordinates-based mixing rate so-called nearest neighbor index was employed to quantitatively examine the different mixing rates along the mixing period according to the variables: filling type and paddles number.

4.2.4.1. Reliability of the single shaft mixer DEM model

To verify the effectiveness of the developed discrete element models, such correlations with real experiments should be found. Invasive sampling techniques are available by thrusting a probe into the mixture either during the mixing operation or at definite mixing intervals by stopping and relaunching the mixing. This method is ineffective as the interaction of the thrust apparatus in the granular bed would impact the particles distribution and similarly when the mixture is interrupted by stopping it several times during the process. An alternative better method is a non-invasive technique. By just analyzing the surface layer of the material in the mixer, I can recognize the similarity rate. For example, in this study I used a high-speed camera to take snaps from the top of the mixer without interrupting the operation, then I analyzed the captured snaps. I divided each capture into 8 cells (Fig. 4.20), and the same for the DEM model. I examined the effectiveness of

the DEM model by checking on the one hand the distribution similarity of yellow particles in each cell. I found an average similarity of 95 % when analyzing snaps captured every 5 s which proves the reliability of our DEM models.

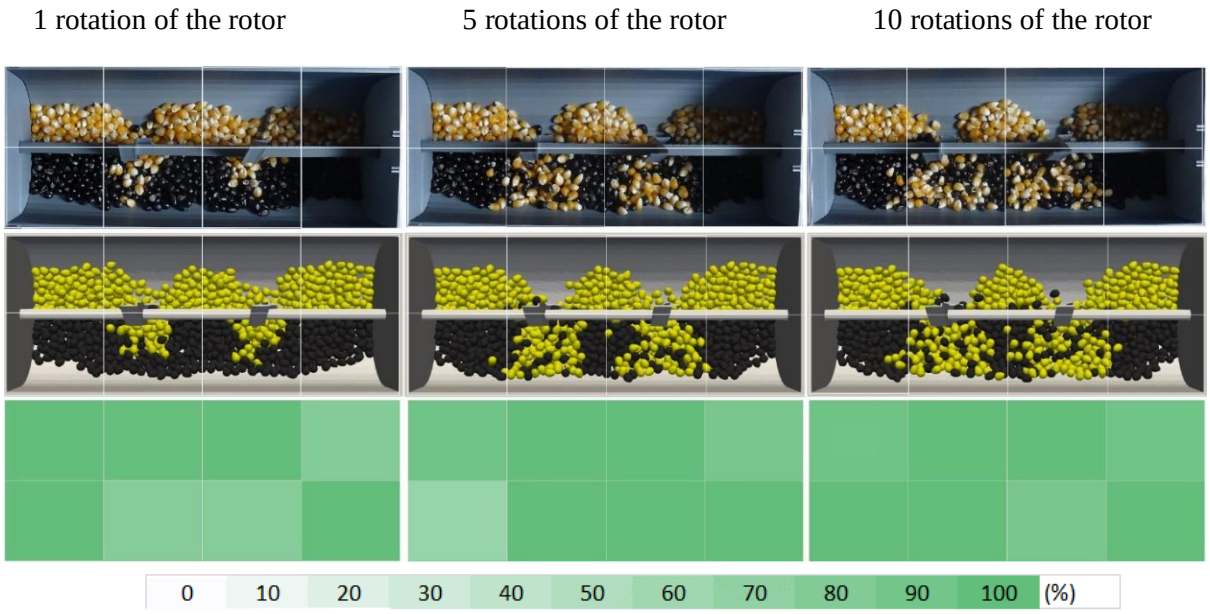

Fig. 4.20. comparison of particle distribution in the mixer with the DEM simulation

On the other hand, I varied the capture speed as follows: 1 image per second, 1 image per 2 seconds, 1 image per 3 seconds, 1 image per 4 seconds, and 1 image per 5 seconds. Applying the quantification of the image analysis described in section 3.11 based on particle variance, the regression lines obtained are shown in Fig. 4.21. The average variance between the two curves is around 5.1 % which confirms the reliability of the DEM model.

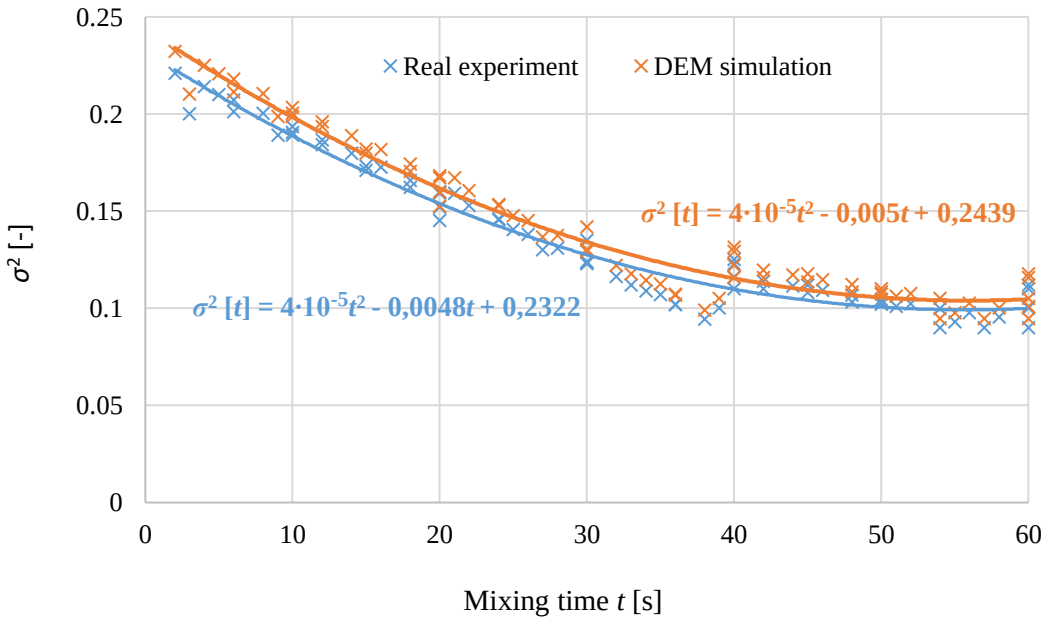

Fig. 4.21. Comparison of mixing curves determined by particle concentration variance

4.2.4.2. Effect of the shape of paddles

I used two different geometries of the paddles illustrated in Fig. 4.22. I conducted two simulations corresponding to run 1 and run 2 in Table 13 with the same particles and mixer configurations, then I calculated the mixing indexes. Results showed that those paddle shapes had no important impact on the mixture uniformity.

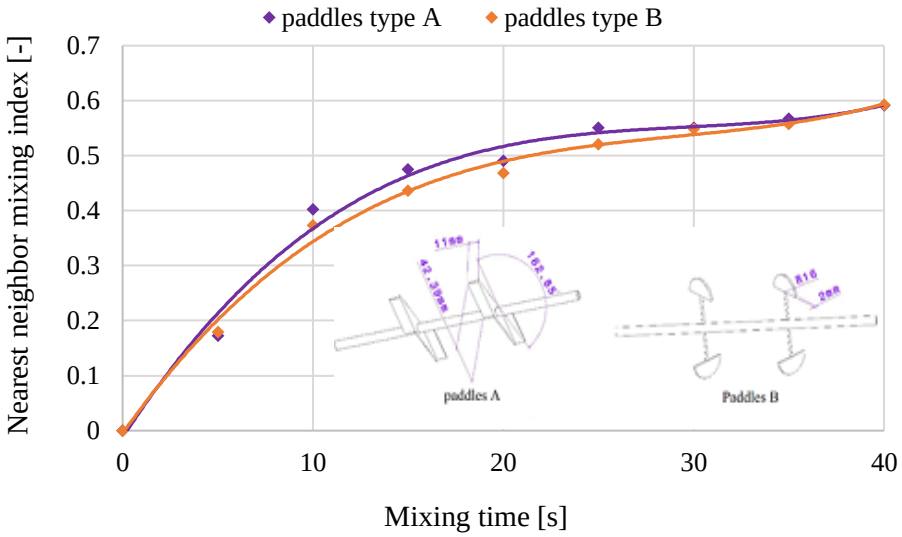

Fig. 4.22. Influence of paddles' shape on the mixing index

4.2.4.3. Effect of number of paddles

The second set of simulations tackled the effect of the number of paddles on the mixing rate. The various number of paddles, while the same shape of paddles was maintained. The distance between every two paddles and between the mixer wall and the paddle are all identical (Fig. 8.3 in Appendix 3).

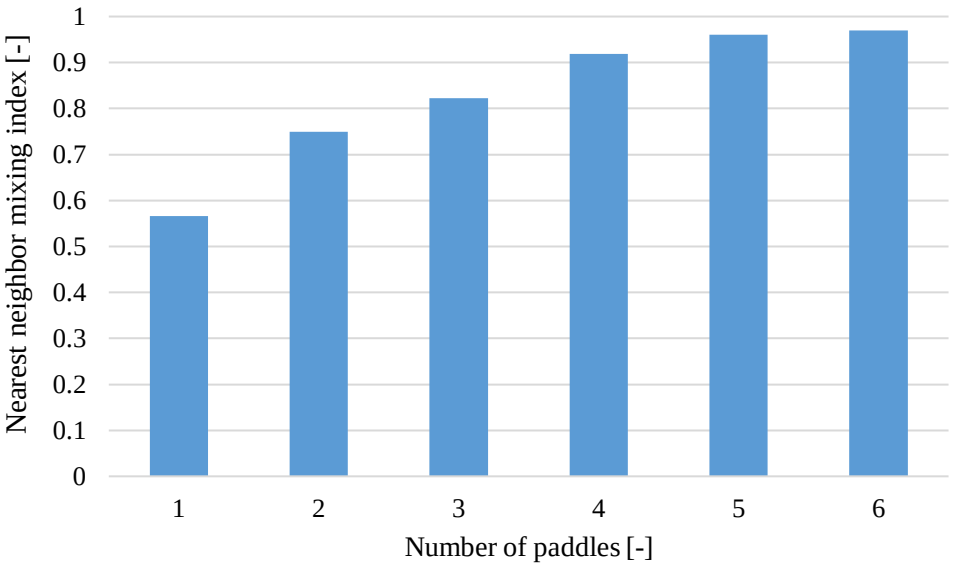

Fig. 4.23. Effect of paddle number on the mixing efficiency

The best mixing index is achieved when using more paddles (Fig. 4.23) while using more than 6 paddles is unnecessary as the difference between 5 and 6 paddles on the mixing index is trivial (around 0.9 % difference as average). The calculated mixing index for every number of paddles used is the average in 90 s mixing time.

The improvement of the mixing rate is achieved because of the elimination of dead zones when using more paddles in the mixer. Fig. 4.24 shows a comparison of the dead regions formed in the mixer when using 2 paddles and 5 paddles after 10 rotations of the paddles and the mixing paddles' rotational speed is fixed at 10 rpm.

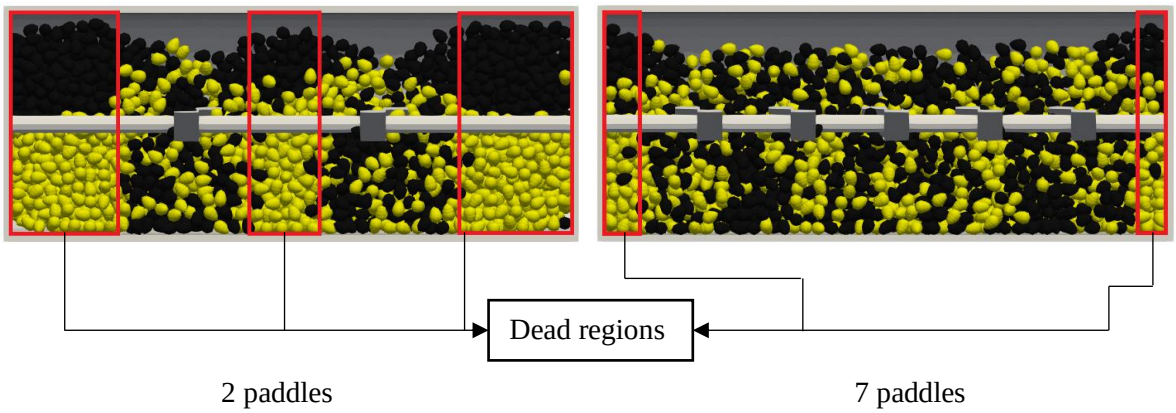

Fig. 4.24. Size of dead regions after 25s mixing time at 10 rpm of the paddles.

4.2.4.4. Effect of grains initial configuration

In this part, I investigated the impact of the initial state of the loaded grains on the mixing index (Fig. 4.25). The first type of filling so-called side-by-side where a cross-sectional splitter is placed and each type of particle is loaded from each section along the mixer, while the second type so-called top-bottom filling where one type of particle is loaded all around the mixer until stagnation, then the other type of particles is loaded on the top of it. The latter is more practical to operate.

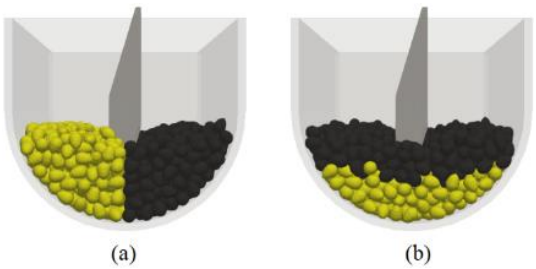

Fig. 4.25. Particles' initial configuration. (a) side-by-side (b) top-bottom

The calculated mixing indexes show that the top-bottom initial filling type accelerates the time of mixing. The best mixing rate is reached at around 12 s mixing time, whilst almost the same mixing rate is achieved at 60 s mixing time in the side-by-side initial filling case. The convective blending resulting in the motion of grains by the force actions from the paddles in the top-bottom filling case would allow grains to move laterally, yet the grains from the top layer would percolate down the mixer in a way that the two types of grains combine swiftly.

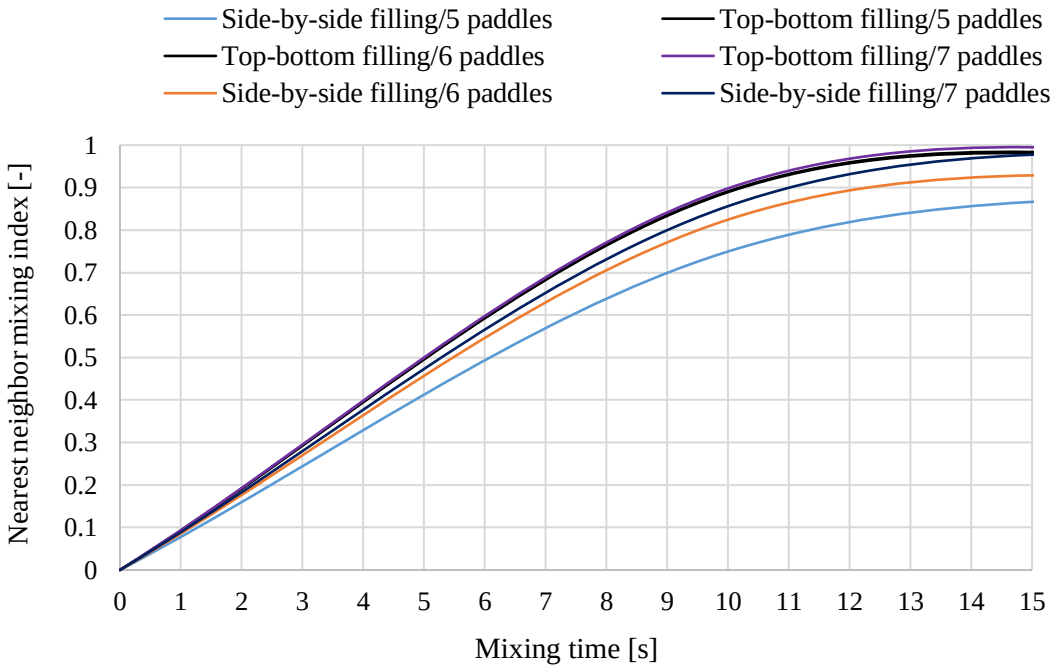

Fig. 4.26. Effect of initial particles filling on the mixing index

4.2.4.5. Mixing of bi-shaped particles

In this part, I studied the mixing of bi-shaped. I used the shapes illustrated with the dimensions in Fig. 4.27. The rotational speed of the paddles was kept constant at 10 rpm. I found that the mixing efficiency of those bi-shaped particles is reached at 2.5 rotations.

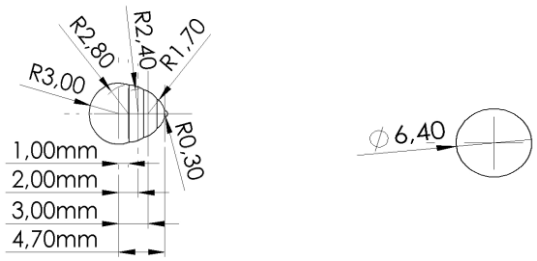

Fig. 4.27. Shape and dimensions of mixed particles

There is an optimal paddle rotation number when mixing bi-shaped particles in the single-shaft paddle mixer to reach the best mixture uniformity while overrunning this number of rotations leads to particle segregation. The mixing efficiency can be approximated using the following polynomial equation:

$$I(N_r) = -0.05424\ {N_r}^2 + 0.259\ N_r - 0.1149 \quad (49)$$

Where: $I(N_r)$: Nearest neighbor mixing index [-], N_r: Number of rotations of the paddles [-]. The equation is valid for 0.7 to 3.5 rotations of paddles. The coefficient of determination is 0.979.

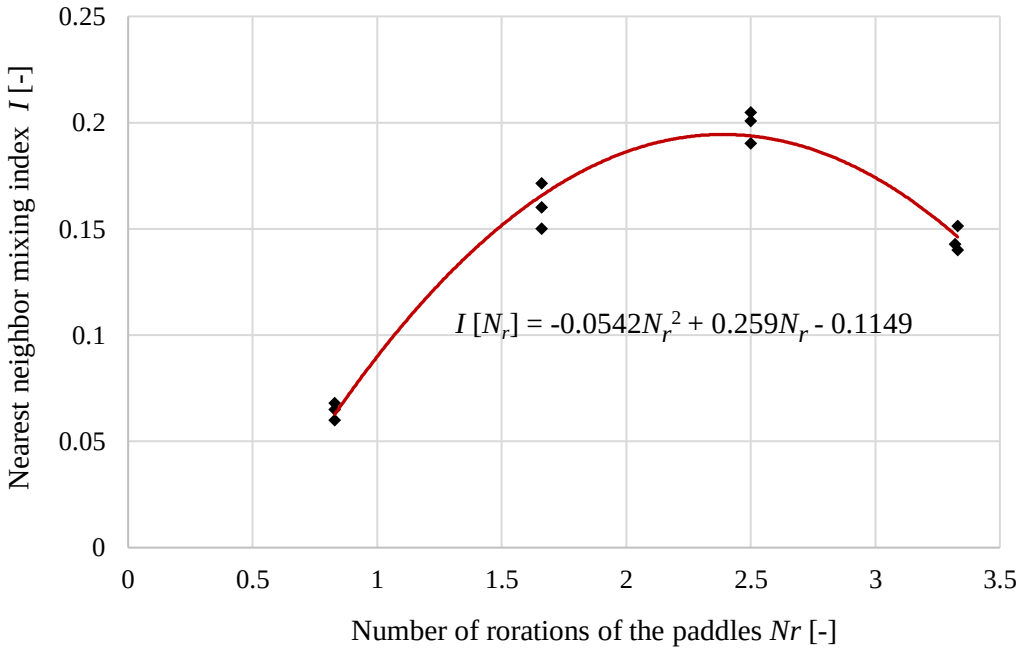

Fig. 4.28 . Optimal number of rotations of the paddles when mixing bi-shaped particles

4.3. New scientific results

4.3.1. Mixing efficiency of a screw mixer with screw pitch length in relation to particle size

I found that the mixing effectiveness in terms of mixing uniformity in the screw mixer based on the screw pitch length and particle average radius rapport can be approximated using the following polynomial equation.

$$I(X) = -0.0019X^2 + 0.0521\,X + \ 0.1362. \tag{50}$$

Where: $I(X)$: Nearest neighbor mixing index [-], X: Screw pitch length to average particle radius ratio [-]. The equation is valid on the condition that X ranges from 3.75 to 18.75, and the coefficient of determination is 0.985.

4.3.2. Optimal number of rotations of the ordinary and paddled drum mixer

I have identified that while mixing a bi-disperse material bed, a mixing to de-mixing transition can be perceived from the curves of the mixing indices for all types of paddled drum mixers. Mixing beyond the optimal number of rotations causes de-mixing for all configurations, independently of the shape and spatial configuration of the paddles.

Using regression analysis, I obtained the following polynomial equation:

$$I(N_d) = 10^{-6}{N_d}^3 - 0{,}0002{N_d}^2 + 0.012N_d + 0.011. \tag{51}$$

Where: $I(N_d)$: Nearest neighbor mixing index [-], N_d: Number of rotations of the drum mixer [-]. This result is valid for ordinary drum mixer and all paddled mixer configurations from 7 to 75 rotations of the mixer. The coefficient of determination is 0.93.

4.3.3. Optimal paddled drum mixer rotational speed

I found that in a paddled drum mixer the mixing uniformity increases until it reaches the peak based on an optimal number of rotations of the drum mixer, while further increasing the number of rotations of the drum will result in a deficiency of the mixing efficiency.
Using regression analysis, I obtained the following polynomial equation:

$$I(\omega) = \ -9 \cdot 10^{-5}\omega^2 + 0.0094\omega + 0.1234. \tag{52}$$

Where: $I(\omega)$: Nearest neighbor mixing index [-], ω: rotational speed of the drum mixer [rpm]. The equation is valid on the condition that ω ranges from 15 to 80 rpm. The coefficient of determination is 0.916.

4.3.4. Optimal number of paddles in the single shaft paddled mixer

I determined that the mixing index increases during the mixing of mono-shaped particles in the single-shaft paddle mixer when the number of paddles increases, while there is no reason to increase the number of paddles above 5 as the mixing index doesn't increase using more paddles. This phenomenon is related to the dead zone arising around the moving paddles, as by increasing the number of paddles, the possible size of dead zones is decreasing.

4.3.5. Optimal number of rotations of the paddles in the single-shaft paddle mixer

I found that there is an optimal paddle rotation number when mixing bi-shaped particles in the single-shaft paddle mixer to reach the best mixture uniformity while overrunning this number of rotations leads to particle segregation. The mixing efficiency can be approximated using the following polynomial equation:

$$I(N_r) = -0.05424\ {N_r}^2 + 0.259\ N_r - 0.1149. \quad (53)$$

Where: $I(N_r)$: Nearest neighbor mixing index [-], N_r: Number of rotations of the paddles [-]. The equation is valid for 0.7 to 3.5 rotations of paddles. The coefficient of determination is 0.979.

5. CONCLUSIONS AND RECOMMENDATIONS

The conclusions of the study concerning mixing enhancement of wheat particles in a hopper bottom screw mixer are the following:

- This two-part study featured qualitative and quantitative assessments of wheat grain mixing. The material was mechanically mixed using a hopper bottom screw mixer under various screw geometric shapes and different orientations of horizontal paddles assembled to the screw axle. Snapshots were captured across the entire periphery of the screw mixer to show the critical characteristics of the mixed materials. It was determined that screw-mated-paddles increased the mixing homogeneity. Furthermore, 4 paddles mated to the screw axle improved the mixing homogeneity compared to other paddles configurations. In case no paddles were used, I found that when the screw pitch length to particle average ratio is 15, the mixing homogeneity reaches the maximum.
- Despite that the qualitative study gives important findings and it does provide an insight into the internal structure of the mixed material, there is a quite limitation of this optical visualization method because it does not provide information to justify the observations. For instance, when many particles are considered, the ratio of the volume to surface area will increase drastically, however, when using laboratory-scale experiments, then it could be a reasonable possibility. Therefore, a quantitative study has been performed in section 4.2.2 by calculating the Lacey mixing index.
- The best mixing index is achieved when using the screw pitch length to average particle radius ratio equals 15. This value improved the mixing uniformity by 11 % compared to the ratio value of 18.75. This means increasing the screw pitch length would decrease the mixing efficiency.

To enhance both mono-disperse and bi-disperse particles in a cylindrical drum mixer, a number of paddles were unevenly installed in the middle of the mixer. The performance of the paddle configurations was investigated by using discrete element simulations, followed by quantitative analysis. The following conclusions can be drawn from the simulation results:

- When mixing bi-disperse granular material, the small particles are mostly located in the core of the drum, that is, the segregation mechanism dominates in the rotating drum.
- Paddles installed in the middle of the mixer related to “Configuration C” enhanced the mixture of the mono-disperse and bi-disperse mixtures by 15.36 % and 13.28 %, respectively.
- Selection of an appropriate mixing time is of vital importance to avoid de-mixing. At 8 rpm drum speed, the mixing homogeneity curve revealed that 40 s mixing time is the optimal time for mixing 5 mm and 10 mm particles.
- Mixing at 60 rpm drum rotational speed in 75 seconds of mixing time has improved the homogeneity of the mixture by 33.87 %, 24.53 %, 16.89 %, 11.08 %, and 5.76 % compared to 16 rpm, 24 rpm, 32 rpm, 40 rpm and 48 rpm, respectively. However, increasing the drum rotational speed adversely impacted the mixing quality as setting the drum at 80 rpm worsened the mixture quality by 2.45 % and 21.32 % compared to 70 rpm and 60 rpm mixer speed, respectively.
- When mixing a bi-disperse material bed at 60 rpm fixed rotational speed, a mixing to de-mixing transition is obtained. Mixing beyond the optimal number of rotations which is 45 causes de-mixing for all configurations, independently of the shape and spatial configuration

of the paddles. An improvement of the mixture uniformity of 10.5 % is achieved at 45 rotations compared to 52.5 rotations of the mixer.
- Sensitivity analysis showed that a maximum of 4 % deviation occurred when setting a 0, 0.001, 0.005, 0.01, and 0.025 coefficient of rolling friction, asserting that the effect of the coefficient of rolling friction on the mixture quality in the drum is trivial.
- At 10 rpm fixed rotational speed, the mixing uniformity improved by 26.5 % at 2.5 rotations compared to 3.25 rotations when mixing bi-shaped particles: clumps of 5 spheres and regular spheres.

As for recommendations, this study revealed that mixing a bi-disperse material at a high filling level of the cylindrical drum is rather complex and challenging. Therefore, novel designs of the drum mixer could be effective in tackling this issue. Furthermore, the same methodology could be utilized to investigate the effect of more particle size ratios and particle shapes on the mixture quality in the drum mixer.

The impact of a number of paddles and initial particle configuration on the mixing of corn grains in a single shaft paddles mixer have been investigated using DEM simulations. The following conclusions can be drawn from our study:

- Satisfactory results were obtained when using a lower Young's moduli of the mixer wall and corn grains to speed up simulation time. This is because of the insignificant change between the average forces acted between particles and between particles and the mixer wall when compared to the DEM case with actual Young's moduli.
- Using DEM modeling to mimic a real mixing case of particles highly depends on the appropriate selection of micro-mechanical properties.
- In the 5 paddles mixer, filling one type of particles all around the mixer, then filling the other type of particles on top of it is more practical and more efficient on the mixture quality compared to the side-by-side filling configuration. The quantitative results display that the best rate of mixing is achieved at 12s mixing time, however, an almost identical mixing rate is reached at 60 s mixing time in the side-to-side initial filling structure.
- Results showed that using more paddles increases the mixing homogeneity, because less dead zones will be formed.
- The optimal number of rotations of the paddles at 10 rpm fixed rotational speed of the paddles to achieve the best homogeneity state when mixing bi-shaped particles is 2.5 rotations, while mixing above this number of rotations of the paddles leads to segregation because the mixing index decreased by 27 % when mixing the particles at 3.33 rotations of the paddles.

This study demonstrates that a lower value of Young's moduli can be used to decrease simulation time while results are reliable to mimic a real mixing case. The grain drop, pendulum collision, and box discharging experiments are effective to determine the different micro-mechanical properties. In addition, the multi-sphere approach to represent a complex shape of grains is adequate in the DEM simulation.

6. SUMMARY

MIXING EFFICIENCY OF SCREW AND PADDLE MIXERS

In the case of a mixing process of solid particles such as the mixing of pharmaceutical powders and chemical products, the main concern is that the different particles should be evenly distributed within the granular assembly. This homogeneous distribution of solid elements could only be achieved if an effective mixing operation is carried out. Therefore, adequate parameters should be set to avoid additional costs and time loss.

My study aims to build reliable DEM models that can be used in real processes to investigate the flow of particles around the mixer and to select the optimal parameters based on several factors such as particle shape, particle type, etc.

I used the discrete element method to describe mixing by mechanical means. This method is powerful and has been developed by many scientists and programmers in recent years. I used EDEM® at first in a small part then I furthered conducting simulations using LIGGGHTS® in a big part of our work because of its flexibility and the possibility to use KIFÜ's Hungarian Supercomputer to run models in a short period. In our models, I decreased the simulation time by reducing the value of Young's modulus by comparing the slope angles results. I proved that Young's modulus magnitude could be decreased to 5×10^6 Pa in a paddle mixer to significantly decrease the computational time without altering the actual result however, it is not always the case when using another type of mixers or particles (it must be always checked).

I employed mixing indices to quantity the different mixtures. This would let us know the uniformity value which ranges from 0 to 1. I coded the nearest neighbor mixing index in java to simplify the calculation, and also to have more accurate results because this method relies on the coordinates of particles inside of the mixer.

I found that the geometry of the drum mixer has an impact on the uniformity of particles. By installing paddles, the uniformity has been improved. In addition, there is an optimal rotational speed of the drum mixer to obtain the best mixture uniformity.

A better mixture homogeneity is obtained when adding horizontal paddles to the screw in a screw mixer because it would let particles move around the mixer wall. I also revealed that there is an optimal screw pitch length, and increasing its length would adversely impact the homogeneity of particles.

Modeling corn grains using the multi-sphere approach in the single-shaft paddle mixer gives acceptable results. I found that the type of particle filling influenced the homogeneity of particles, when filling one type of particle then filling the other type on top of it gave the highest uniformity rate, also there is an optimal number of rotations of the paddles when mixing bi-shaped particles.

The application of DEM in the design of mixing apparatuses is crucial for maximizing their effectiveness and efficiency. Through the simulation of particle behavior and interactions within these systems, DEM offers valuable insights into mixing dynamics. Engineers can utilize this information to refine equipment geometry, enhance mixing efficiency, and mitigate issues related to wear and damage. Such an approach, driven by simulation, not only expedites the design phase but also boosts the dependability and functionality of mixing apparatuses across diverse industrial sectors.

7. ÖSSZEFOGLALÁS (SUMMARY IN HUNGARIAN)

LAPÁTOS ÉS CSIGÁS KEVERŐBERENDEZÉSEK KEVERÉSI HATÉKONYSÁGA

Szemcsehalmazok keverése során általában a legfontosabb feladat a keverék egyenletes eloszlásának biztosítása. Ez az egyenletes eloszlás csak hatékony keverési módszerek alkalmazásával biztosítható. A költségek és a keverési idő csökkentése érdekében szükség van a keverőberendezések optimális működési paramétereinek meghatározására.

Dolgozatom célja megbízható diszkrét elemes modellek létrehozása, melyek felhasználásával modellezni lehet a keverőberendezésekben lezajló szemcsemozgási folyamatokat, és ezek ismeretében meg lehet határozni különböző keverőberendezések optimális működési paramétereit. A diszkrét elemes módszer segítéségével lehetséges a keverés során lezajló mechanikai folyamatok modellezése. A módszer rendkívül hatékony, és az utóbbi évek számítástechnikájának fejlődése lehetővé teszi alkalmazását nagy szemcseszámok esetén is.

Kutatásaim első szakaszában az EDEM kereskedelmi szoftvert használtam, majd azt követően áttértem a LIGGGHTS ingyenes szoftver használatára, amely nagyobb rugalmasságot biztosított a feladatmegoldásban, valamint a KIFÜ szuperszámítógépin is futtatható kódot generált. Kimutattam, hogy a rugalmassági modulus csökkentése jelentősen lecsökkenti a szimulációk időigényét, de nem változtatja meg a keveréssel kapcsolatos eredményeket. Ezt a változtatást azonban nem lehet automatikusan elvégezni minden esetben, hatását minden keverési modell esetében ellenőrizni kell.

Keverési indexeket használtam a különböző keverékek tulajdonságainak kvantitatív elemzésére. A keverési index értéke 0 és 1 között változhat. A „nearest neighbor” keverési index meghatározásának Java kódját elkészítve gyorsítottam fel és pontosítottam az adatfeldolgozás folyamatát.

Forgódobos keverőberendezés belsejében elhelyezett lapátok segítségével sikerült javítanom a berendezés keverési hatékonyságán. Meghatároztam a keverőberendezés optimális fordulatszámát is, amely a legjobb keverési hatékonyságot biztosította.

Csigás keverőberendezésbe beépített keverőlapátok segítségével javítottam a keverési hatékonyságot a fal közelében nyugvó szemcséket is megmozgatva. Meghatároztam a keverőcsiga menetemelkedésének optimális értékét is, mely a legnagyobb keverési hatékonyságot biztosította.

Kukoricaszemek különböző sugarú gömbökből összeállított „clump” modelljét használva egytengelyes lapátos keverőberendezés diszkrét elemes modelljét is elkészítettem. A modell használatával rávilágítottam, hogy a keverőberendezés feltöltési módja hatással van a keverék minőségére. A keverőberendezés optimális működési paramétereit is meghatároztam.

A Diszkrét Elemes Módszer (DEM) alkalmazása a keverőberendezések tervezésében kulcsfontosságú a hatékonyságuk és hatékonyságuk maximalizálása szempontjából. A szemcsék viselkedésének és kölcsönhatásainak szimulációján keresztül a DEM értékes betekintést nyújt a keverés dinamikájába. A mérnökök ezt az információt felhasználhatják az eszköz geometriájának finomításához, a keverés hatékonyságának növeléséhez, valamint a kopás és szemtörés okozta problémák csökkentéséhez. Az ilyen szimulációkra épülő megközelítés nemcsak felgyorsítja a tervezési fázist, hanem növeli a keverőberendezések megbízhatóságát és funkcionalitását.

8. APPENDICES

A1. Bibliography

1. Allen, T. (1968). Particle size measurement, Powder sampling and particle size Measurement. In *Particle Size Measurement* (5th ed., Vol. 1).

2. Applying to Standards, Tests, Assays, and Other Specifications of the United States Pharmacopeia, Bulk Powder Sampling Procedures. (2015). *The United States Pharmacopeial Convention*, 523–536.

3. Arntz, D., den, K., Briels, W. J., Bussmann, P. J. T., Beeftink, H. H., & Boom, R. M. (2008). *Granular mixing and segregation in a horizontal rotating drum: A simulation study on the impact of rotational speed and fill level*. *54*(12), 3133–3146. https://doi.org/10.1002/aic.11622

4. Asachi, M., Nourafkan, E., & Hassanpour, A. (2018). A review of current techniques for the evaluation of powder mixing. *Advanced Powder Technology*, *29*(7), 1525–1549. https://doi.org/10.1016/j.apt.2018.03.03

5. Badmos, A. Y., & H. K. D. H. Bhadeshia. (1997). The evolution of solutions: A thermodynamic analysis of mechanical alloying. *Metallurgical and Materials Transactions*, *28*(11), 2189–2194. https://doi.org/10.1007/s11661-997-0176-5

6. Bao, Y., Li, T., Wang, D., Cai, Z., & Gao, Z. (2020). Discrete element method study of effects of the impeller configuration and operating conditions on particle mixing in a cylindrical mixer. *Particuology*, *49*, 146–158. https://doi.org/10.1016/j.partic.2019.02.002

7. Belheine, N., Plassiard, J.-P. ., Donzé, F.-V. ., Darve, F., & Seridi, A. (2009). Numerical simulation of drained triaxial test using 3D discrete element modeling. *Computers and Geotechnics*, *36*(1-2), 320–331. https://doi.org/10.1016/j.compgeo.2008.02.003

8. Benedetti, C., Abatzoglou, N., Simard, J.-S., McDermott, L., Leonard, G. W., & L. Cartilier. (2007). Cohesive, multicomponent, dense powder flow characterization by NIR. *International Journal of Pharmaceutics*, *336*(2), 292–301. https://doi.org/10.1016/j.ijpharm.2006.12.014

9. Bhatt, B. (2009). *Mixing*. Sector – 3, Pushp Vihar, New Delhi, India: Delhi Institute of Pharmaceutical Science and Research.

10. Boon, C. W., Houlsby, G. T., & Utili, S. (2012). A new algorithm for contact detection between convex polygonal and polyhedral particles in the discrete element method. *Computers and Geotechnics*, *44*, 73–82. https://doi.org/10.1016/j.compgeo.2012.03.012

11. Bridgwater, J. (2012). Mixing of powders and granular materials by mechanical means—A perspective. *Particuology*, *10*(4), 397–427. https://doi.org/10.1016/j.partic.2012.06.002

12. C. González-Montellano, Fuentes Jm, Ayuga-Téllez, E., & Ayuga, F. (2012). *Determination of the mechanical properties of maize grains and olives required for use in DEM simulations*. *111*(4), 553–562. https://doi.org/10.1016/j.jfoodeng.2012.03.017

13. Campbell, H., & Bauer, W. (1966). Cause and Care of Demixing in Solid-Solid Mixers. *Chemical Engineering*, *73*, 179.

14. Carter, F. L. (1978). Quantifying the concept of coordination number. *Acta Crystallographica Section B Structural Crystallography and Crystal Chemistry*, *34*(10), 2962–2966. https://doi.org/10.1107/s0567740878009838

15. Catalano, E., Chareyre, B., & Barthélémy, E. (2013). Pore-scale modeling of fluid-particles interaction and emerging poromechanical effects. *International Journal for Numerical and Analytical Methods in Geomechanics*, *38*(1), 51–71. https://doi.org/10.1002/nag.2198

16. Cleary, P. W. (2000). DEM simulation of industrial particle flows: case studies of dragline excavators, mixing in tumblers and centrifugal mills. *Powder Technology*, *109*(1-3), 83–104. https://doi.org/10.1016/s0032-5910(99)00229-6

17. Cundall, P. A., & Strack, O. D. L. (1979). A discrete numerical model for granular assemblies. *Géotechnique*, *29*(1), 47–65. https://doi.org/10.1680/geot.1979.29.1.47

18. DCS (2016). *gran model hertz model*. Retrieved from CFDEM: https://www.cfdem.com/media/DEM/docu/gran_model_hertz.html

19. DCS (2016). *gran model hooke model*. Retrieved from CFDEM: https://www.cfdem.com/media/DEM/docu/gran_model_hooke.html

20. Fan, L. T., Chen, S. J., & Watson, C. A. (1970). Solids Mixing. *Industrial engineering and mixing, 62(7)*, 53-69.

21. Fan, L. T., Chen, Y., & Lai, F. S. (1990). Recent developments in solids mixing. *Powder Technology*, *61*(3), 255–287. https://doi.org/10.1016/0032-5910(90)80092-d

22. Foldager, F. F., Munkholm, L. J., Balling, O., Serban, R., Negrut, D., Heck, R. J., & Green, O. (2022). Modeling soil aggregate fracture using the discrete element method. *Soil and Tillage Research*, *218*, 105295. https://doi.org/10.1016/j.still.2021.105295

23. Gantt, J. A., & Gatzke, E. P. (2005). High-shear granulation modeling using a discrete element simulation approach. *Powder Technology*, *156*(2-3), 195–212. https://doi.org/10.1016/j.powtec.2005.04.012

24. Gerlach, R., & Nocerino, J. (2003). Guidance for Obtaining Representative Laboratory Analytical Subsamples from Particulate Laboratory Samples. *U.S. Environmental Protection Agency*, EPA/600/R-03/027.

25. Godlieb, W., Gorter, S., Deen, N. G., & Kuipers, J. A. M. (2010). DEM and TFM simulations of solids mixing in a gaz-solid fluidized bed.

26. Harnby, N. (2000). An engineering view of pharmaceutical powder mixing. *Pharmaceutical Science & Technology Today*, *3*(9), 303–309. https://doi.org/10.1016/s1461-5347(00)00283-2

27. Hassanpour, A., Tan, H., Bayly, A., Gopalkrishnan, P., Ng, B., & Ghadiri, M. (2011). Analysis of particle motion in a paddle mixer using Discrete Element Method (DEM). *Powder Technology*, *206*(1-2), 189–194. https://doi.org/10.1016/j.powtec.2010.07.025

28. Hermann, A., Lein, M., & Schwerdtfeger, P. (2007). The Search for the Species with the Highest Coordination Number. *Angewandte Chemie International Edition*, *46*(14), 2444–2447. https://doi.org/10.1002/anie.200604148

29. Hoomans, B. P. B., Kuipers, J. A. M., & van Swaaij, W. P. M. (2000). Granular dynamics simulation of segregation phenomena in bubbling gas-fluidised beds. *Powder Technology*, *109*(1-3), 41–48. https://doi.org/10.1016/s0032-5910(99)00225-9

30. Horváth, D., Poós, T., & Tamás, K. (2019). Modeling the movement of hulled millet in agitated drum dryer with discrete element method. *Computers and Electronics in Agriculture*, *162*, 254–268. https://doi.org/10.1016/j.compag.2019.03.033

31. Horváth, D., Tamás, K., & Poós, T. (2022). Viscoelastic contact model development for the discrete element simulations of mixing process in agitated drum. *Powder Technology*, *397*, 117038. https://doi.org/10.1016/j.powtec.2021.117038

32. Huang, A. N., Cheng, T. H., Hsu, W. Y., Huang, C. C., & Kuo, H. P. (2021). DEM study of particle segregation in a rotating drum with internal diameter variations. *Powder Technology*, *378*, 430–440. https://doi.org/10.1016/j.powtec.2020.10.019

33. Huang, A.-N., & Kuo, H.-P. (2014). Developments in the tools for the investigation of mixing in particulate systems – A review. *Advanced Powder Technology*, *25*(1), 163–173. https://doi.org/10.1016/j.apt.2013.10.007

34. Itasca. (2003). *Particle flow code.* Minneapolis, Minnesota: Itasca consulting group.

35. Jiang, M. J., Yu, H.-S. ., & Harris, D. (2005). A novel discrete model for granular material incorporating rolling resistance. *Computers and Geotechnics*, *32*(5), 340–357. https://doi.org/10.1016/j.compgeo.2005.05.001

36. Jing, L., & Ove Stephansson. (2007). *Fundamentals of Discrete Element Methods for Rock Engineering: Theory and Applications*. Elsevier.

37. Johnson, K. (1985). *Contact Mechanics.* Cambridge: Cambridge University Press.

38. Johnson, M. (1972). Particle size distribution of the active ingredient for solid dosage forms of low dosage. *Pharmaceutica Acta Helvetica.*, 42; 546-559.

39. Jonsson, H., Alderborn, G., & Frenning, G. (2019). Evaluation of bulk compression using a discrete element procedure calibrated with data from triaxial compression experiments on single particles. *Powder Technology*, *345*, 74–81. https://doi.org/10.1016/j.powtec.2018.12.090

40. Keppler, I., Varga, A., Szabo, I., Laszlo Katai, & Laszlo Fenyvesi. (2016). Particle motion around open mixing screws: optimal screw angular velocity. *Engineering Computations*, *33*(3). https://doi.org/10.1108/ec-03-2015-0058

41. Ketterhagen, W. R., Curtis, J. S., Wassgren, C. R., & Hancock, B. C. (2009). Predicting the flow mode from hoppers using the discrete element method. *Powder Technology*, *195*(1), 1–10. https://doi.org/10.1016/j.powtec.2009.05.002

42. Kruszelnicka, W., Macko, M., Łączny, D., Patrycja Bałdowska-Witos, & Lewandowski, J. (2022). The Use of Simulation Software using the Discrete Element Method (DEM) for the Process of Materials Comminution. MATEC Web of Conferences, 357, 07005–07005. https://doi.org/10.1051/matecconf/202235707005

43. Lacey, P. M. C. (2007). Developments in the theory of particle mixing. *Journal of Applied Chemistry*, *4*(5), 257–268. https://doi.org/10.1002/jctb.5010040504

44. Lamboley, A. (1970). *Statistiques. Techniques de l'ingénieur, Ref. A166 V1*.

45. Leuenberger, H. (2002). Martin Physikalische Pharmazie. 4. Auflage; Wissenschaftliche.

46. Leurenberger, H., & Lanz, M. (2005). Pharmaceutical powder technology — from art to science: the challenge of the FDA's Process Analytical Technology initiative. *Advanced Powder Technology*, *16*(1), 3–25. https://doi.org/10.1163/1568552053166683

47. Li, Y., Xu, Y., & Jiang, S. (2009). DEM simulations and experiments of pebble flow with monosized spheres. *Powder Technology*, *193*(3), 312–318. https://doi.org/10.1016/j.powtec.2009.03.009

48. Li, Y., Xu, Y., & Thornton, C. (2005). A comparison of discrete element simulations and experiments for “sandpiles” composed of spherical particles. *Powder Technology*, *160*(3), 219–228. https://doi.org/10.1016/j.powtec.2005.09.002

49. Marigo, M., & Stitt, E. H. (2015). Discrete Element Method (DEM) for Industrial Applications: Comments on Calibration and Validation for the Modelling of Cylindrical Pellets. *KONA Powder and Particle Journal*, *32*(0), 236–252. https://doi.org/10.14356/kona.2015016

50. Marigo, M., Cairns, D. L., Davies, M., Ingram, A., & Stitt, E. H. (2012). A numerical comparison of mixing efficiencies of solids in a cylindrical vessel subject to a range of motions. *Powder Technology*, *217*, 540–547. https://doi.org/10.1016/j.powtec.2011.11.016

51. Massol-Chaudeur, S. D. (2000). *Caractérisation de l’état de mélange de poudres: cas de mélanges faiblement dosés.* Lorraine, France: Institut National Polytechnique de Lorraine.

52. Mathias, L., Saeys Wouter, Tom, L., Pešek Jiří, & Bart, S. (2021). Packing simulation of thin flexible particles using a novel discrete element model. *Computational Particle Mechanics*, *9*(3), 407–420. https://doi.org/10.1007/s40571-021-00419-9

53. Mellmann, J. (2001). The transverse motion of solids in rotating cylinders—forms of motion and transition behavior. *Powder Technology*, *118*(3), 251–270. https://doi.org/10.1016/S0032-5910(00)00402-2

54. Muzzio, F. J., Goodridge, C. L., Alexander, A., Arratia, P., Yang, H., Sudah, O., & Mergen, G. (2003). Sampling and characterization of pharmaceutical powders and granular blends. *International Journal of Pharmaceutics*, *250*(1), 51–64. https://doi.org/10.1016/S0378-5173(02)00481-7

55. Oldal, I., Safranyik, F., & Keppler, I. (2017). Reducing computational time of cohesionless discrete simulations based on particle clusters. *Engineering Computations*, *34*(2), 648–663. https://doi.org/10.1108/ec-12-2015-0388

56. Olivier Dubé, Alizadeh, E., Chaouki, J., & Bertrand, F. (2013). Dynamics of non-spherical particles in a rotating drum. *Chemical Engineering Science*, *101*, 486–502. https://doi.org/10.1016/j.ces.2013.07.011

57. Poole, K., Taylor, R., & Wall, G. (1964). Mixing powders to fine-scale homogeneity : studies of batch mixing. Trans. Inst. Chem. Eng., 42-305.

58. Potyondy, D. O., & Cundall, P. A. (2004). A bonded-particle model for rock. *International Journal of Rock Mechanics and Mining Sciences*, *41*(8), 1329–1364. https://doi.org/10.1016/j.ijrmms.2004.09.011

59. Poux, M., Fayolle, P., Bertrand, J., Bridoux, D., & Bousquet, J. (1991). Powder mixing: Some practical rules applied to agitated systems. *Powder Technology*, *68*(3), 213–234. https://doi.org/10.1016/0032-5910(91)80047-M

60. Prescott, J. K., & Barnum, R. (2000). On powder flowability. *Pharmaceutical Technology*, 24, 60-84.

61. Rosato, A., Strandburg, K. J., Prinz, F., & Swendsen, R. H. (1987). Why the Brazil nuts are on top: Size segregation of particulate matter by shaking. *Physical Review Letters*, *58*(10), 1038–1040. https://doi.org/10.1103/physrevlett.58.1038

62. S368.4, A. (2000). *Compression Test of Food Materials of Convex Shape.* St. Joseph, Michigan: American Society of Agricultural and Biological. Engineers..https://elibrary.asabe.org/abstract.asp?aid=42544&t=2

63. Shenouda, S., & Hoff, A. (2020). Discrete Element Method Analysis for Metal Powders Used in Additive Manufacturing, and DEM Simulation Tutorial Using LIGGGHTS-PUBLIC. *OSTI OAI (U.S. Department of Energy Office of Scientific and Technical Information)*. https://doi.org/10.2172/1656962

64. Shu San Hsiau, & Wen Cheng Chen. (2002). Density effect of binary mixtures on the segregation process in a vertical shaker. *Advanced Powder Technology*, *13*(3), 301–315. https://doi.org/10.1163/156855202320252462

65. Soni, R. K., Mohanty, R., Mohanty, S., & Mishra, B. K. (2016). Numerical analysis of mixing of particles in drum mixers using DEM. *Advanced Powder Technology*, *27*(2), 531–540. https://doi.org/10.1016/j.apt.2016.01.016

66. Susana, L., Canu, P., & Andrea Claudio Santomaso. (2011). Development and characterization of a new thief sampling device for cohesive powders. *International Journal of Pharmaceutics*, *416*(1), 260–267. https://doi.org/10.1016/j.ijpharm.2011.07.003

67. Swaminathan, V., & Kildsig, D. O. (2002). Polydisperse Powder Mixtures: Effect of Particle Size and Shape on Mixture Stability. *Drug Development and Industrial Pharmacy*, *28*(1), 41–48. https://doi.org/10.1081/ddc-120001484

68. Thakur, S. C., Ooi, J. Y., & Ahmadian, H. (2016). Scaling of discrete element model parameters for cohesionless and cohesive solid. *Powder Technology*, *293*, 130–137. https://doi.org/10.1016/j.powtec.2015.05.051

69. Thornton, C., & Randall, C. W. (1988). Applications of Theoretical Contact Mechanics to Solid Particle System Simulation. *Studies in Applied Mechanics*, 133–142. https://doi.org/10.1016/b978-0-444-70523-5.50023-0

70. Thorsten Pöschel, Salueña, C., & Schwager, T. (2001). Scaling properties of granular materials. *Physical Review*, *64*(1). https://doi.org/10.1103/physreve.64.011308

71. Trabelsi, B. (2013). Simulation numérique de l'écoulement et mélange granulaire par des éléments discrets ellipsoidaux.

72. Venables, H. J., & Wells, J. I. (2001). Powder Mixing. *Drug Development and Industrial Pharmacy*, *27*(7), 599–612. https://doi.org/10.1081/ddc-100107316

73. Wang, S., Li, H., Tian, R., Wang, R., Wang, X., Sun, Q., & Fan, J. (2019). Numerical simulation of particle flow behavior in a screw conveyor using the discrete element method. *Particuology*, *43*, 137–148. https://doi.org/10.1016/j.partic.2018.01.016

74. Wen, Y., Liu, M., Liu, B., & Shao, Y. (2015). Comparative Study on the Characterization Method of Particle Mixing Index Using DEM Method. *Procedia Engineering*, *102*, 1630–1642. https://doi.org/10.1016/j.proeng.2015.01.299

75. Wu, C.-Y. (2008). DEM simulations of die filling during pharmaceutical tabletting. *Particuology*, *6*(6), 412–418. https://doi.org/10.1016/j.partic.2008.07.008

76. Yang, R. Y., Zou, R. P., & Yu, A. B. (2003). Microdynamic analysis of particle flow in a horizontal rotating drum. *Powder Technology*, *130*(1-3), 138–146. https://doi.org/10.1016/s0032-5910(02)00257-7

77. Zhao Yong-Zhi, & Yi, C. (2008). Numerical simulation of radial segregation patterns of binary granular systems in a rotating horizontal drum. *Acta Phys. Sin*, 57(1): 322-328. doi: 10.7498/aps.57.322

A2. Publications related to the thesis

1. Garneoui, S., Korzenszky, P., & Keppler, I. (2023). Enhancement of the mixture quality of corn grains in a single-shaft paddle mixer using DEM simulations. Journal of *Mechanical Science and Technology, 37(3),* 1365–1373. https://doi.org/10.1007/s12206-023-0223-1

2. Talafha, S.M., Oldal, I., & Garneoui, S. (2022). Study the particle size impact on the mechanical behaviour of granular material by discrete element method. *FME Transactions, 50(3),* 473–483. https://doi.org/10.5937/fme2203473t

3. Garneoui, S., Korzenszky, P, & Keppler, I (2022): Mixing Enhancement of Mono-Disperse and Bi-Disperse Particles in a Cylindrical Drum Mixer Using Discrete Element Simulations. (2022). *Tehnicki Vjesnik - Technical Gazette*, *29*(3), 752-758. https://doi.org/10.17559/tv-20210303201549

4. Garneoui, S., Keppler, I., Korzenszky, P., & Talafha, S.M, (2021): Numerical study on the impact of particles filling pattern and screw parameters on the mixing uniformity of wheat grains in a screw mixer. *Applied and Computational Mechanics*, *15 (2),* 123-http://dx.doi.org/10.24132/acm.2021.689

5. Garneoui, S., Keppler, I., & Korzenszky, P (2020): Numerical Assessment of a Static Mixer Design for Mixing Free Flowing Granular Materials Using the Discrete Element Method. *Journal of Mechanical Engineering and Technology (JET), 11 (2),* 23-36. https://jet.utem.edu.my/jet/article/view/5972

6. Garneoui, S., Keppler, I., & Korzenszky, P (2020): Mixing Enhancement of Wheat Granules in a Hopper Bottom Lab-Scale Mixer Using Discrete Element Simulations. *FME Transactions, 48 (4),* 868-873. http://dx.doi.org/10.5937/fme2004868G

7. Garneoui, S., Keppler, I., & Korxenszky P (2022): Impact of screw pitch length on the mixture quality of grains in a small-scale silo apparatus. *Mechanical Engineering Letters: R and D: Research and Development, 23,* 4-12. http://dx.doi.org/10.24132/acm.2021.689

A3. Box discharging experiments

The list of conducted experiments in all combinations to calibrate the micro-mechanical properties of the corn particle with the particle-particle CoF, particle-wall CoF, particle-particle CoRF and particle-wall CoRF are listed in Table 8.1.

Table 8.1. List of box discharging experiments

Run	Particle-particle CoF	particle-wall CoF	Particle-particle CoRF	particle-wall CoRF	Slope angle (700p)	Slope angle (1300p)	Slope angle (1500p)
1	0.6	0.4	0.03	0.03	13.05	11.84	8.14
2	0.6	0.5	0.03	0.03	13.1	11.89	8.19
3	0.6	0.6	0.03	0.03	14.2	12.99	9.29
4	0.6	0.7	0.03	0.03	14.3	13.09	9.39
5	0.6	0.8	0.03	0.03	14.4	13.19	9.49
6	0.65	0.4	0.03	0.03	15.5	14.29	10.59
7	0.65	0.5	0.03	0.03	16.6	15.39	11.69
8	0.65	0.6	0.03	0.03	15.7	14.49	10.79
9	0.65	0.7	0.03	0.03	16.8	15.59	11.89
10	0.65	0.8	0.03	0.03	15.9	14.69	10.99
11	0.7	0.4	0.03	0.03	17	15.79	12.09
12	0.7	0.5	0.03	0.03	17	15.79	12.09
13	0.7	0.6	0.03	0.03	17.05	15.84	12.14
14	0.7	0.7	0.03	0.03	17.2	15.99	12.29
15	0.7	0.8	0.03	0.03	17.125	15.915	12.215
16	0.75	0.4	0.03	0.03	18.255	17.045	13.345
17	0.75	0.5	0.03	0.03	17.3	16.09	12.39
18	0.75	0.6	0.03	0.03	18.5	17.29	13.59
19	0.75	0.7	0.03	0.03	19.58	18.37	14.67
20	0.75	0.8	0.03	0.03	18.9	17.69	13.99
21	0.8	0.4	0.03	0.03	18	16.79	13.09
22	0.8	0.5	0.03	0.03	18	16.79	13.09
23	0.8	0.6	0.03	0.03	20.05	18.84	15.14
24	0.8	0.7	0.03	0.03	19.1	17.89	14.19
25	0.8	0.8	0.03	0.03	19.2	17.99	14.29
26	0.6	0.4	0.04	0.04	20.5	19.29	15.59
27	0.6	0.5	0.04	0.04	20.4	19.19	15.49
28	0.6	0.6	0.04	0.04	20.44	19.23	15.53
29	0.6	0.7	0.04	0.04	21.6	20.39	16.69
30	0.6	0.8	0.04	0.04	20.66	19.45	15.75
31	0.65	0.4	0.04	0.04	21.7	20.49	16.79
32	0.65	0.5	0.04	0.04	21.79	20.58	16.88
33	0.65	0.6	0.04	0.04	21.799	20.589	16.889
34	0.65	0.7	0.04	0.04	21.6	20.39	16.69
35	0.65	0.8	0.04	0.04	21.85	20.64	16.94
36	0.7	0.4	0.04	0.04	20.9	19.69	15.99

37	0.7	0.5	0.04	0.04	21.879	20.669	16.969
38	0.7	0.6	0.04	0.04	21.987	20.777	17.077
39	0.7	0.7	0.04	0.04	22	20.79	17.09
40	0.7	0.8	0.04	0.04	23.05	21.84	18.14
41	0.75	0.4	0.04	0.04	22.03	20.82	17.12
42	0.75	0.5	0.04	0.04	23.1	21.89	18.19
43	0.75	0.6	0.04	0.04	24.11	22.9	19.2
44	0.75	0.7	0.04	0.04	26.2	24.99	21.29
45	0.75	0.8	0.04	0.04	26.25	25.04	21.34
46	0.8	0.4	0.04	0.04	26	24.79	21.09
47	0.8	0.5	0.04	0.04	25.9	24.69	20.99
48	0.8	0.6	0.04	0.04	26.1	24.89	21.19
49	0.8	0.7	0.04	0.04	26.6	25.39	21.69
50	0.8	0.8	0.04	0.04	26.49	25.28	21.58
51	0.6	0.4	0.05	0.05	28.5	27.29	23.59
52	0.6	0.5	0.05	0.05	27.799	26.589	22.889
53	0.6	0.6	0.05	0.05	27.97	26.76	23.06
54	0.6	0.7	0.05	0.05	28.61	27.4	23.7
55	0.6	0.8	0.05	0.05	31.1	29.89	26.19
56	0.65	0.4	0.05	0.05	31.08	29.87	26.17
57	0.65	0.5	0.05	0.05	32.6	31.39	27.69
58	0.65	0.6	0.05	0.05	32.4	31.19	27.49
59	0.65	0.7	0.05	0.05	33	31.79	28.09
60	0.65	0.8	0.05	0.05	32.66	31.45	27.75
61	0.7	0.4	0.05	0.05	32.68	31.47	27.77
62	0.7	0.5	0.05	0.05	33	31.79	28.09
63	0.7	0.6	0.05	0.05	33.1	31.89	28.19
64	0.7	0.7	0.05	0.05	32.12	30.91	27.21
65	0.7	0.8	0.05	0.05	33.2	31.99	28.29
66	0.75	0.4	0.05	0.05	34.25	33.04	29.34
67	0.75	0.5	0.05	0.05	33.26	32.05	28.35
68	0.75	0.6	0.05	0.05	34.29	33.08	29.38
69	0.75	0.7	0.05	0.05	35.3	34.09	30.39
70	0.75	0.8	0.05	0.05	34.305	33.095	29.395
71	0.8	0.4	0.05	0.05	35.31	34.1	30.4
72	0.8	0.5	0.05	0.05	35.4	34.19	30.49
73	0.8	0.6	0.05	0.05	36.45	35.24	31.54
74	0.8	0.7	0.05	0.05	36.56	35.35	31.65
75	0.8	0.8	0.05	0.05	36.5	35.29	31.59
76	0.6	0.4	0.06	0.06	36.59	35.38	31.68
77	0.6	0.5	0.06	0.06	37.605	36.395	32.695
78	0.6	0.6	0.06	0.06	37.61	36.4	32.7
79	0.6	0.7	0.06	0.06	37.62	36.41	32.71
80	0.6	0.8	0.06	0.06	38.623	37.413	33.713
81	0.65	0.4	0.06	0.06	39.63	38.42	34.72

82	0.65	0.5	0.06	0.06	38.64	37.43	33.73
83	0.65	0.6	0.06	0.06	39.65	38.44	34.74
84	0.65	0.7	0.06	0.06	37.66	36.45	32.75
85	0.65	0.8	0.06	0.06	38.675	37.465	33.765
86	0.7	0.4	0.06	0.06	39.68	38.47	34.77
87	0.7	0.5	0.06	0.06	39.69	38.48	34.78
88	0.7	0.6	0.06	0.06	39.7	38.49	34.79
89	0.7	0.7	0.06	0.06	40.1	38.89	35.19
90	0.7	0.8	0.06	0.06	40.1	38.89	35.19
91	0.75	0.4	0.06	0.06	40.2	38.99	35.29
92	0.75	0.5	0.06	0.06	40.25	39.04	35.34
93	0.75	0.6	0.06	0.06	40.6	39.39	35.69
94	0.75	0.7	0.06	0.06	39.9	38.69	34.99
95	0.75	0.8	0.06	0.06	41.02	39.81	36.11
96	0.8	0.4	0.06	0.06	42	40.79	37.09
97	0.8	0.5	0.06	0.06	41.5	40.29	36.59
98	0.8	0.6	0.06	0.06	42.3	41.09	37.39
99	0.8	0.7	0.06	0.06	42.2	40.99	37.29
100	0.8	0.8	0.06	0.06	42.35	41.14	37.44

A4. LIGGGHTS input code

In this appendix, I give an example of LIGGGHTS input code. This code would give an insight into the steps and commands that should be defined to run a simulation, also it would help researchers who are not familiar with LIGGGHTS to have a good understanding of how it works.

```
atom_style      granular
atom_modify     map array sort 0 0
boundary        f f f
units           si
communicate     single vel yes

newton          off
variable xmin equal -0.15
variable xmax equal  0.15
variable ymin equal -0.1
variable ymax equal  0.1
variable zmin equal -0.2

variable zmax equal  0.2
variable PI     equal 3.14
variable r      equal 0.0003
variable rho    equal 1163.3
variable G      equal 1.0325e8
variable nu     equal 0.4

variable dt     equal 0.2*((((${PI})*(${r}))*(sqrt((${rho})/(${G})))))/((0.1631*(${nu}))+0.8766))

variable natoms equal 2

variable youngmodulus1 equal    2.891e8         #N/mm²
variable youngmodulus2 equal    5.66e7          #N/mm²

variable        poission1       equal   0.4
variable        poission2       equal   0.235

variable CoR11  equal   0.251
variable CoR12  equal   0.505
variable CoR21  equal   0.505
variable CoR22  equal   0.251
variable sf11   equal   0.6
variable sf12   equal   0.7
variable sf21   equal   0.7
variable sf22   equal   0.6
variable rf11   equal   0.05
variable rf12   equal   0.05
variable rf21   equal   0.05
variable rf22   equal   0.05

#variable       radius1 equal   0.0025  #m
#variable       radius2 equal   0.0025  #m

variable frac1  equal   1.0             #100 %
variable frac2  equal   1.0             #100 %
```

```
variable density1 equal 1163.3 #kg/m³
variable density2 equal 1250 #kg/m³

region reg block ${xmin} ${xmax} ${ymin} ${ymax} ${zmin} ${zmax} units box
create_box 2 reg
neighbor 0.005 bin #default
neigh_modify delay 0 #default

pair_style gran model hertz tangential history rolling_friction epsd2
pair_coeff * * #default
timestep ${dt}
fix integrator all nve/sphere #default
fix gravi all gravity 9.81 vector 0.0 0.0 -1.0 #gravity of 9.81 m/s² in negative z direction

fix m1 all property/global youngsModulus peratomtype ${youngmodulus1} ${youngmodulus2}
fix m2 all property/global poissonsRatio peratomtype ${poission1} ${poission2}
fix m3 all property/global coefficientRestitution peratomtypepair ${natoms} ${CoR11}
${CoR12} ${CoR21} ${CoR22}
fix m4 all property/global coefficientFriction peratomtypepair ${natoms} ${sf11} ${sf12}
${sf21} ${sf22}
fix m5 all property/global coefficientRollingFriction peratomtypepair ${natoms} ${rf11} ${rf12}
${rf21} ${rf22}
fix m6 all property/global Density peratomtype ${density1} ${density2}
fix m7 all property/global characteristicVelocity scalar 2

fix MixerFrame all mesh/surface file mixer_frame.stl type 1 scale 0.001
curvature_tolerant yes
fix MixingRotor all mesh/surface file mixing_rotor_2_paddles.stl type 1 scale 0.001
curvature_tolerant yes
fix Splitter all mesh/surface file splitter.stl type 1 scale 0.001 curvature_tolerant yes

fix walls all wall/gran model hertz tangential history rolling_friction epsd2
mesh n_meshes 3 meshes MixerFrame MixingRotor Splitter

fix pts1 all particletemplate/multisphere 11887 atom_type 1 density constant ${density1} nspheres 5 ntry
1000000 spheres file data/grain1.multisphere scale 1.0 type 1
fix pts2 all particletemplate/multisphere 11887 atom_type 2 density constant ${density1} nspheres 5 ntry
1000000 spheres file data/grain2.multisphere scale 1.0 type 2

fix pdd1 all particledistribution/discrete 32452867 1 pts1 ${frac1}
fix pdd2 all particledistribution/discrete 32452867 1 pts2 ${frac2}

region factory1 cylinder x -0.025 -0.035 0.015 -0.12 0.12 units box
region factory2 cylinder x 0.025 -0.035 0.015 -0.12 0.12 units box

fix ins1 all insert/rate/region seed 86028157 distributiontemplate pdd1 &
nparticles 1320 particlerate 2000 insert_every 1000 overlapcheck yes &
all_in yes vel constant 0 0 0 region factory1 ntry_mc 10000

fix ins2 all insert/rate/region seed 86028157 distributiontemplate pdd2 &
nparticles 1320 particlerate 2000 insert_every 1000 overlapcheck yes &
```

```
all_in yes vel constant 0 0 0 region factory2 ntry_mc 10000

fix        integr all multisphere

variable          simulatefor1s     equal     round(1.0/${dt})
variable simulatefor2s     equal     round(2*(1.0/${dt}))
variable simulatefor40s    equal     round(40*(1.0/${dt}))
variable          dumptime          equal     1.0                                  # Every 1s 1 image
variable          dumpstep          equal     round(${dumptime}/${dt})
variable          dumpstep1         equal     round(0.01/${dt})

dump     dmpparticle               all custom/vtk    ${dumpstep} post/particles_*.vtk id type x y z vx vy vz fx
fy fz radius mass
dump     dmpMixerFrame                   all mesh/stl       ${dumpstep} post/MixerFrame*.stl MixerFrame

dump     dmpMixingRotor                  all mesh/stl       ${dumpstep} post/MixingRotor*.stl MixingRotor

dump     dmpSplitter               all mesh/stl       ${dumpstep} post/Splitter*.stl Splitter

run      ${simulatefor1s}

fix      MoveSplitter              all move/mesh mesh Splitter    linear 0.0 0.0 0.11
run      ${simulatefor1s}

unfix    MoveSplitter
run      ${simulatefor1s}

fix      MoveMixingRotor           all move/mesh mesh MixingRotor rotate origin 0 0 -0.04 axis -1. 0. 0. period
6        #Rotation of paddles (10 rpm)

run      ${simulatefor40s}
```

A5. Nearest neighbor java script

To calculate the mixing index using the nearest neighbor's index, I have coded the model in a java script that finds the mixing rate through a CSV file containing the coordinates in columns x_1, x_2, y_1, y_2, z_1, z_2 of particles type 1 and type 2, respectively.

```
import java.io.*;
import java.util.ArrayList;
import java.util.List;
import java.util.Collections;
import java.util.Comparator;
class Molecule {
    public double x;
    public double y;
    public double z;
    public byte group;
    public static final int seek_count = 12;
    public Molecule(double x, double y, double z, byte group) {
        this.x = x;
        this.y = y;
        this.z = z;
        this.group = group;
    }
}
class Distance {
   public double distance;
   public byte group;

   public Distance(double distance, byte group){
      this.distance = distance;
      this.group = group;
   }
}
public class Main {
   public static void main(String[] args) throws FileNotFoundException {
      ArrayList<Molecule> molecule_list = new ArrayList<>();
      BufferedReader br = new BufferedReader(new FileReader("origfile.csv"));
      String line;
      double x = 0.0;
      double y = 0.0;
      double z = 0.0;
      byte group = 0;
      try {
         while ((line = br.readLine()) != null) {

            String[] tokens = line.split(",");
                                    if(tokens.length == 0){
                                          break;
                                    }
                                    //System.out.println(tokens[0] + ' ' + tokens[1] + ' ' + tokens[2] + ' ' +
tokens[3] + ' ' + tokens[4] + ' ' + tokens[5]);
                                    if(!tokens[0].trim().isEmpty()) {
            x = Double.parseDouble(tokens[0]);
            y = Double.parseDouble(tokens[2]);
```

```
            z = Double.parseDouble(tokens[4]);
            group = 1;
            molecule_list.add(new Molecule(x, y, z, group));
            x = Double.parseDouble(tokens[1]);
            y = Double.parseDouble(tokens[3]);
            z = Double.parseDouble(tokens[5]);
            group = 2;

            molecule_list.add(new Molecule(x, y, z, group));
                                    }
                                    else {
                                    x = Double.parseDouble(tokens[1]);
            y = Double.parseDouble(tokens[3]);
            z = Double.parseDouble(tokens[5]);
            group = 2;
            molecule_list.add(new Molecule(x, y, z, group));
                                    }
          }
        } catch (IOException e) {
          e.printStackTrace();
        }
        double distance = 0.0;
        List<Distance> distance_list = new ArrayList<>();
        double sum = 0;
        for(int i=0; i < molecule_list.size();i++){
          //System.out.println(i+1);
          for(int j=0; j < molecule_list.size();j++){
              if(i != j){
                 // Formula : Distance netween two points
                distance = Math.sqrt(
                    Math.pow(molecule_list.get(i).x - molecule_list.get(j).x, 2) +
                    Math.pow(molecule_list.get(i).y - molecule_list.get(j).y, 2) +
                    Math.pow(molecule_list.get(i).z - molecule_list.get(j).z, 2));
                    distance_list.add(new Distance(distance,molecule_list.get(j).group));
              }
          }
          distance_list.sort((object1, object2) -> Double.compare(object1.distance,object2.distance));
          // Find how many different groups besides itself
          // Formula :  nearest neighbours method
          // 2 * n_dif / n_b
          int n_dif = 0;
          for(int k = 0; k < Molecule.seek_count; k++){
            if(molecule_list.get(i).group != distance_list.get(k).group)
               n_dif++;
          }
          sum += 2.0 * (double) n_dif / (double) Molecule.seek_count; // i --> n times
          System.out.println("Mix Index: " + sum + ", Group: " + molecule_list.get(i).group + ", Diff neighbours:
" + n_dif);
          distance_list.clear();
        }
        double mix_index = sum / 5000.0;
        System.out.println(mix_index);
    }}
```

A6. Technical drawings

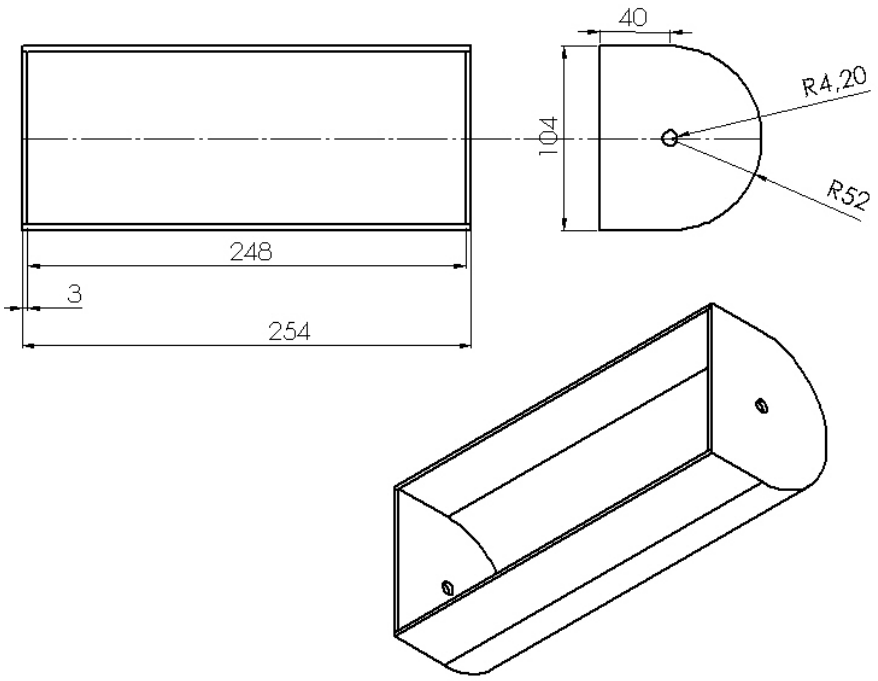

Fig. 8.1. Technical drawing of the Paddle mixer frame

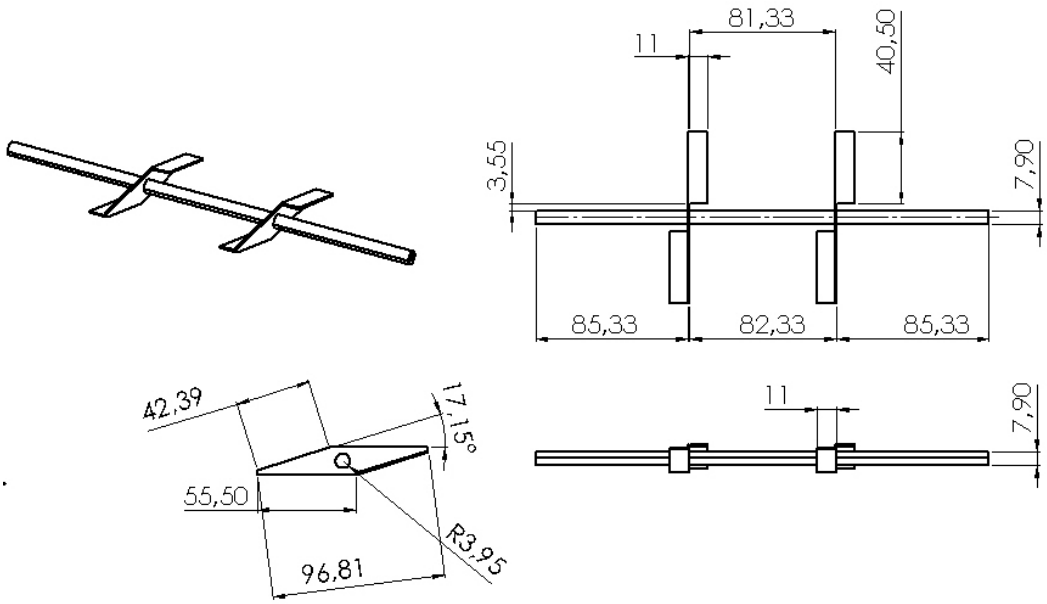

Fig. 8.2. Technical drawing of the Paddle mixer rotor (case of 2 paddles)

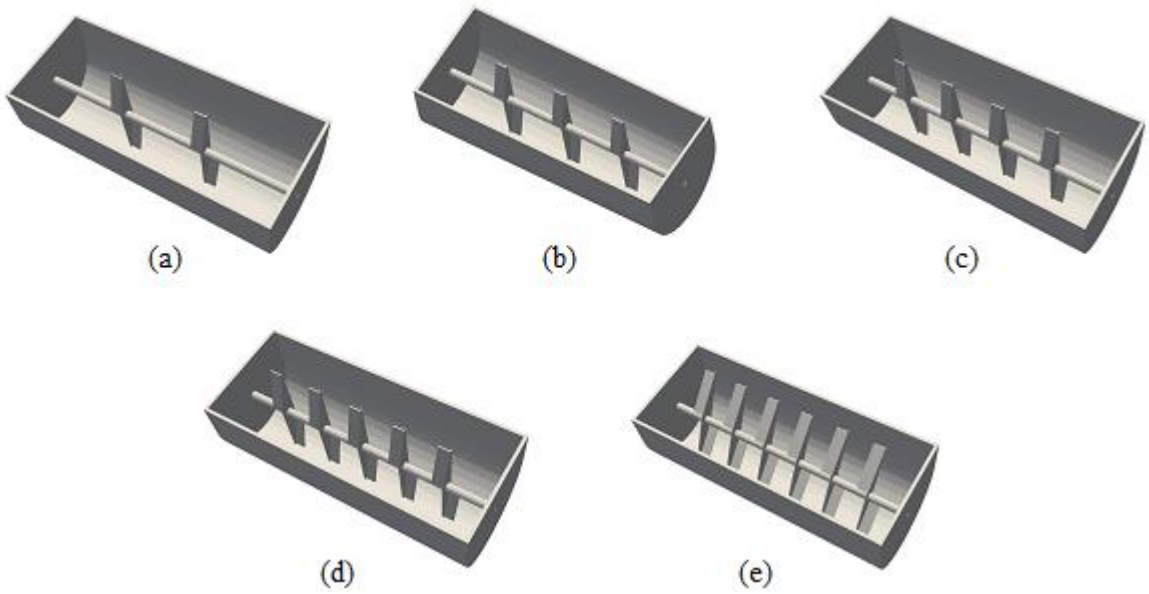

Fig. 8.3. The different number of paddles used in the paddle mixer. (a) 2 paddles (b) 3paddles (c) 4paddles (d) 5 paddles (e) 6 paddles

9. ACKNOWLEDGEMENT

To begin with, I want to thank my mum, brothers and sister for their support and non-vanishing encouragements to keep me motivated and achieve my goals. Also, I thank a lot my friends that were asking about me from my home country, and my friends who I met abroad that made my staying in Hungary like a second home.

I would like to express my thank of gratitude to my supervisor Prof. István Keppler and my co-supervisor Dr. Péter Korzenszky for their guidance and assistance throughout my PhD work. They were very helpful, and it is because of their efforts, research experience and their continuous follow-up all these years, that I succeeded in achieving the PhD requirements.

I acknowledge KIFU for providing us access to supercomputer resources based in Hungary.

Last but not least, I would like to thank the Tempus Public Foundation for the Stipendium Hungaricum scholarship award for having this excellent opportunity to obtain the PhD degree.

Finally, I would like to be grateful for the teachers in our department for giving us courses during the first year of our PhD program, and I appreciate the administrative help whenever asked from all the staff members working in the office of the PhD doctoral school.